BRARY.
-7419 ANL-7419
BRARY.
-7419 ANL-7419
BRARY.
-7419 ANL-7419
BRARY.
-7419 ANL-7419
BRARY.
-7419 ANL-7419
BRARY.
-7419 ANL-7419
BRARY.
-7419 ANL-7419
BRARY.
-7419 ANL-7419
BRARY.
-7419 ANL-7419
BRARY.
-7419 ANL-7419
BRARY.
-7419 ANL-7419

The facilities of Argonne National Laboratory are owned by the United States Government. Under the terms of a contract (W-31-109-Eng-38) between the U. S. Atomic Energy

The facilities of Argonne National Laboratory are owned by the United States Government. Under the terms of a contract (W-31-109-Eng-38) between the U. S. Atomic Energy

The facilities of Argonne National Laboratory are owned by the United States Government. Under the terms of a contract (W-31-109-Eng-38) between the U. S. Atomic Energy

The facilities of Argonne National Laboratory are owned by the United States Government. Under the terms of a contract (W-31-109-Eng-38) between the U. S. Atomic Energy

The facilities of Argonne National Laboratory are owned by the United States Government. Under the terms of a contract (W-31-109-Eng-38) between the U. S. Atomic Energy

The facilities of Argonne National Laboratory are owned by the United States Government. Under the terms of a contract (W-31-109-Eng-38) between the U. S. Atomic Energy

The facilities of Argonne National Laboratory are owned by the United States Government. Under the terms of a contract (W-31-109-Eng-38) between the U. S. Atomic Energy

The facilities of Argonne National Laboratory are owned by the United States Government. Under the terms of a contract (W-31-109-Eng-38) between the U. S. Atomic Energy

The facilities of Argonne National Laboratory are owned by the United States Government. Under the terms of a contract (W-31-109-Eng-38) between the U. S. Atomic Energy

The facilities of Argonne National Laboratory are owned by the United States Government. Under the terms of a contract (W-31-109-Eng-38) between the U. S. Atomic Energy

The facilities of Argonne National Laboratory are owned by the United States Government. Under the terms of a contract (W-31-109-Eng-38) between the U. S. Atomic Energy

ANL-7419
Reactor Technology
(TID-4500)
AEC Research and
Development Report

ARGONNE NATIONAL LABORATORY
9700 South Cass Avenue
Argonne, Illinois 60439

REACTOR DEVELOPMENT PROGRAM PROGRESS REPORT

January 1968

Robert B. Duffield, Laboratory Director
Stephen Lawroski, Associate Laboratory Director

Division	Director
Chemical Engineering	R. C. Vogel
Idaho	M. Novick
Metallurgy	M. V. Nevitt
Reactor Engineering	L. J. Koch
Reactor Physics	R. Avery
Remote Control	D. P. Mingesz (Acting)

Report coordinated by
C. L. Chernick and A. Glassner

Issued February 27, 1968

FOREWORD

The Reactor Development Program Progress Report, issued monthly, is intended to be a means of reporting those items of significant technical progress which have occurred in both the specific reactor projects and the general engineering research and development programs. The report is organized in accordance with budget activities in a way which, it is hoped, gives the clearest, most logical overall view of progress. Since the intent is to report only items of significant progress, not all activities are reported each month. In order to issue this report as soon as possible after the end of the month editorial work must necessarily be limited. Also, since this is an informal progress report, the results and data presented should be understood to be preliminary and subject to change unless otherwise stated.

The issuance of these reports is not intended to constitute publication in any sense of the word. Final results either will be submitted for publication in regular professional journals or will be published in the form of ANL topical reports.

The last six reports issued in this series are:

July 1967	ANL-7357
August 1967	ANL-7371
September 1967	ANL-7382
October 1967	ANL-7391
November 1967	ANL-7399
December 1967	ANL-7403

REACTOR DEVELOPMENT PROGRAM

Highlights of Project Activities for January 1968

EBR-II

No reactor operation was conducted during January because of problems associated with diagnosis and replacement of a damaged control-rod thimble, and checks and measurements on the balance of the control rods to assure that they were in satisfactory condition. Fuel handling was interrupted because of this difficulty and because of a malfunction requiring overhaul of the core-holddown drive mechanism. The accumulated EBR-II operation is 15,541 MWdt.

Production operations were curtailed and surveillance activities were emphasized in the FCF because of a shortage of storage space for refabricated subassemblies. In order to reduce the reactor storage-basket inventory to facilitate the forthcoming exchange of Row-7 and -8 blanket subassemblies with depleted uranium, spent subassemblies were received from the reactor, but no refabricated subassemblies were sent to the reactor.

ZPR-3

With Assembly 51 adjusted to the reference geometry, measurements were made of edge-drawer worths and the temperature coefficient of reactivity. The control rods were calibrated by the inverse-kinetics technique. Measurements of the neutron spectrum by the proton-recoil method were made.

ZPPR

An extensive effort is underway to develop experimental equipment and techniques for the ZPPR program. Bids have been requested for the fission-counter drive mechanism and the drawer conveyor for the loading tube.

Major work by the construction contractor consisted primarily of repair of faulty welds on the seal door bulkheads and on the loading tube. Various cleanup, painting, and leak testing work remains to be done in the mound area, as well as checkout of air-handling systems and replacement of damaged high-efficiency filters.

The reactor-installation contractor has been working in the support wing since December 18. Six thousand matrix tubes were degreased, cleaned, and checked for dimensions.

AARR

The Advisory Committee on Reactor Safeguards has formally advised the Commission that an AARR-type facility can be constructed and operated at ANL without undue hazard to the health and safety of the public. Seismic design criteria have been received from the Commission and will be reviewed; in general, the ANL-originated criteria appear to be conservative.

Initial tests of a revised-design latch system for the outer shroud were satisfactory. Further tests will be performed before the new design is approved.

Initial tests of the beam-tube handling tool were satisfactory. Further tests will include insertion and removal through a simulated coffin.

Assembly of the beam-tube test facility has been completed.

The FLASH computer code for analysis of a loss-of-coolant accident has been modified to plot automatically certain calculated values. Preliminary thermal analysis of the reactor shroud and pedestal, based on assumed values for the film coefficient, indicates high temperatures near the core. The film coefficient must be corrected iteratively before final calculations can be performed.

TABLE OF CONTENTS

	Page
I. LIQUID-METAL FAST BREEDER REACTORS--CIVILIAN	1
A. Fuel Development--LMFBR	1
1. Metallic	1
2. Oxide	2
3. Carbide--Fabrication and Evaluation	2
4. Fuel Cladding and Structure--Jacket Alloys	2
B. Physics Development--LMFBR	6
1. Theoretical Reactor Physics--General Fast Reactor Physics	6
2. Theoretical Reactor Physics--Fast Critical Experiments--Theoretical Support	7
3. Experimental Reactor Physics--Fast Critical Experiments--Experimental Support (Idaho)	7
4. Experimental Reactor Physics--Fast Critical Experiments--Experimental Support (Reactor Physics)	9
5. ZPR-3 Operations and Analysis	10
6. ZPR-6 and -9 Operations and Analysis	14
7. ZPPR Operations and Analysis	17
8. ZPR Fuel and Nonfissile Materials--Procurement	21
9. FTR Critical Experiment Program	25
10. ZPPR Construction	26
C. Component Development--LMFBR	28
1. Sodium Technology Development--Engineering Development	28
2. Reactor Mechanisms Development--Materials Evaluation	30
D. Systems and Plant--LMFBR	35
1. 1000-MWe Plant	35
E. EBR-II	36
1. Research and Development	36
a. Reactor Experimental Support--Reactor Analysis and Testing	36
b. Nuclear Analysis Methods Development	43
c. Reactor System Testing, Surveillance, and Evaluation	48
d. Higher Power Operation	50
e. Fuel Swelling and Driver Surveillance	53

TABLE OF CONTENTS

	Page
f. Mark-II Driver Fuel Element Development	59
g. Equipment--Fuel Related	59
h. Equipment--Reactor and Primary Coolant System	63
i. Secondary Sodium and Power Systems	64
j. New Subassemblies Design and Experimental Support	64
k. Instrumented Subassembly	65
l. Packaged Loop	65
m. Process Chemistry	66
n. Experimental Irradiation and Testing	67
o. FCF Process Analysis and Testing	70
p. FCF Equipment Improvement	71
q. Superheater and EM Pump Study and Test	72
r. Reactor Improvements, Nuclear Instrument Test Facility Study	73
s. Feasibility Study of Fuel Failure Detection	74
t. Hot Fuel Examination Facility (HFEF)--Engineering and Design	75
2. Outside Fuel Procurement	76
3. Operations--Reactor Plant	76
4. Operations--Fuel Cycle Facility	80
Publications	88
II. GENERAL REACTOR TECHNOLOGY	89
A. Applied and Reactor Physics Development--Research and Development	89
1. Theoretical Reactor Physics	89
2. Nuclear Data	95
B. Reactor Fuels and Materials Development	102
1. Fuels and Claddings--Behavior of Reactor Materials	102
2. Fuels and Claddings--Chemistry of Irradiated Materials	109
3. Fuels and Claddings--Thermodynamics of Fuel Materials	109
4. Radiation Damage of Structural Materials--Research and Development	110
5. Techniques of Fabrication and Testing--Basic Fabricability--Research and Development	111

TABLE OF CONTENTS

	Page
C. Engineering Development--Research and Development	113
1. Development of Master-Slave Manipulator Systems	113
2. Instrumentation and Control	115
3. Heat Transfer, Fluid Flow, and Mechanics of Materials	116
4. Liquid-metal Linear Generator	118
5. Engineering Mechanics	118
D. Chemistry and Chemical Separations	119
1. Aqueous and Volatility Processes--Research and Development--Fluoride Volatility Process	119
2. Closed Cycle Processes--Research and Development--Compact Pyrochemical Processes	123
3. General Chemistry and Chemical Engineering--Research and Development	126
Publications	132
III. ADVANCED SYSTEMS RESEARCH AND DEVELOPMENT	133
A. Argonne Advanced Research Reactor--Research and Development	133
1. Instrumentation and Control	133
2. Core Research and Development	134
3. Component Development	139
4. Planning and Administration	140
IV. NUCLEAR SAFETY	142
A. Other Reactor Kinetics--Research and Development	142
1. Fuel Meltdown Studies with TREAT	142
2. Materials Behavior, Equation of State, and Energy Transfer	146
3. Coolant Dynamics	153
B. Operations	157
1. TREAT Operations	157
Publications	158

I. LIQUID-METAL FAST BREEDER REACTORS--CIVILIAN

A. Fuel Development--LMFBR

1. Metallic

a. Fuel Element Performance

(i) U-Pu-Zr Alloy--Irradiation Performance (W. F. Murphy)

Last Reported: ANL-7403, pp. 3-5 (Dec 1967).

Chemical analyses for technetium have been made on annular sections from two additional U-Pu-Zr fuel elements (ND-30 and ND-43) that were irradiated in the EBR-II to burnups of 4.4 and 3.9 a/o, respectively. The samples for analyses were obtained from sections near the midlength of the fuel column. The annular sections (center, middle, and outer) from each element were separated mechanically. The results of the analyses are compared in Table I.A.1 with similar analyses from ND-28.* Data are expressed as 1000 times the ratio of atoms of technetium to the original sum of atoms of uranium and plutonium.

TABLE I.A.1. Technetium Analyses of Annular Zones from Irradiated U-Pu-Zr Fuel

Fuel Element	Atomic Ratios of Zones $[Tc/(U+Pu) \times 10^{-3}]$		
	Center	Middle	Outer
ND-28	2.0	1.1	2.8
ND-30	3.9	0.9	3.5
ND-43	3.1	0.8	3.5

Note: Ratio based on original composition of fuel; accuracy, ± 5%.

The middle zone consistently shows appreciably less technetium than either the center zone or the outer zone. Technetium apparently has migrated from the middle zone to one or both of the other zones.

Fifteen U-15 w/o Pu-10 w/o Zr fuel elements (Group M-3)** were inserted into the EBR-II on November 21, 1967. No additional burnup was acquired in this report period.

*See Progress Report for November 1967, ANL-7399, pp. 1-5.

**See Table II.A.3, Progress Report for December 1967, ANL-7403, p. 4.

2. Oxide

a. Fuel Element Performance

(i) Mixed-oxide Fuel Performance (F. L. Brown and B. J. Koprowski)

Last Reported: ANL-7403, p. 9 (Dec 1967).

Evidence previously acquired* indicated that Capsule HOV-4 probably was responsible for the release of fission-product gas into the primary coolant of EBR-II while undergoing irradiation in experimental Subassembly XO11. No indication of a leak was found in Capsule HOV-10, irradiated in the same subassembly. Both capsules contained vibratorily compacted, mixed-oxide elements in Hastelloy-X cladding.

An axial gamma-activity scan disclosed that the distribution of ruthenium in the two elements differs markedly. Concentrated ruthenium was found only near the bottom of HOV-4, but in several places along the length of HOV-10. Although both elements operated at nearly identical linear heat ratings, about 22.9 kW/ft, neutron radiography indicated probable melting of the fuel in HOV-4. The higher fuel temperatures in HOV-4 probably were the result of the loss of the capsule sodium bond through an as yet unidentified failure in the capsule wall.

3. Carbide--Fabrication and Evaluation

a. Fuel Element Performance (F. L. Brown)

(i) Uranium-Plutonium Carbide

Last Reported: ANL-7403, p. 9 (Dec 1967).

Because the EBR-II has not operated significantly since the last report period, the status of uranium-plutonium carbide fuel elements undergoing irradiation in EBR-II remains unchanged.

4. Fuel Cladding and Structure--Jacket Alloys

a. Irradiation Studies of Fuel Jacket Alloys (R. Carlander)

Last Reported: ANL-7403, pp. 11-13 (Dec 1967).

Void formation due to vacancy clustering has been reported in Types 304 and 316 stainless steel fuel cladding when irradiated in a

*See Progress Report for December 1967, ANL-7403, pp. 35-42.

fast reactor. Volume increases of ~7% at a fluence of 7.8×10^{22} were observed for Type 316 stainless steel due to the formation of these voids.* In order to determine if these volume increases occurred in tensile specimens of irradiated Type 304 stainless steel, V-20 w/o Ti alloy, and Hastelloy-X, the densities were measured. The alloys were irradiated in EBR-II Subassembly XA07 to a nominal fluence of 3×10^{22} at a calculated temperature of 580°C. There was no change in density of the tensile specimens due to irradiation which may be due to the absence of strain during irradiation. The results tend to agree with those reported for Type 316 stainless steel in which it was concluded that stress influenced enlargement of the voids.

b. Sodium Corrosion of Fuel-jacket Alloys (W. E. Ruther, C. F. Cheng, S. Greenberg, D. J. Dorman, and J. C. Tezak)

(i) Development of Refractory-metal Alloys for Service in Oxygen-contaminated Sodium

Last Reported: ANL-7399, p. 14 (Nov 1967).**

Specimens of vanadium alloys have now been exposed to flowing sodium (6.1 m/s) at 600°C for 71 days. Impurity level is controlled with a cold trap at 110°C. V-20 w/o Ti changed most in weight, about +0.3 mg/cm^2, and V-10 w/o Cr changed least, about 0.01 mg/cm^2. The V-20 w/o Ti and V-10 w/o Cr samples appear metallic and brilliant. The V-15 w/o Cr-5 w/o Ti and V-15 w/o Ti-7.5 w/o Cr alloys lost most of the metallic appearing outer film, and now appear dull and dark.

The above experiment at 600°C has been temporarily interrupted to equilibrate vanadium wires with the sodium in the equipment. Simultaneously, other vanadium wires are being equilibrated in a refreshed static system. Using techniques developed by D. L. Smith of our group, the equilibrated wires from the two types of equipment will be compared for O, N, and C contents, hopefully giving a clue to the reason for the more aggressive attack of vanadium alloys in the static system.

Samples of V-20 w/o Ti, V-15 w/o Ti-7.5 w/o Cr, V-15 w/o Cr-5 w/o Ti, V, and V-10 w/o Cr are being exposed in oxygen-refreshed static systems at two cold-trap temperatures (for impurity-level control). Small weight gains (max 1.5 mg/cm^2) were recorded for

*Cawthorne, C., and Fulton, E. J., Voids in Irradiated Stainless Steel, Nature 216 (Nov. 11, 1967).

**Errata in ANL-7399, p. 14. First sentence of last paragraph should read, "Carbon is believed to be a significant sodium impurity when the oxygen level of the sodium has been reduced below 5 ppm by wt, the concentration required to form a vanadium oxide phase." Third sentence of last paragraph should read, "The refractory-metal stabilizers in the stainless steel appear to inhibit the movement of carbon from the test-loop walls to the vanadium-alloy specimens through the sodium."

the first three alloys after an exposure of 7 weeks in the system with the lower impurity level (cold trap at 110°C). The weight loss for the V-10 w/o Cr alloy was about 0.03 mg/cm^2, and for vanadium, about 0.8 mg/cm^2.

All specimens have suffered extensive weight losses of up to 72 mg/cm^2 in 7 weeks of exposure to 700°C sodium cold trapped at 175°C.

(ii) Corrosion of Nickel Alloys in Flowing Sodium

Last Reported: ANL-7382, pp. 83-86 (Sept 1967).

Samples of Type 304 stainless steel (included in all tests as a control), Inconel 600, Incoloy 800, and Hastelloy-X were exposed in the core of EBR-II for a time equivalent to 4 months at full power (7 months total) at temperatures of 510 and 530°C and a velocity of 3.8 m/sec. Fluence was 7.2×10^{20} n/cm^2 ($4.7 \times 10^{19} < 1.35$ MeV). There were no weight or dimensional changes for any of the samples.* Detailed metallographic examination indicated no surface intergranular corrosion. Although the temperatures of exposure (510 and 530°C) were relatively low, the ratio of surface to volume (as pertains to the nickel-alloy samples) was favorable for accelerated thermal-gradient mass transfer. However, microprobe analysis of the specimen surface showed no change in composition** for Type 304 stainless steel and Hastelloy-X. The inherent limitations of the method prevents conclusions relative to compositional changes within 1 micron of the surface. Inconel 600 exhibited a decrease in both nickel and chromium concentrations and an increase in iron concentration to a depth of several microns. In the case of Incoloy 800, there was some decrease in both chromium and iron concentrations, but no change was detected in nickel concentration. These are comparisons of concentration in surface and bulk for each element. The fact that selective dissolution did take place for Inconel 600 and Incoloy 800 in in-reactor sodium at relatively low temperature enhances the significance of no change of surface composition for Type 304 stainless steel and Hastelloy-X. Iron-rich surfaces are normally observed for Type 304 stainless and high-nickel alloys exposed to sodium at 650°C in ex-reactor stainless steel loops.†

(iii) Corrosion of Brazed Material in Sodium. A sodium-filled calandria was to be used for conducting heated zone experiments by the

*See Progress Report for June 1967, ANL-7349, pp. 81-82.

**Typical compositions of pertinent high-nickel alloys are, in w/o: Hastelloy-X, Ni-18 Fe-9 Mo-1.5 Cr-1 Co-1 Mn-1 Si-0.6 W-0.01 C; Inconel 600, Ni-17 Cr-8 Fe-2.75 Nb-0.1 max C; Incoloy 800, Fe-32 Ni-20.5 Cr-0.75 Mn-0.35 Si-0.30 Cu-0.04 C.

†Thorley, A. W., and Tyzack, C., The Corrosion Behavior of Iron and Nickel-based Alloys in High Sodium, TRG Report 1356(C) (1966); Hopenfield, J., and Darley, D., Dynamic Mass Transfer of Stainless Steel in Sodium Under High Flux Conditions, NAA-SR-12447 (July 1967); Brush, E. G., Sodium Mass Transfer: XVI--The Selective Corrosion Component of Steel Exposed to Flowing Sodium, GEAP-4832 (June 1965).

Reactor Physics Division in ZPR-9. However, sodium leaked at the brazed joints of a prototype calandria after 39 thermal cycles between room temperature and 600°C at a heating or cooling rate of 2 hr per half-cycle. This calandria was fabricated from Type 304 stainless steel in the shape of a rectangular can containing five rows of five, 12-in.-length tubing (0.350-in. OD x 0.010-in. wall), equally spaced in a 2-in. square tube sheet (0.220-in. thick) at each end. All tubings were brazed to the tube sheets with Nicrobraze 50 (77% Ni, 10% P, 13% Cr) and the tube sheets were welded to the can by the tungsten-inert-gas technique. The calandria was purged with argon to remove the entrapped air and filled with sodium under vacuum to an equivalent inside volume of 100% at 600°C and 80% at room temperature. After insulation, the calandria was heated with a "Calrod" inserted in the center tube. The failure occurred at the upper end, where the tubes were alternately exposed to sodium vapor and liquid sodium. Microexamination of the upper end fillet braze revealed selective leaching of phosphorus from the braze structure. The corresponding lower-end fillet braze, exposed only to the less severe condition of liquid sodium, was not attacked during this short exposure of 156 hr. Similar selective leaching of phosphorus from Nicrobraze 50 fillets has been observed by Thorley and Tyzack* in a 650°C flowing sodium loop, and by Hoffman et al.** in a seesaw test in static sodium with a hot-zone temperature of 815°C and a cold-zone temperature of 595°C.

* Thorley, A. W., and Tyzack, C., The Corrosion Behavior of Iron and Nickel-based Alloys in High Sodium, TRG Report 1356(C) (1966).

** Hoffman, E. E., et al., An Evaluation of Corrosion and Oxidation Resistance of High Temperature Brazing Alloys, ORNL-1934 (Nov 1956).

B. Physics Development--LMFBR

1. Theoretical Reactor Physics--General Fast Reactor Physics (H. H. Hummel)

Last Reported: ANL-7403, pp. 14-16 (Dec 1967).

a. Dynamics Studies

(i) Calculations of Temperature-dependent Cross Sections in the QX1 Program. Doppler reactivity feedback is treated by interpolation of capture and fission cross sections between computed temperatures. The user first prepares a library tape in XLIBIT* format. Four sets of data are entered for each temperature-dependent isotope, representing capture and fission cross sections at four different temperatures. At problem run time the QX1 program forms temperature-dependent mixture cross sections at these four temperatures, using these values and the input atom densities for each isotope in the mixture. The interpolation coefficients $a_{x,g}$, $b_{x,g}$, and $c_{x,g}$ for each energy group of each mixture are determined by substitution of the known values of $\Sigma_{x,g}$ at temperatures T_0, T_1, T_2, and T_4 in the expression

$$\Sigma_{x,g}(T) = \Sigma_{x,g}(T_0) + \int_{T_0}^{T} \left[\frac{a_{x,g}}{\sqrt{T}} + \frac{b_{x,g}}{T} + \frac{c_{x,g}}{T^2} \right] dT, \qquad (1)$$

where the subscript x refers to capture or fission and g to the energy group.

During problem execution, the macroscopic composition cross sections in each spatial region are computed from current atom densities and temperatures of each mixture in the composition by means of Eq. (1) with the precalculated coefficients $a_{x,g}$, $b_{x,g}$, and $c_{x,g}$ for each mixture. The increments of capture and fission cross sections from reference to current temperature are added to the transport cross section of each group. The current system reactivity is then computed from the composition cross sections and fluxes, and the initial adjoints.

There is no provision for including the potential scattering dependence of cross sections at the present time.

*Sparck, S., XLIBIT--ANL Cross-section Library Code, ANL-7112 (Feb 1966).

2. Theoretical Reactor Physics--Fast Critical Experiments--Theoretical Support (F. W. Thalgott, R. B. Nicholson and R. G. Palmer)

Last Reported: ANL-7399, p. 16 (Nov 1967).

The RABBLE code has been extensively modified for the purpose of studying thin-foil measurement in ZPR assemblies. More exact integral transport theory has been used, thus eliminating the boundary-current approximations. The flat-source approximations of RABBLE have been replaced by a linear source variation. The new version, called RABID, has been developed on the CDC-1604 prior to conversion to the IBM-360/75. Preliminary results for ZPR plate sizes indicate a gain in accuracy of around 1%, with about the same computation time as RABBLE. More significant improvement is expected for thin-foil studies.

Further one- and two-dimensional studies are in progress to determine the shape-factor curves for cores in the size range of interest for ZPPR.

A code, called WINDOW, has been written for the CDC-1604 for the purpose of comparing the spectrum obtained from MC^2 calculations with that measured by the proton-recoil spectrometers. The code smoothes the fine-group output through a Gaussian window corresponding to the spectrometer resolution.

3. Experimental Reactor Physics--Fast Critical Experiments--Experimental Support (W. G. Davey)

Last Reported: ANL-7403, pp. 17-18 (Dec 1967).

a. Neutron Spectrometry. Considerable emphasis has been placed on preparation of the proton-recoil spectrometer for measurement of neutron spectra in the FTR critical presently in ZPR-3. The live-time clock system was completed and operationally tested. It worked well under test conditions and is a valuable addition to the system. The measurements in ZPR-3 are underway and represent the initial operational use of the general-purpose, computer-based, proton-recoil spectrometer system. Preliminary tests of the system in AFSR were promising.

b. Heterogeneity Studies. One of the major remaining concerns about the usefulness of the counting methods being developed is that of sensitivity in large ZPPR cores. A long, low-level irradiation was made in AFSR to simulate possible ZPPR conditions. The irradiation gave a total of about 10^9 fissions in a ^{235}U sample. The analysis so far indicates that count rates will be at least adequate to obtain the desired statistical precision. Qualitatively, the analysis also shows that fission-product isotopes having lifetimes between about 30 min and 10 or 15 hr will be the most useful.

The irradiation was also used to estimate count rates for systems-design purposes. The rates obtained were low enough to allow multiplexing of several counter systems into one fast analog-to-digital converter. The requirement for handling large numbers of foils, however, dictates that there will be a large volume of multichannel data. Systems using fast multichannel analyzers as buffer storage are being compared to systems using A/DC's with direct computer access.

Work is continuing on the analysis of spectra from irradiated ^{235}U foils with the aid of the 1620 and 1604 computers. Though originally requiring the use of both computers, the program is being compacted to run completely on the 1620.

An anti-Compton system will be necessary to achieve the desired precision in the determinations of fission-product activity. Some simplified setups are being developed, using 2- x 2-in. sodium iodide detectors.

Irradiation of ^{238}U has started. In addition to fission-product gamma spectra, spectra from ^{238}U capture products (^{239}U and ^{239}Np) will be investigated to determine if other techniques, such as coincidence counting, will be necessary to establish the amount of ^{238}U capture.

New equipment has been ordered which should improve the detector-system resolution, especially at high counting rates. Irradiations of ^{239}Pu and ^{232}Th are also planned.

c. Computer Applications. The request for proposal for the ZPPR computer is being reviewed by the Applied Mathematics Division for technical content prior to Laboratory approval for submission to industrial suppliers. A justification and design study has also been completed and is being reviewed within the Idaho Division.

Many experimental devices have been designed to input directly into the ZPPR computer. In order to operate these devices prior to the time when the computer will be on line, a special data-collection system is being fabricated. This system will allow rapid collection of data and storage of digitized information on magnetic tape. The design requirements are such that the equipment will be easily converted to form part of the on-line computer interface equipment at a later date. This equipment is described under ZPPR Operations and Analysis.

4. Experimental Reactor Physics--Fast Critical Experiments--Experimental Support (R. Gold)

Last Reported: ANL-7371, p. 62 (Aug 1967).

a. Neutron Spectrometry

(i) Response Corrections for 4π Hydrogen-recoil Counters. The proton-recoil technique has been under development at Argonne for use in conjunction with zero-power critical assemblies fueled with ^{235}U and plutonium.

The large spontaneous fission source, especially in plutonium-fueled assemblies, requires the use of small counting tubes for optimum results, and these tubes generally show a departure from ideal in their response. We have, consequently, found it necessary to treat in detail the various effects producing nonideal behavior and have developed procedures to correct for these effects.

One source of nonideal counter response is the well-known wall-and-end effect in which proton-recoil tracks are truncated by passage from (or into) the effective counting volume. One can effectively avoid this problem by restricting measurements to low energy, but a restriction of this kind would be unfortunate since it would eliminate a large part of the region of interest in fast reactors from the measured result.

Wall-and-end effects do not constitute the only reason for departure of the response of detectors from ideal. The finite effective length of detectors, desensitized near ends by an increased anode diameter, produces an effect similar to wall-and-end effects but independent of proton energy.

Using directly measured response functions for the detector together with a numerical unfolding procedure, we have been able to correct observed proton-recoil distributions up to about 3 MeV. Errors introduced into spectrum measurements because of the unfolding are small, partly as a consequence of the fact that neutron spectra as derived using the raw input data do not differ greatly from spectra derived from the unfolded data. In general, the response correction is a perturbation on the spectral measurement.

An example of the extent to which these nonideal detector response effects alter a spectrum measurement is shown in Fig. I.B.1, which gives a spectrum as analyzed from the raw proton-recoil data directly and as analyzed with the various response corrections (including wall-and-end effect) made. The data are from ZPR-3 Assembly 48; statistical fluctuations and resonance peaks have been smoothed over to better show response-function effects that vary continuously with energy.

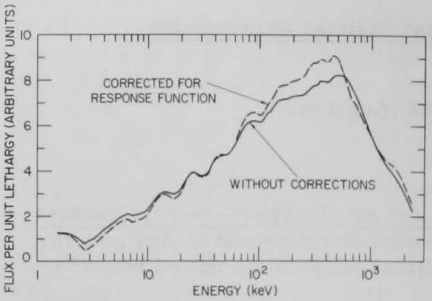

Fig. I.B.1. The Effect of Nonideal Counter Response upon Measurement of a Neutron Spectrum

5. ZPR-3 Operations and Analysis (W. G. Davey and R. L. McVean)

Last Reported: ANL-7403, pp. 19-20 (Dec 1967).

a. Doppler Coefficient. The modified Doppler equipment has been completely checked out and is ready for use except for the stand for supporting the drive mechanism. This stand is being fabricated.

b. Mockup Studies. Assembly 51, the first assembly in the Fast Test Reactor (FTR) critical program, was designed with two drawers in adjacent horizontal matrix positions comprising a "cell." The composition of this "cell" approximates a nominal composition proposed for the FTR.

As stated in ANL-7403, after obtaining initial criticality and measurement of safety-rod worths, the worths of all eight safety rods were increased by transfer of plutonium from adjacent matrix positions above and below the safety rods. The worth of a safety-rod drawer with both loadings is shown in Fig. I.B.2.

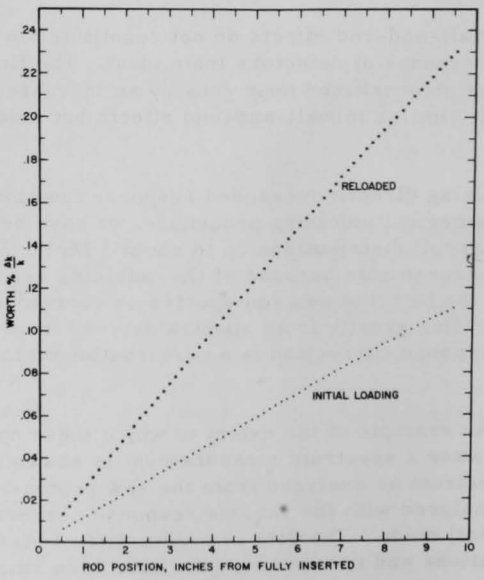

Fig. I.B.2. Curve for Safety-rod Worth in Assembly 51

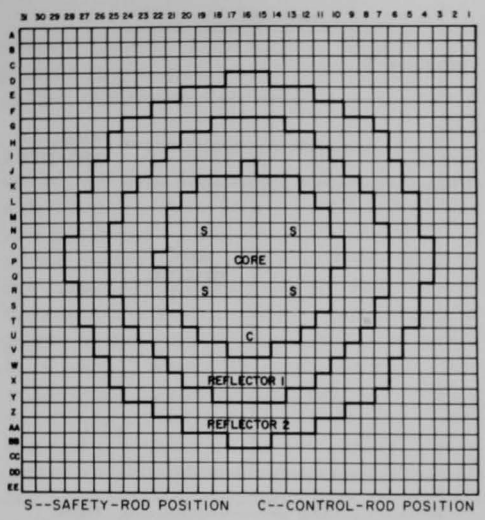

Fig. I.B.3. Reference Core for Assembly 51

The reference geometry for the assembly is shown in Fig. I.B.3. With this geometry, measurements have been made of the temperature coefficient of reactivity and the edge-drawer worths and control rods have been calibrated.

Because of the variety of drawer lengths and variation of material densities in the sodium cans, there are three zones in Radial Reflector I. These zones and the as-built compositions of the reference geometry are given in Tables I.B.1-3. Figure I.D.4 is an axial view of the reactor, in which the cylindrical zones have a volume equal to the volume of the zones in the reference geometry.

The control rod used in Assembly 51 has been calibrated and the effective source has been measured. To check the experimental

TABLE I.B.1. Core Compositions for Assembly 51

atom density (x 10^{-24} cm^3)

Drawer Type	$^{239,241}Pu$	$^{240,242}Pu$	^{235}U	^{238}U	Mo	Na	C	O	Al	Fe	Cr	Ni	Mn	Si
Core Type A[a]	0.001972	0.000170	0.000012	0.005703	0.000224	0.010262	0.003113	0.011479	0.000110	0.01528	0.003803	0.001664	0.000159	0.000186
Core Type A*[a]	0.001498	0.000175	0.000018	0.008306	0.000431	0.008244	0.003113	0.014093	-	0.01600	0.003530	0.001544	0.000147	0.000173
Cell Average	0.001736	0.000172	0.000015	0.007005	0.000328	0.009253	0.003113	0.01279	0.000055	0.01564	0.003666	0.001604	0.000153	0.000180
Control Rod	0.001990	0.000162	0.000015	0.007144	0.000197	0.010123	0.002746	0.008241	0.000124	0.016047	0.003992	0.001747	0.000167	0.000196
Safety Rod	0.002990	0.000329	0.000032	0.014635	0.000796	0.004039	0.000916	0.005362	0.000026	0.017198	0.003829	0.001675	0.000160	0.000188
Drawer above Safety Rod	0.000902	0.000119	0.000012	0.005705	0.000224	0.010340	0.004150	0.017212	-	0.016122	0.003561	0.001558	0.000149	0.000175
Drawer below Safety Rod	0.000597	0.000056	0.000013	0.005829	0.000208	0.010340	0.004150	0.017212	-	0.015803	0.003482	0.001524	0.000145	0.000171

[a] A--Drawers in even-numbered matrix columns; A*--Drawers in odd-numbered matrix columns.

TABLE I.B.2. Reflector Compositions

atom density (x 10^{-24} cm^3)

Location	Na	Ni	Fe	Cr	Mn	Si	C
Axial Reflector	0.010321	0.028926	0.010426	0.002583	0.000182	0.000126	
Radial Reflector I							
Zone A	0.004156	0.056349	0.007637	0.001878	0.000228	0.000092	
Zone B	0.004115	0.056338	0.007539	0.001854	0.000227	0.000091	
Zone C	0.004156	0.056335	0.007511	0.001847	0.000226	0.000091	
Radial Reflector II	-	0.000494	0.074860	0.001153	0.000560	0.000055	0.000561

TABLE I.B.3 Spring Gap Composition

atom density (x 10^{-24} cm^3)

	Fe	Cr	Ni
Spring Gap[a]	0.01654	0.00444	0.00218

[a] The spring gap is 0.66 cm long and consists of the back of the front drawer, plus the spring, plus the front of the back drawer.

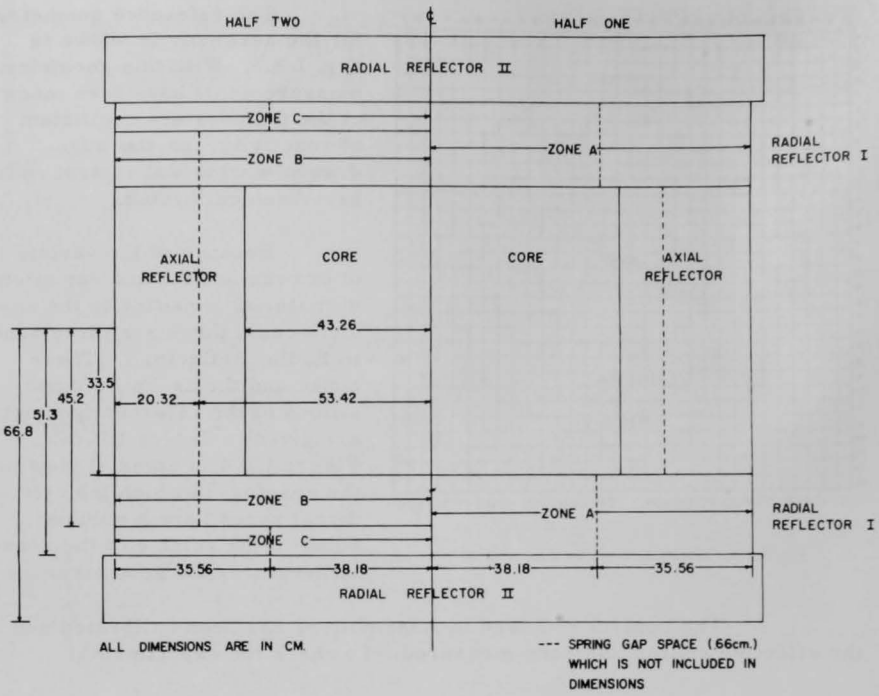

Fig. I.B.4. Equivalent Cylindrical Loading for Reference Core of Assembly 51

equipment, three different equipment arrangements were used to measure the rod worth by the inverse-kinetics technique. Methods utilizing the dc electrometer and the voltage-to-frequency converter as a current-to-frequency converter were in agreement, and indicate an accuracy better than 1%, whereas use of the vibrating-reed electrometer was clearly inferior. Uncertainties in the delayed-neutron parameters are the major source of uncertainty in the final calibration.

In the inverse-kinetics technique a constant reactor power level is established with the rod to be calibrated fully inserted. The rod is then withdrawn at constant speed while the flux history is recorded with a multichannel time analyzer. The control rod is fuel-bearing, so the reactor power decreases during the measurement. Knowledge of the effective neutron source permits calculation of reactivity as a function of time by means of the kinetics equations. Rod speed and starting time can then be used to obtain the rod-calibration curve.

The effective neutron source must be obtained from a separate measurement. This may be inferred from the unstable period produced in a rod bump experiment. This source is used to calculate an initial rod calibration.

An additional experiment is necessary to refine both the source value and the rod calibration: rod position is measured at two different subcritical power levels. The initial rod calibration is used to convert the rod positions to reactivities, and these are plotted against the reciprocal of the power level. This plot can be extrapolated to infinite power, giving the just-critical rod position and reactivity. The reactivity difference between this just-critical position and the rod position at a finite subcritical power is the amount the reactor is subcritical at that power level. Then $S_1 = -nk_{ex}$, where S_1 is the source strength and n is the power level corresponding to the subcritical k_{ex}. The initial rod-calibration curve is recalculated using this new source, giving corrected reactivity values for the rod positions at the two power levels, and a corrected source. This iterative procedure converges very quickly. The source value is valid for the particular instrument used to measure power level, and a different value is required for each instrument depending upon its sensitivity.

The final rod calibration is obtained by fitting a fifth-order polynomial to the data. The polynomial fit is shown in Fig. I.B.5. The data points did not depart noticeably from the line.

To achieve good accuracy with the inverse-kinetics method, the flux measuring system must be stable and linear. To achieve the desired stability and linearity various methods of driving the voltage-to-frequency converter were investigated. It may be driven directly from the detector using the voltage-to-frequency converter as a current-to-frequency converter in the 10^{-6}-Amp range, or with either a dc electrometer or a vibrating-reed electrometer providing the intermediate current-to-voltage conversion. The results of the three equipment configurations are shown in Fig. I.B.6. After rod motion has stopped, reactor power continues

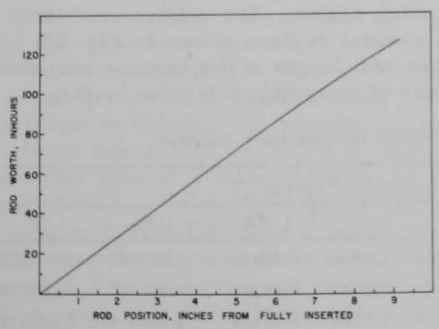

Fig. I.B.5. Calibration of Control Rod for Assembly 51

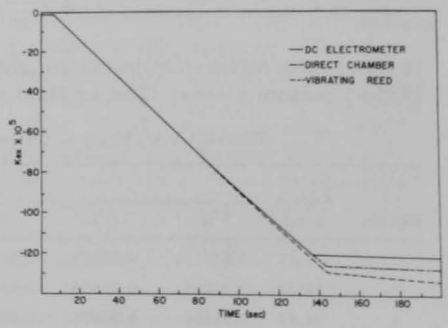

Fig. I.B.6. Reactivity vs. Time for Three Equipment Configurations

to decrease, but the calculated reactivity should remain constant. The continual decrease of the results obtained with the vibrating-reed electrometer indicates excessive nonlinearity in that instrument. The dc electrometer and the "chamber direct" method gave different results because rod motion differed: 0.0 to 9.0 in. for the dc electrometer and 0.0 to 9.5 in. for the other two methods. The dc electrometer result agrees well with "chamber direct" at the 9.0-in. position. Data from the "chamber direct" method were used to obtain the reported rod calibration. The dc electrometer could be used when greater sensitivity is required.

The results of the control rod calibration are now being used to interpret the edge worth measurements and the temperature coefficient of reactivity.

Proton-recoil spectrum measurements are now underway on Assembly 51. Measurements are planned at four locations: core center, midway between core center and core edge, core edge, and in the nickel-sodium radial reflector.

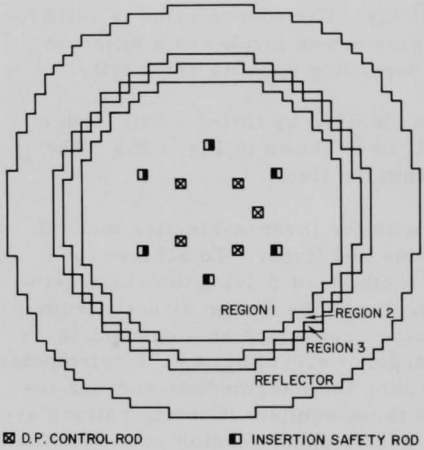

Fig. I.B.7. Regions in Assembly 6 of ZPR-6

6. ZPR-6 and -9 Operations and Analysis

a. Integral Studies of Large Systems (W. Y. Kato)

Last Reported: ANL-7399, pp. 30-31 (Nov 1967).

(i) ZPR-6. Assembly 6 of ZPR-6 went critical on December 26, 1967. Figure I.B.7 shows a cross-sectional view of one half of the assembly and Table I.B.4 gives the concentrations of the materials in each region. The existence of the various regions shown in Fig. I.B.7 is due to the difference in the weight per unit length of the various enriched (93%) uranium plates. The critical mass of Assembly 6 for the loading

TABLE I.B.4. Material Concentrations in Assembly 6 of ZPR-6

Region	Outer Radius (cm)	Atoms (x 10^{-24}) per cc						
		^{235}U	^{238}U	Na	O	Fe	Ni	Cr
1	77.17	0.001150	0.005796	0.009142	0.01465	0.01410	0.001365	0.002788
2	85.53	0.00107	0.005790	0.007790	0.01465	0.01572	0.001582	0.003254
3	90.87	0.00156	0.005780	0.008310	0.01465	0.01524	0.001518	0.003115
Blanket	120.63	0.0000827	0.04008	-	-	0.0042282	0.0005665	0.001215

shown in Fig. I.B.7 is 1817 kg of ^{235}U. This value of the critical mass is corrected for excess reactivity only. Measurements of other parameters are underway.

(ii) ZPR-9. A pneumatic sample hanger was installed in ZPR-9. Samples are oscillated into and out of the reactor, and the reactivity change is measured by an accurately calibrated autorod. The sample changer may be remotely positioned to measure worth values at any point along the radius of Assembly 19. The accuracy of the measurements is about ±0.002 Ih, which is about one percent for most of the samples.

The following measurements, which are part of the generalized zone studies and experimental program, have been made on ZPR-9 using the pneumatic sample changer:

a. central worths for Na, ^{235}U, ^{238}U, boron, Ta, Al, stainless steel, and C;

b. radial worth traverses for Na, ^{235}U, ^{238}U, boron, Al, stainless steel, and C;

c. a detailed calibration of the autorod;

d. measurements to check the effect of neutron streaming in the sample changer tube and neutron-spectrum distortion caused by the sample changer tube.

b. Doppler Effect (C. E. Till)

Last Reported: ANL-7391, p. 26 (Oct 1967).

(i) Doppler Measurements in ZPR-9 Assembly 18. The sensitivity of the measured Dopper reactivity effect to the details of the test-sample environment has been of continuing concern in the series of small-sample Doppler measurements in ZPR-6 and -9. Figure I.B.8 summarizes the results of an extensive series of Doppler measurements performed in ZPR-9 Assembly 18 to explore the effects of environment. The test sample in all of the tests was a 1-in.-dia x 12-in. natural UO_2 sample. The sample can, oscillator drawer, and matrix tube which surround the sample constitute the equivalent of about 1/4 in. of stainless steel which is always interposed between the sample and the core. In the measurements, this normal annular filter of 1/4 in. was augmented by interposing additional annular filters of stainless steel or depleted uranium between the sample and the core. As an example of typical results, the measurements of the Doppler reactivity effect between room temperature and 1100°K as a function of additional filter thickness are shown in Fig. I.B.8, where the results are normalized to the configuration without any additional filter (i.e., with only the built-in 1/4-in. stainless steel filter).

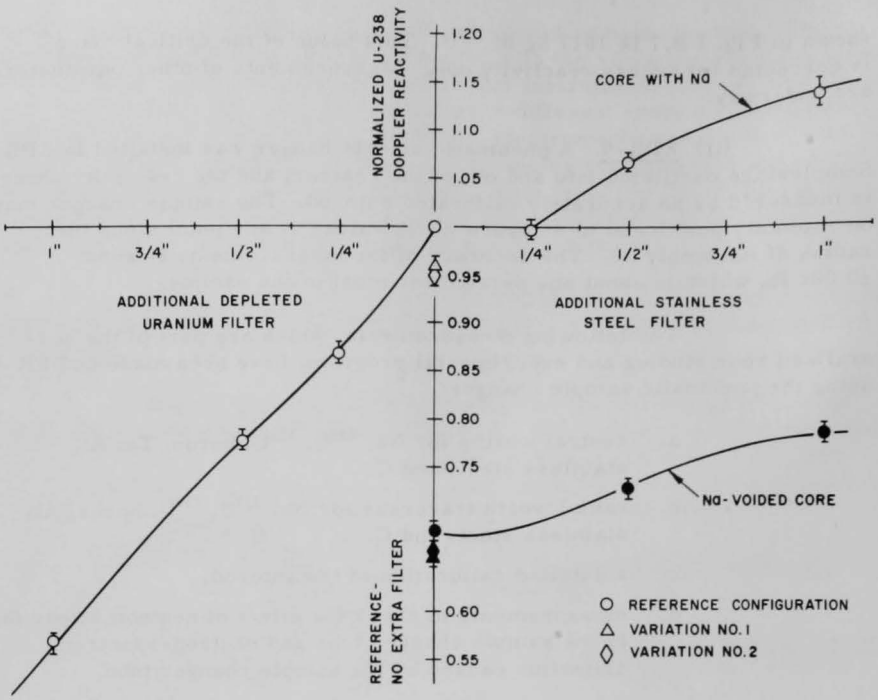

Fig. I.B.8. ^{238}U Doppler Reactivity Effect as a Function of Sample Environment, Normalized to Reference Environment, for ZPR-9 Assembly 18

The data points shown in the figure as Variations Nos. 1 and 2 refer to local variations of plate orientation in the case where only the basic 1/4-in. filter is present. Variation No. 2 is the local plate orientation which consists of the unchanged vertical pattern characteristic of the ZPR assemblies. There is a measureable effect, amounting to 4-5%, due to local plate changes in some configurations.

The results shown in the figure have not been fully analyzed. However, the results are in conformity with preliminary analysis. There are two competing effects in operation: gross flux levels, and therefore the Doppler effect, are affected by the filter materials; stainless steel increases the gross low-energy flux at the sample position, whereas depleted uranium decreases it. The resonance interaction effects between cold resonances in the sample environment and hot resonances in the sample have the net effect of enhancing the Doppler effect. Thus, interposing scattering material and decreasing the interaction reduce the Doppler effect. The measurements confirm that the built-in 1/4-in. filter is in the range of filter thicknesses over which the competing effects nearly balance so that the results are quite insensitive to filter thickness.

c. Heterogeneity Effects (C. E. Till)

Last Reported: ANL-7391, pp. 27-29 (Oct 1967).

Refined analysis of the heterogeneity effect on measurements in Assembly 5 of ZPR-6 is in progress. These measurements have been reported in previous Progress Reports: ANL-7329, pp. 25-33 (April 1967); ANL-7342, pp. 55-59 (May 1967); ANL-7382, p. 58 (Sept 1967); and ANL-7391, p. 27 (Oct 1967).

Very carefully prepared samples for heterogeneity-effect measurements in Assembly 6 of ZPR-6, a uranium oxide system with an enrichment of 16.43% by weight, are being fabricated. These samples will have the same composition but different internal geometry. One type of geometry will be the normal plate-type heterogeneous samples. A second type will be homogeneous samples, and a third type will be rodded samples. The relative reactivity worths of these samples will be measured in the normal plate surrounding and in a surrounding that has the same geometry as the samples. Considerable information on the heterogeneity effects in this rather soft-spectrum system is expected from these measurements.

7. ZPPR Operations and Analysis (W. G. Davey and P. I. Amundson)

Last Reported: ANL-7391, pp. 30-31 (Oct 1967).

a. Basic Studies of Large Plutonium Systems

(i) Program. ZPPR will be utilized to its fullest capacity in the study of large systems. Studies will be aimed particularly at establishing the pertinent physics criteria involved in the design of very large systems (1000 MWe) and their proper relationship to the design of a demonstration reactor of possibly 350-400 MWe. Such parameters as critical size, neutron-energy spectrum, fission ratios, and reactivity worths of various materials will be measured to help establish cross sections which can be used confidently in calculations pertaining to reactors of large size.

Preliminary examination of the detailed design of the first core to be built in ZPPR has been initiated.

(ii) Experimental Equipment. A considerable effort is being devoted to the development of experimental equipment for the ZPPR program.

The major reactor-associated experimental devices that will be initially available on ZPPR include: a radial traverse drive for fission counters with a 15-unit fission counter changer, a radial traverse

drive for reactivity perturbation samples with a 50-unit perturbation sample changer, an axial traverse drive with a 10-unit sample changer (for samples up to 2 x 2 x 6 in.), a sample transfer system for removing samples (up to 2 x 2 x 6 in.) from the reactor cell without shutting down the reactor or violating the cell containment, a radial Doppler-sample traverse drive and Doppler-sample "rod," low-worth and high-worth autorods for precision reactivity measurements, a temperature-measuring system with up to 90 thermocouple inputs, and a 28-channel data-acquisition system to be used for data recording prior to procurement of the ZPPR computer. Additional equipment of a type common to all experimental devices is the 12-unit absolute digital-position readout system. The system provides for rapid position readout with an accuracy of ±0.001 in., for recording all movable experimental devices in the reactor.

Some of the above items are out for construction bid or are being purchased; these include the radial fission-counter traverse drive and fission-counter chamber, the radial traverse drive for perturbation samples, the digital-position readout system, the autorod control system, and the purchase items for the Doppler system. Other items are currently being designed or are in detail drafting; these include the Doppler sample drive system, the perturbation-sample changer, the axial traverse drive and sample changer, the sample-transfer system, and the autorod drives. The data-acquisition system is currently being specified, as are the radial fission-counter designs and reactivity perturbation samples.

b. Doppler Coefficients. Strong efforts are being made to ensure that ZPPR utilizes the best available techniques for Doppler measurements. A vigorous program of equipment selection and, where necessary, development has been undertaken.

The ZPPR Doppler program will start with the "Hot Sample-Cold Reactor" type of reactivity Doppler experiment that has been developed and utilized at Argonne with such a high degree of success. Special efforts have been directed toward solving the problems of performing such measurements in a facility as large and as complex as the ZPPR. Specifically, the experiment will be performed through a radial rather than axial penetration. This eliminates interference with control and safety rods, and provides a more optimum geometry for the long, cylindrical Doppler samples in the large and highly "pancaked" cores which will be built. The Doppler samples will consist of oxides of various fissile and fertile compositions, will be about 1 in. in diameter by 12 in. long, and will be about 1 kg in mass. Previous measurements have shown that as the core volume increases, the spectrum softens so that the total reactivity signal from heating the sample will be adequate for precise reactivity measurements in even the very large cores. The Doppler samples will be interchangeable with those used in ZPR-6 and -9 to allow for intercalibration and cross comparison of the samples in different reactors and spectra.

The design of the entire Doppler system has been laid out and checked for compatibility with the ZPPR reactor and the design criteria. The Doppler "rod" (that part of the system that contains the Doppler "sample" and actually penetrates the reactor) is entering the final design stages and will be ready for construction soon. The mechanical drive and oscillator will be ready for final detailing as soon as three different driving systems are analyzed in relation to the rigid design criteria for ZPPR. Items which can be specified now have been sent out for bid or purchase. As soon as the drive system is specified, the remainder of the commercially available items will be purchased and construction will begin.

c. Sodium Coefficients. A vigorous program of technique evaluation, equipment procurement, and, where necessary, development is being initiated to ensure that sodium reactivities can be measured accurately and efficiently in ZPPR.

The importance of the sodium-void coefficient dictates that the experimental program include not only an investigation of the effects of gross changes of sodium density throughout the system being studied, but also space-dependent studies under both in-cell (heterogeneous) and cell-average (pseudohomogeneous) conditions.

These investigations will utilize a multipurpose remote sample-changing mechanism for the in-cell measurements. This will provide measurements in an infinite plane geometry which can be well described by analytical techniques. Since the geometry can be described accurately in computations, any ambiguities due to core heterogeneity are effectively removed.

The remote sample changer that will be utilized for these measurements is presently being designed. This equipment will also serve other functions in the ZPPR program (see Sect. I.B.7.e).

d. Higher Isotope Fuel Studies. The objectives of these studies will be to investigate the neutronics features of large, fast breeder reactors which depend on the isotopic composition of the fuel. The necessity for these studies derives from the large variation in composition of plutonium that can occur in the lifetime of the reactor, particularly the variation in ^{240}Pu content. The limited availability and high cost of fuels containing large fractions of ^{240}Pu (and to a lesser degree of importance ^{241}Pu and ^{242}Pu) means that these studies are performed with limited quantities of fuel in zoned configurations.

Initial efforts have centered on intercompatible fuel forms and element design. These efforts are being coordinated between members of

the Idaho and the Reactor Physics Divisions. Fuel requirements will be specified by the Laboratory as a result of the coordinated programmatic requirements between the divisions.

e. Reactor Technique Development. Although the basic techniques of most fast critical experiments are well established, the precise application of these techniques depends on the mechanical aspects of the assembly machine and on the types and sizes of assembly under investigation. In addition, the large size of the ZPPR cores results in such soft neutron spectra that problems of heterogeneity of core materials are more severe than in smaller assemblies.

The initial study of adaptation of experimental techniques to ZPPR falls into four broad categories:

(1) Precise measurements of reactivity effects under experimental conditions that can be accurately described by computational techniques and thus analyzed. Initial efforts have centered on a theoretical study of the ZPPR autorod design. An analysis of the stability of the autorod control system proposed for ZPPR is now in progress. This system utilizes error plus error derivative control ($E + dE/dt$). No unstable oscillations are indicated, although the possibility of a stable oscillation exists for certain values of control parameters. This would confirm an oscillation observed in a test of the ($E + dE/dt$) controller on ZPR-3. Other work (by Bennett and Long) has been expanded to consider a reactor with a source, and also the effects of the time constants of a detector and an autorod drive; $E + dE/dt$ control has also been included. Using Bennett's assumption that the rod-noise spectrum is white, $W(\omega) = W_0$, estimates of the percentage of increase in the error due to the source have been obtained. Future work involves eliminating the white spectrum assumption.

(2) As a special case of (1), the improvement of measurements of Doppler effects in very large cores, where the experimental signal may be small, is being studied. A preliminary evaluation of Doppler-rod balancing techniques has also been initiated. An IBM-1620 computer program has been written to aid in balancing the reactivity swing of the Doppler rod and minimize the use of reactor time. Preliminary checkout is encouraging. A final test will be made on the next ZPR-3 Doppler experiment. If successful, the program could cut balancing time with the reactor by a substantial amount. The program would then be adapted to the ZPPR Doppler rod.

(3) Measurements of capture and fission rates using small foils which can map the detailed fine structure of reaction rates within a cell of a critical assembly are planned. This is necessary to avoid gross perturbation of the neutron flux by detectors and thus provide data which

can be analyzed accurately. The technique requires development of sophisticated counting and data-reduction techniques. The preliminary work centers around technique development and is described in Sect. I.B.3.

(4) The automation of data acquisition and reduction is necessary to improve the speed of experiments for better reactor utilization, to increase accuracy and variety of practical experiments, and to reduce the labor, and hence time, in data analysis prior to publication. Efficient use of modern, automatic data-processing methods is possibly the most important single aspect which will lead to the most efficient utilization of ZPPR. Present efforts center on digital-position indicators and a computer-compatible data-acquisition and -recording system. With regard to the digital-position indicators, preliminary design of the control logic, multiplexer unit, output shift register, and display unit is complete. Some of the components for the breadboard and prototype have been received, and breadboarding of this system will start in the near future. With regard to the data-acquisition and -recording system, preliminary requirements have been established. Several suppliers of the basic components of the system have been contacted, and specifications are being written on the portion of the system to be purchased.

8. ZPR Fuel and Nonfissile Materials--Procurement (A. B. Shuck)

Last Reported: ANL-7399, pp. 34-37 (Nov 1967).

a. Process Materials

(i) Plutonium. The present order with Atlantic Richfield Hanford Co. (ARHCo) is for production of 1200 kg of ingots, blended to 11.5 ± 0.5% ^{240}Pu content. As of January 1, ARHCo has produced 574.2 kg of finished ingots. During January 1968, blending lot 16 containing 168 kg of plutonium was ingoted for a cumulative total of approximately 740 kg of one-kg ingots. It has been necessary to use plutonium from a number of sources including commercial reactors. Some of this plutonium contains comparatively large percentages of ^{238}Pu and ^{241}Pu, but it has been possible to keep the ingots within the specified limits of 0.1% ^{238}Pu and 2.5% ^{241}Pu.

(ii) Jacket Fabrication. An additional 1000 jacket sleeves and 2000 end plugs were fabricated by Central Shops to meet February requirements for 100 additional jackets by Dow and 894 jackets by NUMEC for fabrication of plutonium fuel elements. To January 15, 1968, 5,764 sets of fuel element jacket components had been completed and shipped. Two-shift production of fuel-element jackets has been scheduled to complete the requirement for 20,000 sets of jackets in order that the tooling can be released for contract manufacture of the sodium and sodium carbonate elements.

(iii) Fabrication of Fuel Elements. The Dow production for January was at a slightly lower level than for previous months. This reflected the effects of year-end inventory, tooling up to produce 1-in. elements, and the need to replace a number of 4-in.-core plates, which were found to have deterioriated in storage. The 1-in.-core plates required fixtures to adapt them to the tooling used to machine the longer-core plates. Minor changes were also required in the welding fixtures and tooling. About 10 days were lost to the production of the 4- to 8-in. sizes while the tooling changes were being made; 128 one-in. core plates were machined, and the tooling was returned to production of regular sizes of fuel elements.

During the production the 891 five- and seven-in. fuel elements required for the December ZPR-3 FFTF critical experiment, 335 four-in. core plates were salvaged from the casting ends. These were wrapped in aluminum foil and sealed from the argon-atmosphere machine line in polyethylene pouches. The sealed pouches were placed individually in stainless steel vessels with room atmosphere in the space between the vessel and the pouch.

After 3 to 5 weeks storage, some of the pouches were opened in the air-filled fuel-element assembly glovebox. The core plates were found to be severely corroded. The fine dust was highly pyrophoric, characteristic of hydride-metal powder. Ninety of the core plates were cleaned and jacketed by the normal technique, which provides about 1/2-atm pressure of inert gas in the jacket. Some of the rejacketed fuel elements swelled within two weeks. Upon dejacketing, a number of the core plates showed evidence of further corrosion.

This prompted the inspection of the remainder of the 4-in.-core plates in storage. Although there were varying degrees of corrosion, nearly all showed some evidence of corrosion and intergranular attack. It was postulated that moisture diffused from the air through the polyethylene pouch. In the intert atmosphere, the moisture and plasticizer decomposed to active hydrogen and oxygen, and the nascent hydrogen combined with the plutonium. The attach appeared to be of a penetrating grain-boundary nature, which caused deep corrosion of the core plates. Unfortunately, plutonium hydride is not completely decomposed at temperatures which would not damage the core plates. As there appeared to be no other means of reclaiming the core plates with assurance that all hydride is eliminated, all 335 core plates were remelted and cast. Procedures were developed for future storage.

Nonremeltable residues from U-Pu-Mo alloy have been separated into two classes. Those which can be returned to production by simple dissolution, selective precipitation, calcining, fluoridizing, and reduction are classed as fast-recycle residues. Those residues that require

more extensive chemistry and ion-exchange separation are classed as slow-recycle. Work has been started on the recovery of the fast-recycle residues. Present thruputs to precipitation and calcining appears to be about 4 kg/day. As of January 29, residues containing 112.6 kg of plutonium were dissolved, and 50 kg were fluoridized and reduced to metal.

NUMEC has had the usual broad range of startup problems. Most have now been solved.

The first difficulty was in obtaining good castings in all six mold cavities. After failing to develop a gating design that would fill all six 15-in.-long molds simultaneously, NUMEC developed a sprue which filled the center cavities first and then would overflow to the outer cavities in sequence. This filled each cavity sufficiently fast to overcome the cold-shut defects that originally occurred.

Abrasive cut-off methods did not work with the U-Pu-Mo alloy in the inert atmosphere. NUMEC installed a milling machine to saw core plates from the castings. They have improved the life of the carbide milling cutters by the way in which these are ground by developing further the relieved tooth contours originally used at ANL. A serious accident on one of the milling machines occurred to an employee on December 14, 1967.

NUMEC bases their yields on a possible 90 in. of core plates from the six 15-in.-long casting. They have gradually improved from an average of less than 50 to about 75% of the 90 in. in useable core plates. The yields, based upon metal charged, are considerably less, although the sprues and casting croppings can be remelted. Crucible skulls and machine chips amount to over a kilogram per melt. Efforts to reclaim these by remelting have not been successful to date. The problem of how to best recover the NUMEC "fast recycle" has been assigned as a NUMEC Research and Development task.

The casting-cleaning operations have been very well developed. Both as-cast faces of the core plates are wire-brushed to bright metal. The core plates are then passed to an ultrasonic-cleaning station where they are cleaned in absolute isopropyl alcohol. The isopropyl alcohol is continuously refiltered through submicron filters and is frequently changed. The castings are vacuum dried and immediately loaded into the jacket sleeves. NUMEC has loaded core plates through paper funnels that protect the edges of jacket sleeve from contamination. ANL demonstrated that fine shreds and scrappings of paper can be introduced to the jacket while loading. Stainless steel funnels were ordered, but as of January 30 were not yet in use for core loading.

NUMEC has used a set of developmental welding fixtures. These were all-copper, and with repeated assembly and disassembly have become quite worn. The later welds have suffered the effects of these worn fixtures. New fixtures were designed of stainless steel with copper-chill inserts. These were received during the last week of January and are being tested.

The cumulative production status for U-28.3 w/o Pu-2.5 w/o Mo fuel elements and production from December 29, 1967, through January 26, 1968, was as follows:

	Dow		NUMEC	
	Month	Cum	Month	Cum
Batches cast	74	405	55	116
Inspected core plates	892	3215	622	947
Assembled fuel elements	702	2874	629	916
Inspected fuel elements	593	2675	644	799
Fuel elements shipped	352	1366	536	691
Fuel elements on order	-	3862	-	5379

Ten percent of the Dow production has been sent to Illinois for gamma-scan assay. The balance of Dow-produced elements is being shipped directly to Idaho. The completed fuel elements are presently being held at Dow pending acceptance of the ZPPR vaults from the construction contractor. NUMEC shipments are being made to Argonne, Illinois for inspection and gamma-scan plutonium assay.

The quantity of fuel elements completed and inspected and on order by size is as follows:

	Nominal Element Length (in.)					
	1	4	5	6	7	8
Completed by Dow (1/26/68)	92	287	1001	197	582	516
On Order at Dow	100	684	1026	684	684	684
Completed by NUMEC (1/26/68)	-	137	197	131	122	212
On order at NUMEC	-	978	1467	978	978	978

(iv) Inspection of Fuel Elements Received. An inspection area complete with gauges for fuel-element dimensions and with microscopes for weld inspection was set up in the fuel-element-receiving area (Building 16, Room 55). The receiving inspection of the fuel elements is being done by the field-inspection teams who are rotated between Dow and ANL, and NUMEC and ANL, supplemented by ANL technicians. As of January 31, the first

nine shipments from NUMEC were inspected. Several rejectable and marginally rejectable welds were encountered. Three elements were returned to NUMEC as illustrative of weld defects that were getting past inspection. The dimensional conformity of the first nine shipments from NUMEC has been good.

(v) Sodium and Sodium Carbonate Elements. The contract with DK Aerospace Co. for sodium-filled elements and sodium carbonate-filled elements was signed on January 17, 1968. Representatives are bringing the schedule of production, process-control procedures, and quality-control manual to ANL January 31 for evaluation and approval. In the meantime, tooling and preproduction activities have been initiated by DK so that production can commence by mid-February. DK reports that their schedule will be in accordance with the contract, which in turn is based on ANL test requirements.

The request for proposal for sodium carbonate wafers to be furnished to DK for loading is out for bid. The placing of this contract will be expedited since delivery of these wafers is very tight in terms of requirements in DK's schedule.

Central Shops is fabricating an additional 3800 sodium-filled elements and final delivery is scheduled for February 22, 1968. Current progress indicates this delivery will be met. The 1050 sodium carbonate elements being fabricated by Central Shops is scheduled for delivery on March 2, 1968, and current progress indicates the delivery date will be met.

(vi) Iron Oxide Elements. The iron oxide elements are on order with Lake Products. The preproduction samples were received, but were out of specifications relative to dimensional requirements. They are to submit another group of preproduction samples made with new tooling by February 15. In the meantime, chemical analyses are being obtained on the samples already submitted.

9. FTR Critical Experiment Program (D. Meneghetti)

Last Reported: ANL-7403, pp. 22-25 (Dec 1967).

The proposed Assembly IIa is a cylindrical-shaped, uniform-composition core similar to that of Assembly I (ZPR-3 Assembly 51) except for the presence of an axial gap which separates the core into two equal driver regions. The proposed composition of the gap is 80 v/o sodium and 20 v/o stainless steel. The critical mass of the core will depend upon the gap width and the cross-sectional area-profile of each driver half.

The critical masses of a series of cores having no gap, two-drawer-wide gap (~11 cm), and three-drawer-wide gap (~17 cm) have been calculated using the two-dimensional, x-y geometry, SNARG program in the S_2 approximation. The six-group cross-section set number 29601 was used. In these calculations the peripheral radial profiles of the drivers approximated sectors of circles wherein the chord length was held constant at 41.4 in. A 30-cm radial reflector with composition identical to the nickel-containing inner radial reflector of Assembly 1 was used.

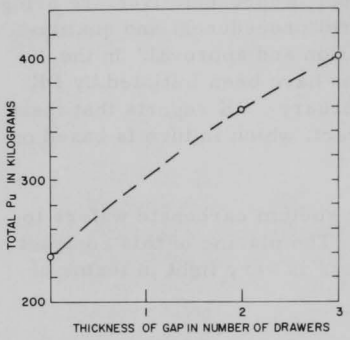

Fig. I.B.9. Calculated Critical Masses of Proposed Assembly IIa as Function of Gap Width

Effects of axial diffusion leakages from the various regions were approximated by $D_j \pi^2/H^2$ quantities, where the diffusion constants D_j are regional and group-dependent and where H is the equivalent bare extrapolated axial height.

The results are shown in Fig. I.B.9. The calculated values have been normalized to an experimental value for the case of zero gap. The ordinate is total plutonium containing 90% fissile and 10% fertile components. The use of $D_j \pi^2/H^2$ for approximating vertical leakage effects represents one of the uncertainties in the calculations. An estimate of the error resulting from use of this approximation indicates, however, that the curve of Fig. I.B.9 should overpredict the critical mass by a few percent at the three-drawer gap position.

10. <u>ZPPR Construction</u> (H. Lawroski)

Last Reported: ANL-7403, pp. 25-27 (Dec 1967).

Design of the fission-counter drive mechanism was completed and sent out for bids on January 10. The bids are due February 8. Bid packages on the drawer conveyor for the loading tube were sent out December 27 and bids are due January 24.

Visual inspection of the 285 AEC-type high-efficiency filters in place revealed 24 filters damaged on the exterior of the filter media, i.e., the portion of the filters visible from the catwalk of the weather protective enclosure. Inspection of the interior surfaces of the filters could not be performed because a protective wire mesh had been wired in place over these filter surfaces. The contractor was instructed to install the proper stud fasteners for the wire mesh.

Major work by the construction contractor consisted primarily of repair of faulty welds on the seal-door bulkheads and on the loading tube. Satisfactory leak tests were achieved for the electrical penetration bulkheads on all seal doors, for the north portion of the seal pit, and for the loading tube. The ventilation and piping bulkheads at seal door 0-67 were satisfactorily leak tested. Bulkheads at seal doors 0-65, 0-69, 0-73, and 0-74, the sourth half of the seal pit, the seal pit cover, and the escape tunnel transition connection have not been leak tested satisfactorily.

During the initial testing and checkout of the reactor-cell temperature controls and air-handling units on December 27, the four Norbatrol components which convert the temperature signal to a control signal were found inoperative because of two burned-out elements. The units were shipped to the factory for repairs on December 28. Repairs were made and the units were returned to the site January 22. Work was started immediately on testing and checkout of the cell air-handling system.

The following work remains to be done in the mound area: cleanup and checkout of the fuel-storage vault and workroom; satisfactory leak testing of the previously mentioned bulkheads and tunnel; aligning, adjusting, and testing of the seal doors; painting of the reactor cell area and corridors; adjusting, balancing, and checkout of the air-handling systems in the mound area; and cleanup, replacement of damaged filters, and leak testing of the backup containment structure.

A construction progress meeting was held at the site with DRDT, COO, and ANL personnel on January 17. Consideration is now being given to having ANL align, adjust, and leak test the seal doors to facilitate the completion of the construction project and to allow the installation of the reactor components.

The reactor-installation contractor has been working in the support wing since December 18. Six-thousand matrix tubes were degreased, cleaned, and checked for dimensions. Groups of tubes with the same vertical dimensions will be separated for each layer in the reactor matrix. The height dimension, which is critical, will be matched for each half of the reactor. Other miscellaneous cleanup was performed in preparation for movement of reactor components into the reactor cell.

Containers for the lead to be used in load testing the bed and tables were received on January 22. Ten of the 38 containers have been filled with lead bricks and the remainder are in the process of being filled.

Additional information for the safety analysis of ZPPR which was requested by DRDT is being assembled by ANL.

C. Component Development--LMFBR

1. Sodium Technology Development--Engineering Development (S. D. Skladzien)

Last Reported: ANL-7403, pp. 27-29 (Dec 1967).

a. Sodium Quality Measurement

(i) In-line Techniques. In a series of five tests of a plugging meter installed in the Sodium Analytical Loop, faster sodium flow was found to result in higher plugging temperatures. This indicates that the accuracy of sodium-purity measurements with plugging meters depends on the sodium flow rate and/or the rate of cooling at the meter. The 36°F spread in plugging temperature indicates a substantial variation (3-6 ppm, depending on which solubility data are used) in oxygen content, but the five sodium-plugging runs were conducted within 6 hr while the Sodium Analytical Loop maintained sodium purity constant at 7 ppm oxygen (chemical analysis). These findings point to the need for better understanding and standardization of plugging-meter design, operation, and calibration.

The plugging-meter portion of the loop consists of a manually operated, serrated-stem plugging valve in the cooling-loop section, and a dc electromagnetic pump and magnetic flowmeter on the hot side of a counterflow heat economizer.

After the five plugging runs, 1.830 g of NaOH pellets, equivalent to 13.4 ppm oxygen, were added to the main vessel of the Sodium Analytical Loop and the response of the various in-line purity-measuring instruments was observed. Figure I.C.1 shows the responses of a plugging meter and of two oxygen meters (electrochemical cells made by United Nuclear Corp.). The plugging temperature increased 41°F within the first 24 hr (the sodium flowed through the meter at 0.33 gal/min and was cooled 10.7°F/min). The oxygen meters responded very well in this test; the change in output voltage after 3 days was 22.7 and 25.5 mV for Oxygen Meters Nos. 202 and 203, respectively (in previous reports, these meters were called Nos. 1 and 2). A dc absolute-resistivity meter measured a 0.3-microhm increase in sodium resistance in the same 3 days; in other words, the resistance changed 0.0067%/ppm oxygen. Chemical-analysis data for oxygen in the sodium and for hydrogen in the blanket gas are not yet available.

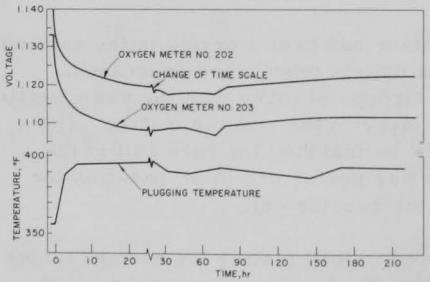

Fig. I.C.1. Response of Oxygen Meters and Plugging Meter to NaOH Addition to Sodium Analytical Loop

b. Sodium Quality Control. Construction of the prototype submerged oxide collector has been completed, and the unit has been delivered. It will be installed in the sodium reactor mockup tank when the support superstructure has been installed.

Preliminary tests of the direct water-reaction method for determining the content of a spent cold trap continued. Mixtures of sodium metal and sodium oxide were reacted with steam, and the evolved hydrogen was collected and measured. The results, shown in Table I.C.1, indicate an undesired hydrogen-producing side reaction with the stainless steel container whenever the oxide content of the mixture was high. The stainless steel surface, examined after the reaction had been completed, was etched where the surface had contacted the sodium oxide at the start of the test. A new container material will be tried.

TABLE I.C.1. Tests of Steam-reaction Method for Determining Content of Spent Cold Trap

Weight of Na (g)	Weight of Na_2O (g)	Hydrogen Produced (liters at STP)		
		Calculated	Observed	Error (%)
6.20	0	3.02	3.00	-0.7
3.94	7.91	1.92	1.93	+0.5
3.91	59.0	1.91	2.01	+5.0
3.07	40.6	1.50	1.62	+8.0
1.41	62.3	0.69	0.90	+31.0

An algebraic analysis of the steam-reaction method, which consists of reacting steam or water with the contents of a spent cold trap and measuring the weight of the residue (A), the alkalinity of the resulting solution (B), the amount of hydrogen evolved (C), and the amount of water used in the reaction (D), indicates some limitations. The corresponding algebraic expressions are

$$A = 61.994\, X_{Na_2O} + 40.005\, X_{NaOH} + 24.005\, X_{NaH} + 22.997\, X_{Na};$$

$$B = 2X_{Na_2O} + X_{NaOH} + X_{NaH} + X_{Na};$$

$$C = X_{NaH} + 0.5\, X_{Na};$$

$$D = X_{Na_2O} + X_{NaH} + X_{Na},$$

where X_{Na_2O}, X_{NaOH}, etc., are the number of moles of sodium oxide, sodium hydroxide, etc., initially present in the residue. On first examination, the four algebraic expressions appear to be independent, making an exact solution possible. Unfortunately, this is not so.

The four equations are said to be dependent if constants K_1, K_2, K_3, and K_4 exist, not all zero, such that

$$K_1A + K_2B + K_3C + K_4D = 0.$$

If this equation holds only when all the constants are equal to zero, then the four equations are independent. If we let $K_1 = -1$, $K_2 = 40.005$, $K_3 = 2.016$, and $K_4 = -18.016$, then the above test indicates that the four equations are dependent.

Three of the above four equations are, however, independent, and if the concentration of at least one of the four unknowns is low compared to the other three, then an algebraic solution becomes possible. We may also obtain exact relative solutions, such as total oxygen and total hydrogen, for all conditions:

$$\text{Total oxygen} = X_{Na_2O} + X_{NaOH} = B - D;$$

$$\text{Total hydrogen} = X_{NaOH} + X_{NaH} = B + C - 2D.$$

2. Reactor Mechanisms Development--Materials Evaluation

a. Physicochemical Mechanics of Metals (F. A. Smith)

Last Reported: ANL-7399, p. 41 (Nov 1967).

(i) Effect of 1200°F Sodium on Butt-welded Type 304 Stainless Steel Pipe. To determine the susceptibility of a section of heliarc butt-welded Type 304 stainless steel pipe to intergranular attack by flowing sodium, samples of 4-in.-dia pipe were immersed in 1200°F flowing sodium for 35 days. These and control samples were subjected to accelerated corrosive attack by being immersed in a boiling Strauss reagent solution for 6 hr. At 1-hr intervals, the structural attack was determined by measuring the electrical resistance between five sets of points in the pipe parent metal, the as-cast weld metal, and the weld-heat-affected zone (see Fig. I.C.2).

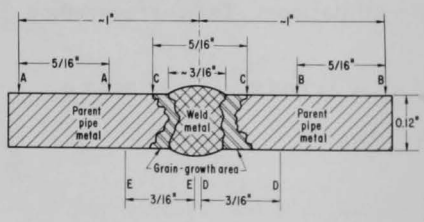

Fig. I.C.2. Location of Points between Which Electrical Resistance Was Measured

The parent metal was affected the most (electrical resistance increased as much as 70% over the original values) Resistance in the grain-growth zone of the pipe increased up to 60%. In contrast, the resistance of the weld metal increased only 20-25%. Visual observations and photomicrographs have confirmed the microstructural changes indicated by the resistance measurements. Physical-property data are being acquired on another set of test and control specimens.

It should be noted that the pipe section tested had been removed from part of the Core Component Test Loop (CCTL) during preoperational modifications. The pipe section previously had been radiographed, leak-tested with helium, and certified as acceptable. Type 308 stainless steel weld rod had been used for the butt-weld because the nickel depletion that occurs during welding would result in a postweld composition very close to that of the Type 304 stainless steel base metal.

b. Sodium Effects on Wear Properties of Materials (E. S. Sowa)

Last Reported: ANL-7403, pp. 29-30 (Dec 1967).

The Clarite vee-blocks and Carboloy shafts whose weartests were reported in ANL-7403 are shown in Figs. I.C.3 and I.C.4. The shaft that had operated in argon picked up considerable metal from the vee-blocks. The vee-blocks that operated in argon show greater wear and scoring than their counterparts that operated in sodium.

Fig. I.C.3. Shaft and Vee-blocks That Had Been Weartested in Argon

Fig. I.C.4. Shaft and Vee-blocks That Had Been Weartested in Sodium

Further analysis of the data has shown that the friction coefficients were higher than was reported in ANL-7403. For example, the friction coefficient for the samples tested in argon was ~1.10 during the first 30 min, fluctuated considerably, and then dropped to ~0.680 toward the end of the 2-hr run at 300°F, by which time fluctuations were much less. By the end of the 1200°F run, the coefficient had dropped to 0.450. The coefficients of the samples tested in sodium fluctuated less.

The samples tested in argon wore faster at 300°F than did the samples in sodium at 300 and 500°F. However, at 700°F the samples in

sodium wore faster than did those in argon. Both sets of samples wore about equally at 900°F, but wear of both sets increased markedly at 1200°F. Additional tests will be performed to verify these results.

Comparison of the data shows the effects of the two environments on wear; the data on operation at various temperatures shows the influence of sodium lubrication and wetting, as well as how the changes in material properties with temperature affect the wear rate. The ultimate objective is to determine the reasons for the importance of the mechanisms over the range of operating temperature.

The Component and Material Evaluation Loop (CAMEL), which will be used for dynamic tests, has been charged with sodium. A temperature profile taken over the loop before and after filling showed considerable normalization of temperatures caused by redistribution of heat by the sodium. However, a plug developed in the gas-circulation system, demonstrating the need for vapor traps at the terminations. The sodium was frozen in situ so these traps can be installed.

c. Fuel Pin Thermocouple Development (A. E. Knox)

Last Reported: ANL-7403, p. 30 (Dec 1967).

(i) Electrical Insulators. Thoria insulators have been found to change from an as-received light yellow to a dark gray color when heated to high temperatures in the presence of helium and tantalum. A spectrographic analysis has shown that such a color change is not caused by tantalum contamination, but probably by a loss of oxygen. To verify this, a darkened thoria insulator (previously heated at 2400°C for 25.7 hr in the presence of helium and tantalum) was fired at 1000°C to a constant weight in air. During this air-firing, the insulator gained weight and underwent a color change from dark gray to yellow-orange. This indicates that the darkened thoria is substoichiometric thoria. How this change in stoichiometry affects the resistivity of thoria will be investigated.

(ii) Thermoelement Properties. The emf output of a tantalum-sheathed, thoria-insulated W-3% Re/W-25% Re thermocouple has been found to be stable within 1%, with no observable drift, at 2400°C for 310 hr. The thermocouple was helium filled and was not thermally cycled. The thoria insulator beads in the thermocouple were large (0.206-in. OD) with loose-fit thermoelements (0.010-in. wires in 0.030-in. holes). Under these conditions, it appears that the emf output of the W-3% Re/W-25% Re thermoelement combination is stable in the presence of thoria insulation and a tantalum sheath. This thermocouple test will be continued for ~200 hr more (for a total of ~500 hr), at which time the effects of thermal cycling will be determined.

(iii) Prototype Thermocouples. To initiate the purchase of prototype thermocouples built to ANL specifications, a request for proposal is being prepared. A candidate thermocouple (of ~1/16-in. OD) is being constructed at the Laboratory.

(iv) In-pile Tests. Four companies have indicated they would respond to a request for proposal to build irradiation capsules and perform the necessary in-pile tests. Three of these companies indicated an additional interest in performing both pre- and post-irradiation tests. Drafts of the proposal request are being reviewed.

d. Fission Gas Pressure Transducer Development (J. R. Folkrod)

Last Reported: ANL-7403, pp. 30-31 (Dec 1967).

(i) Null-balance System. As reported, the first MSA null-balance pressure transducer was removed from test when the instrument gave incorrect and erratic readings above 400°F. The exact cause of the trouble has not been determined, but it should be noted that the instrument continues to function satisfactorily below 400°F.

The second unit performed like its predecessor, apparently shorting out above 400°F. When the bellows of this second unit began to leak after 24 hr, testing was terminated. The manufacturer had previously tested the unit at 1200°F and claimed success. However, the operation at 1200°F could have weakened the bellows. Experience at the Laboratory with nickel bellows has shown that they are very weak after use at elevated temperatures.

The pressure controller satisfactorily increased pressure, but in decreasing pressure the system would hunt and the relay would chatter very badly.

e. Signal-Lead Connectors for Sodium Service (A. P. Grunwald)

Last Reported: ANL-7403, pp. 32-33 (Dec 1967).

The prototype connector design for FTR has been reviewed and approved. Parts are being fabricated.

A 0.5-in.-ID line for inserting flux wires into the FTR core has been incorporated in the design. Because of the already tight space, some modifications were required. A new support structure and vessel cover have been designed so the test apparatus can accommodate this prototype connector.

(i) Test of Electrical Connector in Sodium Vapor. The insulation resistance of another 36-pin connector (Physical Sciences Corp. Type T10-22-36P-TC4) has been measured in sodium vapor through the range 410-700°F. The connector was welded into the top of a 2-in.-dia, 3.5-in.-high, stainless steel vessel containing 35 g of sodium. In Fig. I.C.5 are plotted the maximum and minimum readings of the resistance of the Durock insulation as measured between each of eight connector pins and the stainless steel body of the connector. Except where noted otherwise in Fig. I.C.5, argon gas in the vessel was maintained at ~2 psig during the test.

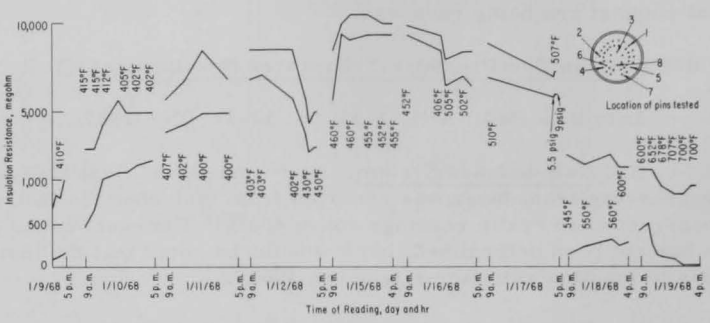

Fig. I.C.5. How Electrical Resistance of Durock Insulation (between each of eight pins and connector body; only maximum and minimum values are plotted) Varied when Connector Was Exposed to Sodium Vapor in Argon at Various Temperatures Indicated

f. Failed Fuel Locating Method Development (F. Verber)

Last Reported: ANL-7403, pp. 33-34 (Dec 1967).

The design for the Failed Fuel Test Loop (see Progress Report for November 1967, ANL-7399, p. 45) was reviewed jointly by AEC, PNL, and ANL. As a result, the design was modified to approximate more closely the sodium-flow condition through a fuel subassembly of the FFTF and to improve detection of the krypton-85 gas to be injected in the sodium loop. (1) The gas injector will be located 70 in. below the 4-in. sodium-pipe section of the sodium loop in a straight vertical run of 1-in. pipe. (2) The 1/2-in.-dia exit holes in the 1-in. section of the sodium loop will be lowered and another row of 1/2-in.-dia exit holes will be added. (3) A sodium surge tank will be installed near the inlet to the electromagnetic pump. (4) The window in the gas-detector loop will be relocated near the sodium-vapor trap; the window is being fabricated.

Another improvement in the gas-detector loop involves substitution of a 0.001-in.-thick, 1-in.-dia Mylar window for the 0.010-in.-thick, 2-in.-dia stainless steel window. This will increase the efficiency of measurement of the radiation from the krypton-85 tracer in the gas-recirculating loop.

D. Systems and Plant--LMFBR

1. 1000-MWe Plant (L. W. Fromm)

Last Reported: ANL-7403, pp. 34-35 (Dec 1967).

a. The Babcock & Wilcox Co. Subcontract. The B&W reference concept was described at a meeting with the AEC. B&W has continued to refine its reference concept and has selected the plant steam cycle.

Task-II design descriptions are being written, and work is continuing on Task-III parametrics. Four additional trade-off studies have been completed and are in the process of being reported.

The architect-engineer is continuing support studies.

b. Westinghouse Corp. Subcontract. All Task-I technical work has been completed; seven topical reports and a Task-I report are being written.

Work on seven Task-II work packages has begun.

A successful computer run of the plant-optimization code has been achieved as part of methods development for the Task-III parametric analysis. Computer-code cost representation of the intermediate heat exchanger has been completed; a similar representation for the steam generator is about 50% complete.

c. General Electric Co. Subcontract. The Task-I reference design has been chosen and all other Task-I technical work has been completed. A cursory review was conducted to determine the influence of a higher plutonium alpha value on the Task-I core-design alternates. This higher alpha value is based on recent British experiments. The Task-I report is being prepared.

Systems and major equipment are being designed in Task III. Work has begun to identify parametric studies, trade-off studies, and parametric ranges to be evaluated during Task III.

d. Combustion Engineering, Inc., Subcontract. The reference design is being refined in respect to control, radial-blanket modifications, and moderator insertion. Accident analysis for the reference design is continuing. The Third Quarterly Technical Report has been submitted to ANL.

e. Atomics International Subcontract. The Atomics International 1000-MWe Follow-on Study work is approximately 20% complete. Nuclear and fuel-cycle analyses of the range of core parameters being studied in Task I have been completed, as has a study of plant-safety criteria. System-selection studies related to the core-parameter variations continue; an optimization code is being revised to include effects of availability. Technical notes have been prepared that describe the bases and criteria for much of the work performed and the selections made to date.

E. EBR-II

1. Research and Development

a. Reactor Experimental Support--Reactor Analysis and Testing (R. R. Smith)

Last Reported: ANL-7403, pp. 35-49 (Dec 1967).

(i) Postirradiation Examination of Driver Subassemblies Discharged from Run 26. The results of postirradiation examinations conducted on driver subassemblies discharged from Run 25 indicate that decreases in button-to-button dimensions exceeded the number of increases by a factor of approximately three (see ANL-7391, pp. 58-60, Oct 1967; ANL-7399, pp. 55-56, Nov 1967). Since compressional effects of this nature may affect the power coefficient, similar measurements were conducted on subassemblies discharged from Run 26. The results for 13 of the 28 subassemblies from Run 26 are summarized in Table I.E.1.

Values given in the column labeled Deviation are the deviations from the results of preirradiation measurements. In some cases, the results of original measurements indicated that one set of flats was either slightly under or over specifications. This fact was taken into account by comparing the original measurement with the most extreme postirradiation measurement (in the same direction). Since the precision limits of pre- and postirradiation measurements are each ±0.001 in., the precision limit of all deviations given in the last column of Table I.E.1 is ±0.0014 in. Accordingly, only deviations of 0.002 in. or larger are considered significant.

The results indicate that of the 39 individual measurements made across 39 sets of flats, 21 indicated significant decreases, 9 indicated significant increases, and 9 indicated no significant change. The sum of all indicated decreases (regardless of significance) amounted to 83 mils; the sum of all indicated increases amounted to 31 mils. The net change per set of flats, a decrease of 1.3 mils, is essentially the same as that established from measurements conducted with subassemblies discharged from Run 25.

(ii) Feedback Model for Run 26. Attempts have been made to employ mathematical models to describe the reactivity feedback which was established at 22.5 MWt during Run 26. These attempts indicate that the net feedback may be described as the sum of four, or possibly five, individual components. A comparison of the calculated results for three slightly differing models with actual rod-drop results are given in Fig. I.E.1. Comparisons of calculated results with actual transfer-function data are summarized in Figs. I.E.2-4 (all for 22.5 MWt and full-flow conditions). Inspection of the data indicate that model I gives the best fit in the frequency

TABLE I.E.1. Button-Button Measurements

Specified Tolerance--2.318 ± 0.001 in.

Subassembly	Flats	Preirradiation Dimension (in.)	Postirradiation Dimension (in.)	Deviation (in.)
B-349	1-4	One set 2.321	2.315	-0.003
	2-5	Others in spec	2.313	-0.004
	3-6		2.318	-0.003
B-350	1-4	One set 2.321	2.316	-0.002
	2-5	Others in spec	2.317	-0.001
	3-6		2.322	-0.001
B-351	1-4	One set 2.320	2.318	0.000
	2-5	Others in spec	2.322	-0.002
	3-6		2.318	0.000
B-353	1-4	One set 2.319	2.312	-0.006
	2-5	Others in spec	2.305	-0.013
	3-6		2.311	-0.008
C-265	1-4	One set 2.315	2.317	-0.001
	2-5	Others in spec	2.322	+0.004
	3-6		2.313	-0.002
C-292	1-4	In spec	2.316	-0.002
	2-5		2.315	-0.003
	3-6		2.319	+0.001
C-296	1-4	One set 2.316	2.321	+0.003
	2-5	Others in spec	2.321	+0.003
	3-6		2.318	+0.002
C-297	1-4	One set 2.316	2.320	+0.004
	2-5	Others in spec	2.315	-0.001
	3-6		2.315	-0.003
C-2025	1-4	In spec	2.319	+0.001
	2-5		2.316	-0.002
	3-6		2.316	-0.002
C-2035	1-4	In spec	2.313	-0.005
	2-5		2.314	-0.004
	3-6		2.316	-0.002
C-298	1-4	In spec	2.315	-0.003
	2-5		2.322	+0.004
	3-6		2.318	0.000
C-2028	1-4	In spec	2.316	-0.002
	2-5		2.322	+0.004
	3-6		2.320	+0.002
C-2030	1-4	In spec	2.321	+0.003
	2-5		2.316	-0.002
	3-6		2.314	-0.004

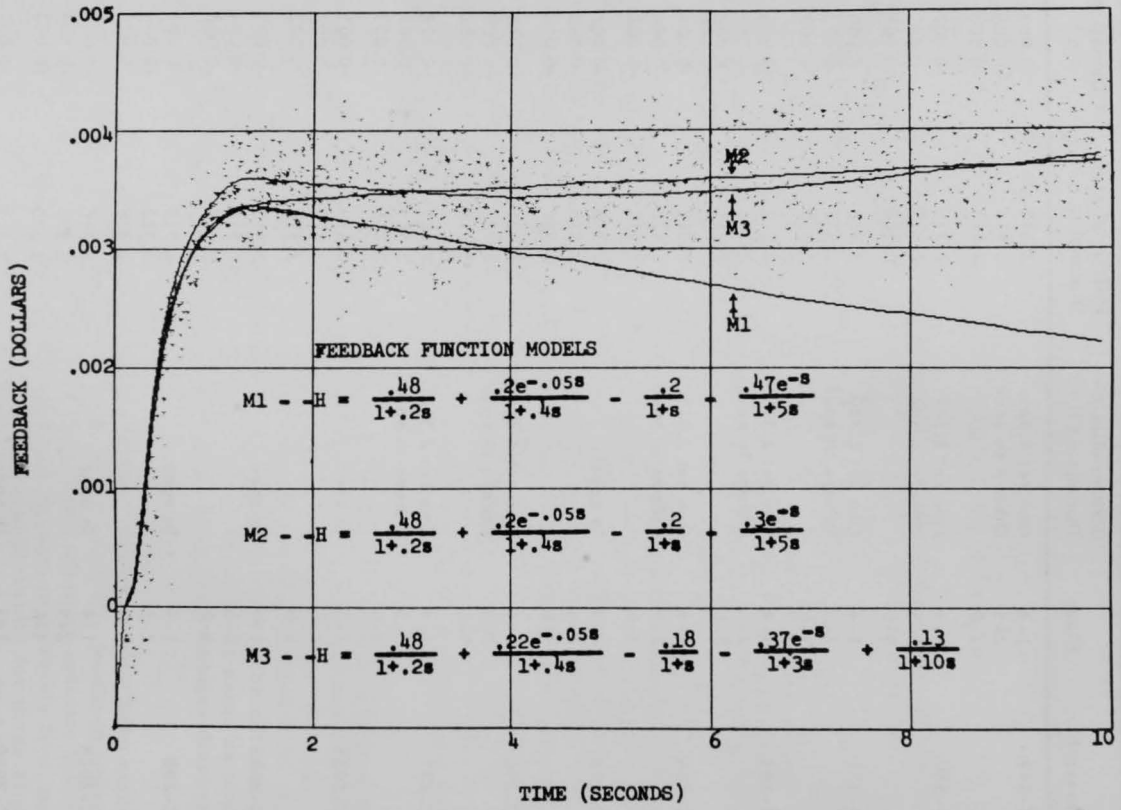

Fig. I.E.1. Rod-drop Experiment at 22.5 MW during Run 26B

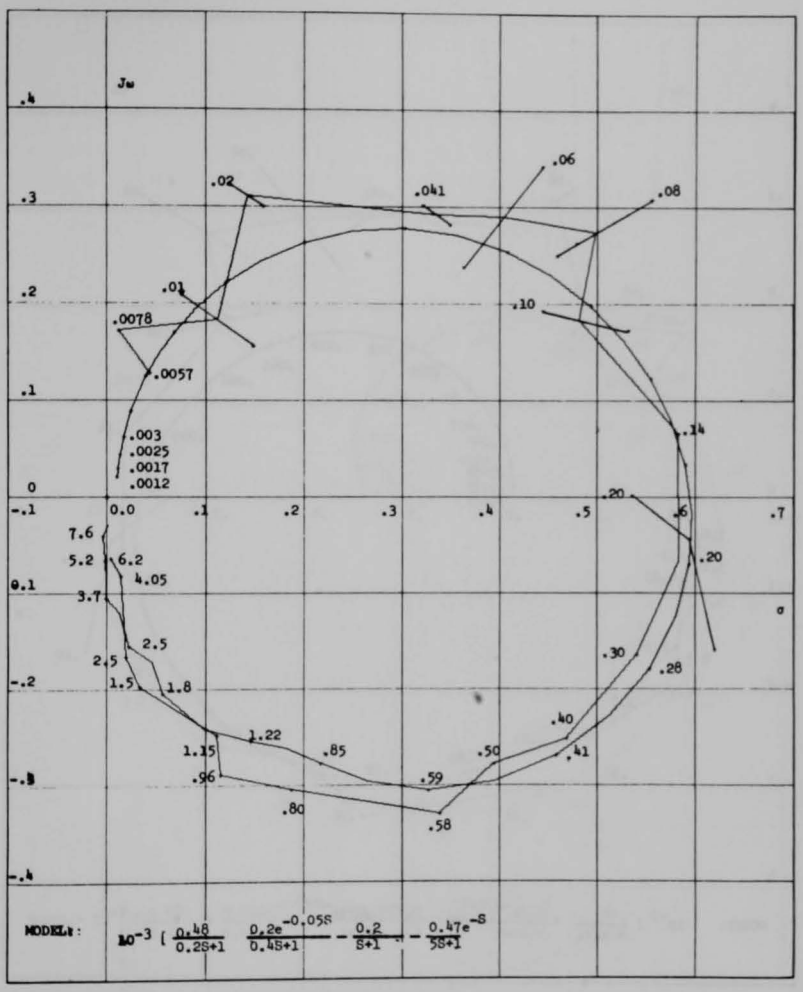

Fig. I.E.2. Feedback (H) Measured Curve and Model I

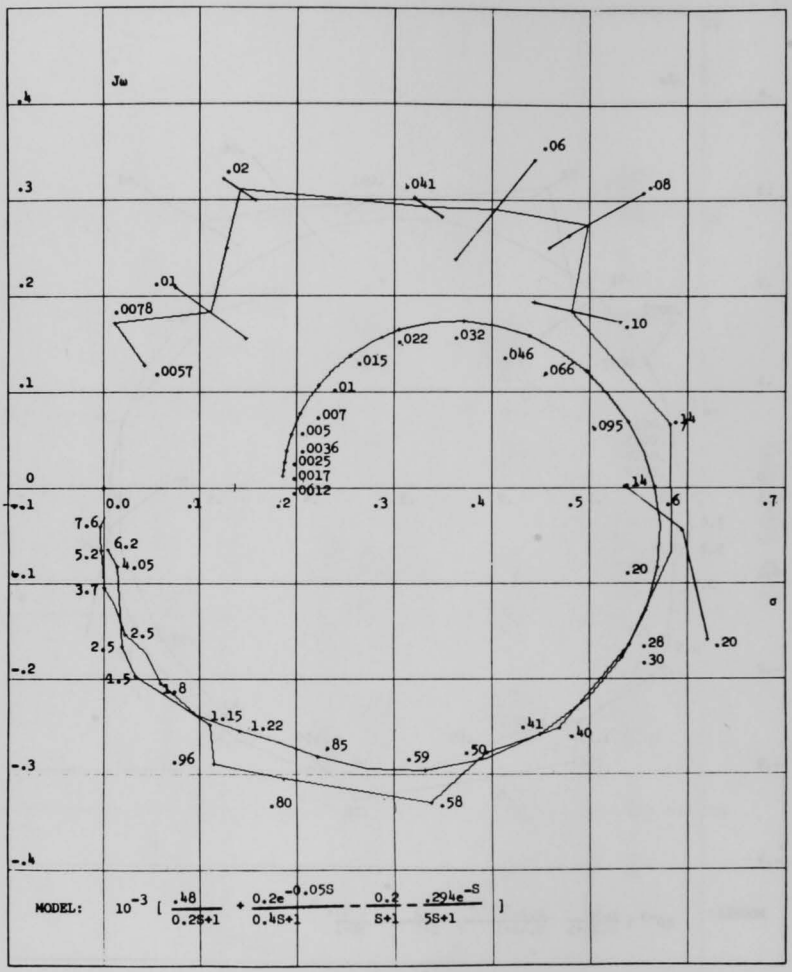

Fig. I.E.3. Feedback (H) Measured Curve and Model II

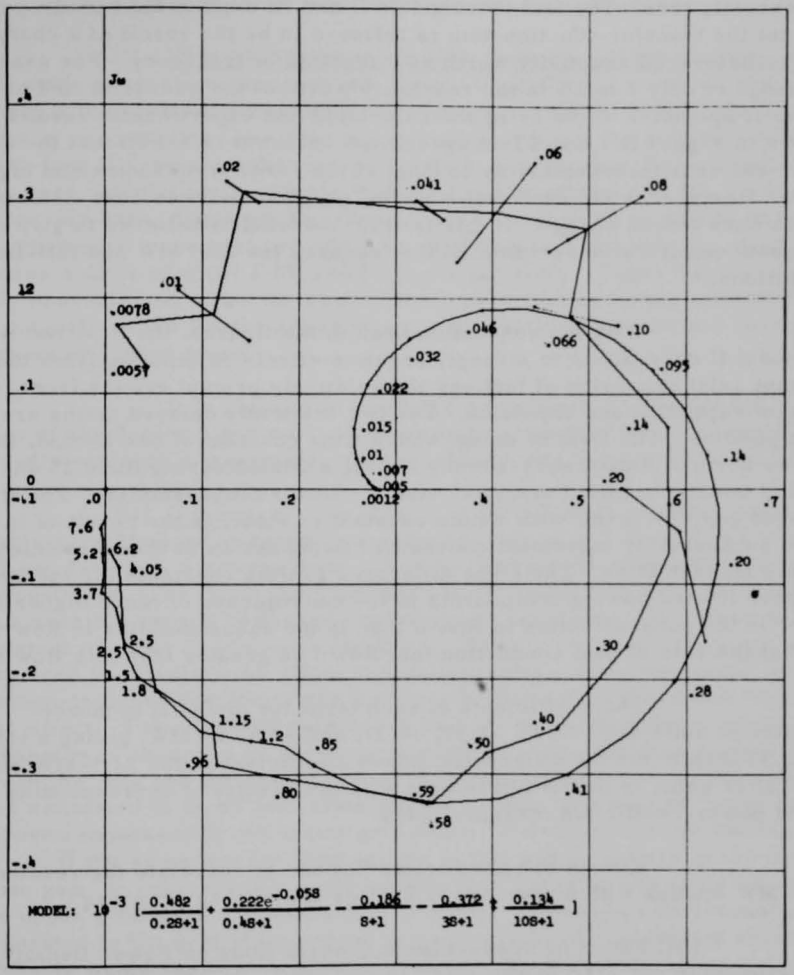

Fig. I.E.4. Feedback (H) Measured Curve and Model III

domain, whereas models II and III give the best fit in the time domain. Superficially, it would seem that the data are inconsistent, but this is not necessarily true. The fact that models II and III explain the rod-drop data but not the transfer-function data is believed to be the result of a change in oscillator-rod reactivity worth as a function of frequency. For example, a change of only 1 to 2% in the reactivity worth of the oscillator rod at the lower frequencies would bring the calculated and experimental results shown in Figs. I.E.3 and 4 into agreement. Since it is known that the oscillator rod rubs (presumably by bowing) at the lower frequencies and higher power levels, it is believed that its axial position and therefore its reactivity worth does indeed change. If this is true, model II is believed to give an adequate empirical description of the feedback for 22.5 MW and full-flow conditions.

With the convention used in the figures, the first two terms of model II correspond to strongly negative effects originating from the prompt axial expansion of fuel and the relatively prompt effects from sodium expansion and expulsion. The two relatively delayed terms are both positive. The first of these, with a time constant of one second, involves normal inward subassembly bowing assisted during Runs 25 and 26 by inward bowing in Row 7 stainless steel reflector subassemblies. The strongly delayed positive term, with a time constant of 5 sec, is the result of inward subassembly movement caused by bowing action in Row 8 stainless steel subassemblies. The large difference in time constants for the two positive inward bowing components is the consequence of much higher flow rates in the subassemblies in Row 6 than in the subassemblies in Row 9, so that the rate of heat conduction into Row 7 is greater than into Row 8.

The coefficients of each term for model II in power-coefficient units are -0.885, -0.37, +0.37, and +0.55 Ih/MW, giving a total of -0.33 Ih/MW for the differential power coefficient in the 22.5-MW region. The latter value is in fair agreement with the results of corresponding static power-coefficient measurements.

Efforts to effect better fits and to correlate the results of 22.5-MW studies with higher power studies are still in progress.

(iii) Effect of Boron-loaded Control Rods on Power Density. A preliminary calculation was made to determine the effects on power density of converting to a system of poison-loaded control rods without any fuel sections. The assumptions included a typical 91-subassembly core loading and the replacement of eight standard metal-fueled control rods with an equal number of control rods loaded with ^{10}B (involving a total of 300 g of ^{10}B still inserted in the core for control at criticality). Results of the calculations show that driver-fuel enrichment would have to be increased by 10% to achieve criticality. It follows that for the same specific power, flux levels will be significantly decreased by the use of poison-loaded control rods as compared with the present control-rod design

b. Nuclear Analysis Methods Development (P. J. Persiani)

Last Reported: ANL-7403, pp. 49-51 (Dec 1967).

(i) Physics Analysis--Statics; Control-rod System Improvement. The study program to improve the control capability of an 8-rod system includes a fuel-control poison-follower design. A series of SNARG calculations in r-z geometry has been started to investigate the influence of a 6-in.-long B_4C poison follower, with a 6-in. gap between fuel and follower. The base calculation is with the control-rod fuel entirely in the core. From this base, dropping the control rods 6 in. (bottom of poison follower at upper core boundary) and 14 in. (control rod fuel entirely out of core) causes a $\Delta k/k$ of about 1.5% and 6.5%, respectively. These figures are only approximate, since the spatial mesh used for the initial calculations is not well-suited for the cases of interest; calculations are now being made with an improved mesh.

It is planned to investigate synthesis techniques for the purpose of developing a control-rod computational method which correlates two-dimensional x-y geometry representation with r-z geometry calculations.

(ii) Dynamics. Calculation of EBR-II heat-transfer time constants gave "lumped-element" approximate values of 0.43, 4.9, 4.1 and 5.9 sec for core, stainless steel reflector, and two blanket subassemblies, respectively. The inner shell (upper) and retaining ring were investigated as a possible source of dynamic influence on reactivity. An effective time constant of about 25 sec was calculated. Bump's computer "bowing" code was used to calculate the effect of retaining-ring expansion caused by plenum-temperature rise since previous bowing calculations had negelected this effect. The effect did turn out to be negligible, probably because the expansion is absorbed by the large number of subassemblies present between the ring and the reactor core. The upper-grid-plate time constant was estimated to be 48 sec, assuming no sodium flow upward in the gap between subassembly and upper grid plate. The time constant becomes 19 sec if the same leakage flow occurs in this gap as occurs in the lower plate gap. A subassembly would have to be a few mils out of its seat in the upper grid plate for such a flow to exist. The amount of internal power generated in the grid plate proved to be so small that grid-plate expansion probably would result only if inlet coolant temperature variation exists. It is assumed at present that the coolant inlet temperature does not vary; so, the grid plate seems to be eliminated as a cause of relatively fast dynamic effects.

(iii) Analysis of the Power Coefficient for Run 26

(a) Run 26 Results. In Fig. I.E.5 are presented the experimental results for various power-reactivity measurements during Run 26, with rod-bank effects still present. As can be seen, the results

of the measurement at the end of Run 26C (Dec 11) fall considerably outside the band of the other curves. The uniqueness of Run 26C is still obvious when the rod-bank effects have been subtracted out, as can be seen from Fig. I.E.6.

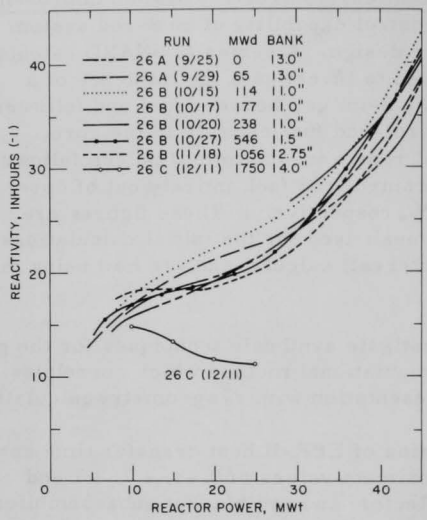

Fig. I.E.5. Measured Power Reactivity during Run 26; Rod-bank Effect Still Included

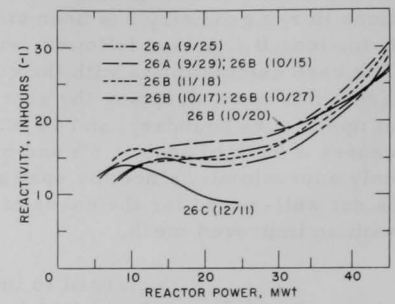

Fig. I.E.6. Measured Power-reactivity Curves during Run 26; All Rod-bank Effects Corrected Out

The determination of and results for the linear and nonlinear components of the total power coefficient have been described (see ANL-7403). The linear component due to fuel expansion was determined from partial-flow experiments at different times during Run 26, whereas the calculated value of the sodium power coefficient was assumed to apply during the entire run; these two components make up the linear feedback. The linear feedback was then subtracted from some of the curves in Fig. I.E.6 to determine the behavior of the nonlinear component during Run 26. The results indicated that both the linear and nonlinear components were increasing during the run.

(b) Possible Behavior for Run 27. Since the mechanisms which cause the changes in the linear and nonlinear coefficients described above in Sect. I.E.1.b.(iii).(a) are not completely understood, it is quite difficult to predict the shape of the power coefficient curve during Run 27. However, based on observations for Runs 25 and 26, an attempt to scope the possible curves can be made for several assumptions as to the behavior of the linear and nonlinear components. These assumptions are somewhat speculative, and it obviously remains for the measurement to determine the actual behavior.

It is possible that the power coefficient at the start of Run 27 will be essentially the same as that for the beginning of Run 26A, as shown in curve I of Fig. I.E.7 (Table I.E.2 summarizes the assumptions made for this figure). This would be consistent with the observed reactivity effects at the start of Run 25 and 26. However, one can make more pessimistic assumptions, leading to the other curves in this figure. Since for the start of each run there will be about the same number of fresh fuel elements, it seems reasonable to assume that the linear (fuel and sodium) feedback is about the same at the start of each run. On the other hand, the nonlinear (bowing) component increase during Run 26 could be due to increased subassembly clearances. If this were the case, it is not clear which subassemblies now have the most influence on the bowing, nor in which case the replacement of part of the fuel subassemblies before Run 27 will affect the bowing feedback strongly. Then one can postulate that the nonlinear feedback for the start of Run 27 will be similar to that near the middle, or even the end, of Run 26. These two assumptions give curves III and IV of Fig. I.E.7.

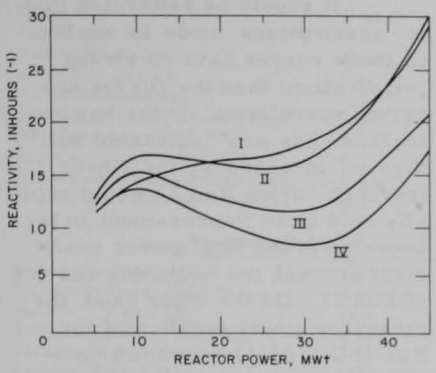

Fig. I.E.7. Possible Power Reactivity at Start of Run 27 for Several Assumptions. Rod-bank effect is not included.

The behavior of the power coefficient during Run 27 is of course even more difficult to predict. During Run 26 the nonlinear feedback increased about 20%, based on the curves for 26A (start) and 26C (average) shown in Fig. II.E.8, p. 50, of ANL-7403. Whether the increase in the bowing has saturated out or will continue during Run 27 will only be determined by experiment. However, presuming that during Run 27 the nonlinear feedback also increases by 20%, while the linear component changes as it did during Run 26, leads to the curves labeled B in Fig. I.E.8 for the end of Run 27. Table I.E.3 gives the assumptions for this figure. In this figure the same assumptions were made for the start of the run as those for curves III and IV of Fig. I.E.7. The effect of the rod bank for its expected position at the start

TABLE I.E.2. Assumptions Made for Curves in Fig. I.E.7

Curve	Linear Feedback	Nonlinear Feedback
I	26A (start)	26A (start)
II	26B (end)	26B (end)
III	26A (start)	26B (end)
IV	26A (start)	26C (average)

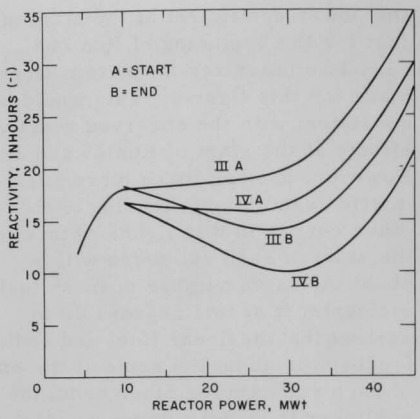

Fig. I.E.8. Possible Power Reactivity Behavior during Run 27 for Several Assumptions. Rod-bank effect is included.

and end of the run has been added to show what the measured curve would be for these assumptions.

It should be reiterated that the assumptions made to arrive at these curves have no strong justification; thus the curves are rather speculative. If the bowing increase has now "saturated out," then an increase in the linear feedback during Run 27 would actually lead to an improvement in the behavior of the total power coefficient between the beginning and end of Run 27. On the other hand, the measured power coefficient for Run 26C (12/11) as shown in Fig. I.E 6 was not used in the analysis to determine the nonlinear feedback at the end of Run 26; if it were, then even more pessimistic curves than those shown in Figs. I.E.7 and I.E.8 would result.

TABLE I.E.3. Assumptions Made for Curves in Fig. I.E.8

	Curve	Linear Feedback	Nonlinear Feedback	Position of Control-rod Bank (in.)		Curve	Linear Feedback	Nonlinear Feedback	Position of Control-rod Bank (in.)
Start	IIIA	26A (start)	26B (end)	11	Start	IVA	26A (start)	26C (average)	14
End	IIIB	26C (average)	1.2 x 26B (end)	11	End	IVB	26C (average)	1.2 x 26C (average)	14

(c) Power Coefficient Study

(1) Core Configuration and Size Effect. The calculations of the components of the power coefficients of Runs 16, 24, 25 and 26B were completed, with the results presented in Table I.E.4. The results were obtained using a second-order transport code with an r-z representation and 1×10^{-6} convergence. Cross-section Set 23806 with core, reflector, and blanket weighted cross sections was employed.

The input values of the dimensions were obtained from engineering drawings and were corrected for temperature. The fuel loadings were provided by the Idaho Division, and the compositions of the structure and coolant were determined from engineering drawings and reports. The Idaho Division calculated the temperature of the fuel, steel, and coolant in the regions of EBR-II. Computer programs were used to prepare some input data and punch the input cards. These programs are being merged into one program which will punch all the cards for calculating the components of the power coefficient.

TABLE I.E.4. Calculated Values of the Components of the Power Coefficient and Associated Data

Item	Run 16 (end)	Run 24 (end)	Run 25 (end)	Run 26 (start)
No. S/A in Core	75	81	88	91
Rings 7, 8	Depl U	Depl U	Steel	Steel
Fuel Type	Mk-I	Mk-IA	Mk-IA	Mk-IA
Axial Blkt Matl	Depl U	Steel	Steel	Steel
Axial Blkt Design	Pin	Pin	50 pin/13 triflute	33 pin/31 triflute
No. of Experiments	5	9	11	13
Avg Core Sodium Temp (°F)	791	787	792	792
Avg Fuel Temp (°F)	911	911	911	911
Avg Core Steel Temp (°F)	830	825	828	828
Expansion of Core Radius (cm)	0.0347	0.0349	0.0364	0.0370
Avg Up Refl Sodium Temp (°F)	881	876	884	884
Reactivity Defects ($-\Delta k \times 10^5$) and Temp Coef ($-\Delta k/\Delta°F$) x 10^5				
Sodium in Core (Δk)	44.7	40.7	43.6	40.8
Sodium in Core ($\Delta k/\Delta°F$)	0.494	0.465	0.481	0.462
Sodium, Up Refl (Δk)	29.6	30.9	40.7	40.1
Sodium, Up Refl ($\Delta k/\Delta°F$)	0.160	0.189	0.223	0.222
Sodium, In Refl (Δk)	5.9	7.2	3.6	3.2
Sodium, Total (Δk)	80.4	79.0	88.2	84.5
Fuel (Δk)	44.6	43.6	42.3	41.5
Fuel ($\Delta k/\Delta°F$)	0.211	0.206	0.200	0.196
Steel Expansion				
Axial (Δk)	8.7	9.1	12.4	17.9
Axial and Radial (Δk)	119.6	118.2	122.0	129.3
Radial (Ih/mil)	3.8	3.4	3.3	3.3
45 MW				
No Radial Exp (Δk)	135.2	138.1	152.1	147.7
Radial Exp (Δk)	255.3	250.3	255.7	253.9

The power coefficients in Table I.E.4 are given in units of $-\Delta k \times 10^5$ or $\Delta k/\Delta°F \times 10^5$ between zero and full power.

The calculated values of the power coefficients for 45-MW operation do not differ greatly in the four runs of EBR-II considered here. There are some small variations of the individual components. The fuel coefficient decreased from Run 16 to 26B while the axial expansion coefficient increased. The sodium coefficient for the upper reflector increased and that for the inner blanket-reflector decreased upon the addition of the steel radial reflector (Run 25 and 26B). The steel-expansion coefficient changes little in these calculations.

Although the calculated value of the power coefficient does not change greatly for Runs 16 through Run 26B, the value of the reactivity defect at full power may be quite different, depending on the nature of the radial movement of the core, reflector, and blanket. For example, the reactivity defect would be considerably larger for a reactor which only expands radially upon going to full power, compared to one which contracts during part of the approach to full power.

Studies are now being conducted to calculate the reactivity effects due to radial expansion and contraction of the core, inner blanket-reflector, and outer blanket.

The above arguments apply to possible changes in the power coefficient due to the "core size" effect. The fact that the power coefficients do not change greatly with core size (or number of core subassemblies) does not mean that the reactivity defect at full power is insensitive to core size. In fact it may be reasoned that the nature of the radial core movement is influenced by the core size. The study of the radial movement also includes investigating core-size effects.

c. Reactor System Testing, Surveillance, and Evaluation (B. C. Cerutti)

Last Reported: ANL-7403, pp. 51-53 (Dec 1967).

(i) Leak-rate Testing of Containment Building. A complete analysis is being made of the containment building penetrations for the secondary sodium pipes, and of the equipment and procedures for leak testing these penetration seals. The annual leak-rate test for these penetrations presently requires that the secondary sodium system be completely drained to storage and the pipe line cooled down before installation of leak-test apparatus. This necessitates a prolonged reactor shutdown and an adverse effect on reactor plant factor. A means for conducting this leak-rate test with the secondary sodium system hot and operative is under investigation.

(ii) Fuel-handling Subassemblies Holddown. After extensive overhaul, the unit was checked for engagement at various core locations, with alignment adjustments being made in an attempt to find a setting that was satisfactory for all reactor positions. This was not entirely successful, as there seems to be a positioning error which increases with distance from the core centerline. This problem was first noted when fuel handling began after the initial filling of the primary tank with sodium. The problem gradually disappeared as clearances in the upper shroud tube increased, but these additional clearances caused dragging in the shroud tube. When the proper clearances in the shroud were restored, the slight misalignment problem at the reactor face returned. Investigation of this problem is in progress and further alignment checks will be conducted when time permits.

(iii) Removal and Replacement of No. 12 Control-rod Thimble. Control rod L-446 (see Sect. I.E.3.a) was inspected in the air cell at the FCF. A series of scratch and rub marks, about 3/8 in. wide and $14\frac{1}{2}$ in. long starting near the top of one flat of the hex, were observed. Two major scratches extend downward to the hex bushing guide, and a single major

scratch extends from that guide downward. The scratches were assumed to have been caused by a deformed area at the top of the control-rod thimble on the flat adjacent to core position 5-C-4.

Subassembly C-2039 was removed from position 5-C-4 and inspected in the FCF Air Cell after greater than normal force was required to lift it in its grid position. The flat of this subassembly adjacent to the thimble in position 5-C-3 had been heavily scratched. Light scratches were visible on the three flats of the subassembly opposite the thimble.

The scratches on the control rod and the adjacent subassembly and the results of the gauging accomplished using specially designed fixtures operated through the auxiliary gripper hole pointed conclusively to a damaged control-rod thimble in position 5-C-3. The thimble was removed from this position and found to be damaged at the top of the flat which was adjacent to position 5-C-4. The dimensions of the deformation are shown in Fig. I.E.9.

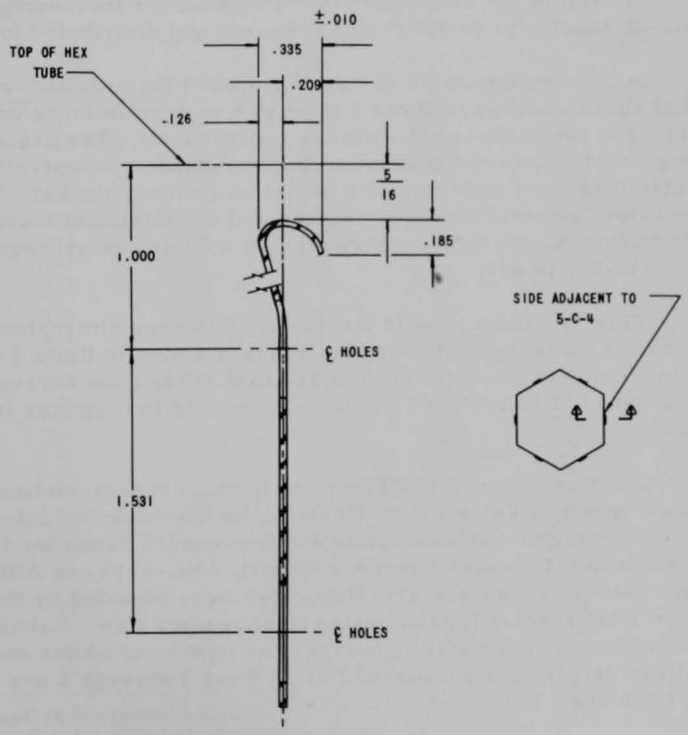

Fig. I.E.9. Dimensions of Deformation of Control-rod Thimble Removed from Reactor Grid Position 5-C-3

(iv) Rotating Plugs. Surveillance of the large and small rotating-plug-seal system continued. The entire large plug trough and a 30° section of the small plug trough were cleaned. Eighty-one pounds of dross were removed from the large plug trough and 6 lb from the small plug trough.

Samples of black powder from both plugs are to be analyzed. Several blade thermocouples were replaced or repaired.

d. Higher Power Operation (R. E. Rice)

Last Reported: ANL-7403, p. 54 (Dec 1967).

The first 70%-enriched driver-fuel subassembly was completed and placed in reactor grid position 4-B-1. The subassembly contains 19 fuel elements enriched to 70%, located in the center of the subassembly and surrounded by standard Mark-IA driver-fuel elements.

A draft of the revision of the "Proposal for Increasing the Power of the EBR-II Reactor to 50 MWt" was prepared and distributed for comment.

A plant modification has been proposed for reorificing the driver-fuel subassemblies in Rows 1 through 6 to provide more uniform temperatures in the subassemblies in the reactor core. The proposed reorificing would reduce the maximum fuel and cladding temperatures with either a stainless steel reflector or a depleted-uranium blanket. The maximum power-to-flow ratio would be reduced and the minimum increased. The more uniform temperature distribution is a desirable prerequisite to operation at higher power.

This reorificing would involve the following dimensional changes: upper-row inlet holes in the driver-fuel subassemblies in Rows 1 through 5 would be increased in diameter from 0.314 to 0.359 in.; the corresponding holes in subassemblies in Row 6 would be increased in diameter from 0.259 to 0.297 in.

The flow rates of 800°F sodium through subassemblies in Rows 1 through 6 are given in Table I.E.5. These flows are based on out-of-pile calibration of prototype subassemblies at the pressure drops for the various rows given in the Hazard Summary Report, ANL-5719 and ANL-5719 Addendum. Individual subassembly flow rates were adjusted by the ratio of measured total reactor flow to design total reactor flow. Calculated maximum fuel temperatures at higher reactor power levels for standard and reorificed driver-fuel subassemblies in Rows 1 through 6 are given in Tables I.E.6 and I.E.7.

TABLE I.E.5. Subassembly Flow Rates at 800°F

S/A Type and Location		Stainless Steel Reflector		Uranium Reflector		Design Flow at 41 psi (ANL-5719 Addendum)		
Row	Type	Standard S/A's (gpm)	Reorificed S/A's (gpm)	Standard S/A's (gpm)	Reorificed S/A's (gpm)	Standard S/A's (gpm)	Reorificed* S/A's (gpm)	Ratio
1, 2	Driver	151	141	141	131	141	141	1.0
3	Driver	133	131	124	122	124	131	1.057
4	Driver	97.6	102	91	95	91	102	1.122
5	Driver	82.6	90	77	83.6	77	90	1.170
6	Driver	71.4	78	66.5	72.5	66.5	78	1.173
3	Safety	90.6	84.5	84.5	78.5			
5	Control	64.4	60	60	55.8			

*These flows and ratios are for the 41 psi ΔP of the original design. Actually total flow will not change and ΔP inlet to outlet will be slightly less.

TABLE I.E.6. Temperatures at 50-MWt Reactor Power

Row[a]		Flow (gpm)	Fuel (°F) Center	Radial Avg	Surface	Clad ID	Sodium Outlet (°F)
1	a	151	1040	984	933	915	865
	b	141	1052	996	945	927	877
	c	141	1043	988	940	922	873
	d	131	1056	1001	953	935	886
2	a	151	1038	982	932	912	864
	b	141	1050	994	944	924	876
	c	141	1042	986	940	922	872
	d	131	1055	999	958	935	885
3	a	133	1048	993	947	928	881
	b	131	1052	997	951	932	884
	c	124	1051	999	953	937	889
	d	122	1054	1002	956	940	892
4	a	97.6	1078	1033	992	975	927
	b	102	1068	1023	982	965	917
	c	91	1085	1040	1000	984	937
	d	95	1075	1030	990	974	927
5	a	82.6	1054	1014	978	964	921
	b	90	1036	996	960	946	903
	c	77	1073	1037	1002	986	946
	d	83.6	1054	1018	983	977	937
6	a	71.4	1049	1017	986	974	936
	b	78	1029	997	966	954	916
	c	66.5	1044	1014	984	972	937
	d	72.5	1025	995	965	953	918

[a] a--Standard driver-fuel subassembly, stainless reflector.
b--Reorificed driver-fuel subassembly, stainless reflector.
c--Standard driver-fuel subassembly, uranium inner blanket.
d--Reorificed driver-fuel subassembly, uranium inner blanket.

TABLE I.E.7. Temperatures at 62.5-MWt Reactor Power

Row[a]		Flow (gpm)	Fuel (°F) Center	Radial Avg	Surface	Clad ID	Sodium Outlet (°F)
1	a	151	1125	1055	992	969	906
	b	141	1140	1070	1107	984	921
	c	141	1123	1060	1000	978	916
	d	131	1145	1077	1016	994	933
2	a	151	1123	1053	990	965	905
	b	141	1138	1068	1005	980	920
	c	141	1128	1058	1000	978	915
	d	131	1144	1074	1017	994	931
3	a	133	1135	1067	1009	985	926
	b	131	1140	1071	1014	990	930
	c	124	1139	1074	1016	997	937
	d	122	1143	1078	1020	1000	940
4	a	97.6	1173	1116	1065	1044	984
	b	102	1160	1104	1053	1031	971
	c	91	1182	1125	1075	1055	997
	d	95	1169	1113	1063	1043	984
5	a	82.6	1143	1093	1048	1030	977
	b	90	1120	1070	1025	1008	954
	c	77	1166	1121	1078	1058	1008
	d	83.6	1143	1098	1054	1047	996
6	a	71.4	1137	1096	1057	1043	995
	b	78	1111	1071	1032	1018	970
	c	66.5	1130	1093	1055	1040	996
	d	72.5	1107	1069	1031	1016	973

[a]a--Standard driver-fuel subassembly, stainless reflector.
b--Reorificed driver-fuel subassembly, stainless reflector.
c--Standard driver-fuel subassembly, uranium inner blanket.
d--Reorificed driver-fuel subassembly, uranium inner blanket.

e. Fuel Swelling and Driver Surveillance

(i) Mark IA--Investigation of Anomalous Fuel Swelling (F. G. Foote and K. F Smith)

Last Reported: ANL-7403, pp. 54-59 (Dec 1967).

(a) Extended Burnup of MC-S-type Fuel Pins. Fuel-pin swelling has been determined on fuel elements taken from Subassembly C-292. Twenty-two pins from casting batch 4137 (MC-S-3) showed an average swelling of 4.64% at an average burnup of 1.03% (1.155% max). Seventeen pins from casting batch 4142 (MC-S-4) showed an average swelling of 4.96% at the same burnup. Pins from casting batches 4135, 4136, 4139, and 4140 (all MR-type melts) showed swellings ranging from 9.2 to 15.2%, that is, some two to three times the swelling of the MC-S-type fuel. Subassembly C-291, which contains only pins from low-swelling casting batches 4137 and 4142, is being held in the fuel-transfer storage basket for possible reinsertion in the core for additional burnup.

(b) High-burnup Irradiations of Mark-IA Fuel in EBR-II. Seven encapsulated fuel elements in experimental irradiation Subassemblies XO15 and XO17 remain in the core, and will be further irradiated during reactor Run 27.

(c) Effect of the Change to Mark-IA Design upon Fuel Swelling. Sodium levels in fuel elements from Subassemblies C-297 and C-298 are being measured.

(d) Effect of Enrichment Increase from 48% (Mark I) to 52% (Mark IA). Subassembly C-283 contained Mark-IA fuel elements, approximately half of which were of 48% enrichment and half of 52%. This subassembly was irradiated in Reactor Grid Position 1-A-1 in a highly uniform flux. Fuel swelling has been calculated from measured changes in sodium level. The results are summarized in Table I.E.8. On the average, these numbers seem to indicate that fuel with higher enrichment swells less than fuel with lower enrichment, although there is considerable overlap of casting batches 0301 and 4129. Pins from casting batch 4108, made from virgin metals, show appreciably less swelling than pins from either of the regular melt-refining ingots. Fuel-element temperatures are not yet available.

TABLE I.E.8. Effect of Fuel Enrichment upon Swelling

Fuel Enrichment (%)	Number of Elements	Casting Batch	Melt Refining Number	Calculated Burnup (%)		Percent Swelling	
				Max	Avg	Range	Avg
48	45	0301	MR-99	1.15	1.02	6.53-12.41	9.84
52	38	4129	MR-93	1.25	1.11	5.14-10.82	8.47
52	7	4108	EUF-21B	1.25	1.11	5.30- 6.62	5.97

These results are somewhat unexpected in that the pins of lower enrichment, operating presumably at a lower temperature and to a lower burnup, swell somewhat more than those operating at higher temperature and to a higher burnup. However, it was realized in setting up the experiment that it is difficult to prepare melts that differ only in fuel enrichment. In particular, trace-element impurities vary from melt to melt and may have a greater influence upon swelling behavior than does enrichment. Specimens of these casting batches are being chemically analyzed. Preliminary results indicate that the alloy swelling least (4108) contains 175 ppm silicon, and that the alloy swelling most (0301) contains only 120 ppm.

A second subassembly containing a different assortment of casting batches has reached target burnup but has not yet been disassembled.

(e) Effect of Position and Orientation in the Casting Bundle upon Fuel Swelling. Subassembly C-2035 reached target burnup at the end of reactor Run 26 but has not yet been disassembled.

(f) Effect of Trace-element Impurities upon Fuel Swelling. Subassembly C-2111, suspected of containing a leaking fuel element, has been disassembled and the fuel elements examined. No fuel-jacket leaks were found. So far no leaking fuel elements have been found in either Subassemblies C-2111 or C-2113. Detailed examinations continue.

(g) Effect of Pressure upon Swelling of U-5 w/o Fs Alloy. Density measurements of fuel-pin sections that were irradiated in Capsule P-2 to an estimated burnup of 1.8% have been completed. Table I.E.9 gives the data.

TABLE I.E.9. Density Data for P-2 Pressure Specimens Undergoing Estimated 1.8 a/o Burnup

Specimen Number	Cast Pin Number[a]	Mean In-reactor Fuel Temp (°C)	Mean[b] In-reactor Pressure (psia)	Preirradiation Density (g/cc)	Postirradiation Density, Avg of 3 (g/cc)	% $\Delta V/V$[c]
1	53-4	582	2060	18.02	14.94	20.6
2	-10	549	1140	18.03	13.21	36.5
3	-6	582	600[d]	18.01	9.45	90.6
4	-12	549	211	18.03	9.89	82.3
5	-2	582	148	18.01	8.63	108.6
6	-8	549	108	18.05	9.01	100.3

[a]All of Melt No. 409.
[b]Effects of fuel swelling and gas evolution are not included.
[c]Calculated from density change.
[d]Pressure to clad rupture only.

A graph of % $\Delta V/V$ versus in-reactor ambient pressure for both P-1 and P-2 fuel pins appears in Fig. I.E.10. The trend toward reduced swelling for higher pressure is evident in both test series. The

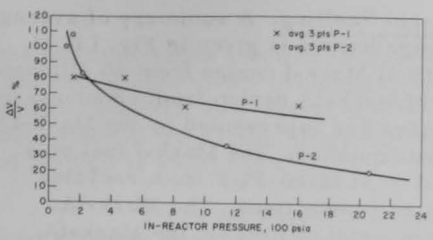

Fig. I.E.10. Swelling vs. In-reactor Pressure

scatter for the P-2 points is much less than that for P-1 because of better specimen condition in P-2.

Capsule P-3 is to be subjected to postirradiation examination shortly.

(h) Effect of Heat Treatment upon Swelling of U-5 w/o Fs Alloy. Table I.E.10 gives the identifications, heat treatments, and irradiation parameters of the three capsules of this test series. These test specimens are being irradiated without restraining jackets.

TABLE I.E.10. Schedule of Heat Treatments for U-5 Fs Specimens To Be Irradiated in Capsules in CP-5

Position in Capsule	Capsule Number	Cast Pin Number	Melt Number	Heat Treatment	Ambient Pressure	Target Fuel Temp (°C)
1	H-1	56-2	409	As cast	~Atmospheric	~600
2		-1	409	1 hr @ 500°C, A.C.[a]		
3		-3	409	2 hr @ 980°C, W.Q.[b]		
4		-5	409	2 hr @ 980°C, W.Q., 1 hr @ 500°C, A.C.		
5		-6	409	16 hr @ 740°C, W.Q.		
6		-8	409	16 hr @ 740°C, W.Q., 1 hr @ 500°C, A.C.		
1	H-2	13-1	0450SR	As cast	~Atmospheric	~600
2		-2	0450SR	1 hr @ 500°C, A.C.		
3		-3	0450SR	2 hr @ 900°C, W.Q.		
4		-5	0450SR	2 hr @ 900°C, W.Q., 1 hr @ 500°C, A.C.		
5		-6	0450SR	16 hr @ 740°C, W.Q.		
6		-8	0450SR	16 hr @ 740°C, W.Q., 1 hr @ 500°C, A.C.		
1	H-3	63-1[c]	409	1 hr @ 500°C, A.C.	~Atmospheric	~600
2		-12	409	1 hr @ 500°C, A.C.		
3		29-1[c]	0450SR	1 hr @ 500°C, A.C.		
4		-12	0450SR	1 hr @ 500°C, A.C.		
5		-2	0450SR	2 hr @ 900°C, W.Q., 1 hr @ 500°C, A.C.		
6		-11	0450SR	2 hr @ 900°C, W.Q., 1 hr @ 500°C, A.C.		

[a]A.C. = air cooled.
[b]W.Q. = water quenched.
[c]In Table II.E.8, p. 57, of ANL-7403 (Dec 1967), the cast pin numbers were reported as 54 instead of 63, and 47 instead of 29. The pins first selected for this capsule were radiographed and found to contain voids which made them unacceptable.

Capsule H-1 reached an estimated burnup of 1.2% and was removed from CP-5. Preliminary examination of the specimens revealed no marked effect of heat treatment. All of the specimens had about the same appearance, with some surface cracking, and all increased in volume approximately 65%. More detailed examination is in progress.

Capsule H-2 is accumulating burnup and is scheduled for removal from CP-5 about February 1, 1968. Capsule H-3 is being assembled.

(i) Hot Laboratory Examination of Irradiated Fuel

(1) Fuel Surveillance. Sodium-level measurements have been completed on approximately 450 driver fuel elements removed from EBR-II at the end of reactor Run 25. Calculation of fuel swelling has been completed on 247 of these, taken from ten different subassemblies and representing 38 different casting batches. The swelling results are being tabulated and evaluated.

(j) Analysis of Fuel-pin Swelling. A summary of average fuel-pin swelling as a function of average burnup is given in Fig. I.E.11. Results are available for 1124 fuel pins of Mark-I design from 60 different subassemblies and for 1446 fuel pins of Mark-IA design from 68 subassemblies. Some 132 different casting batches are represented by the Mark-IA fuel elements. Four fuel types are distinguished. The Mark-I fuel pins were cast at Illinois from virgin metal or at Idaho-FCF from recycled fuel pins. The results are reasonably self-consistent. The Mark-IA, SL-type fuel pins were cast from virgin metal at Illinois; the Mark-IA, MR-type at Idaho-FCF from clean recycled fuel; and the Mark-IA, MRC-type at Idaho-FCF from scrap pin and casting heels. The plotted points represent the average swelling and burnup of at least five pins of a given melt irradiated in a given subassembly.

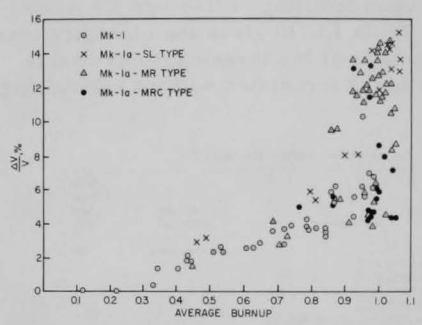

Fig. I.E.11. Swelling of EBR-II Driver Fuel as a Function of Average Burnup

The SL-type fuel in the Mark-IA design swells to a greater extent than the Mark-I, although the difference in behavior is appreciable only beyond about 0.75% average burnup. Most of the MR-type fuel swells to a greater extent than does the Mark-I fuel and to about the same degree as the SL-type fuel. However, an appreciable number (30%) of the MR-type fuel pins swell no more than the Mark-I fuel pins and, in some cases, considerably less. Most of the MRC-type fuel swells to about the same or to a lesser extent than the Mark-I fuel, although a few melts (20%) swell to about the same extent as the MR-type and SL-type fuel. The general conclusion is that factors other than the fuel source and fuel-element design are affecting the swelling behavior.

(ii) Thermal Conductivity of Irradiated Mark-IA Fuel (H. Berger)

The thermal conductivities of several specimens cut from irradiated U-5 w/o Fs EBR-II driver fuel pins (Types MRC, MR, and SL) have been determined. For each specimen, burnup, swelling and irradiation temperature of the surface, and center and center of mass have been calculated so that the effects of those parameters on the postirradiation value of the thermal conductivity could be evaluated.

A relation was found between the percentage decrease in conductivity with irradiation and swelling. This relation involves the three types of EBR-II driver fuel investigated and indicates that, despite the different swelling characteristics of the three, it is possible to predict

the postirradiation thermal properties of V-5 w/o Fs from the swelling. The dependence of the conductivity on the swelling means that the loss in conductivity will be greatest, not at the region where the burnup is greatest, but rather at the region where the center-of-mass irradiation temperature of the fuel is about 515°C.

Fuel Type SL had the largest losses of conductivity. A 30% loss of conductivity was accompanied by a 14.1% swelling at a burnup of 0.9 a/o and a center-of-mass irradiation temperature of 517°C. A specimen from fuel Type MRC had a 10% loss in conductivity for a 4% swelling at a burnup of 0.8 a/o and a center-of-mass irradiation temperature of 484°C.

The porosity volume was calculated for each specimen, and the conductivity calculated by means of several porosity-corrected formulas. Reasonably good agreement with the experimental results was achieved with a modified Maxwell-Eucken equation:*

$$K_P = K_{100} \frac{(1 - P)}{(1 - \beta)P},$$

where

P = pore volume;

K_{100} = conductivity of solid material;

K_P = conductivity of material with pores.

β is an empirical constant that can vary from 0.5 to 1.5 and is dependent on pore shape.

(iii) EBR-II Mark-IA TREAT Experiments (P. J. Persiani)

A series of TREAT experiments is being planned for irradiated Mark-IA fuel elements. The objective of the experiments are:

1. to check the dimensional stability of Mark-IA fuel up to and including failure;

2. to check possible changes in failure thresholds, from the known Mark-I behavior, for "high swelling" type Mark-IA fuel;

3. to attempt measurement of axial fuel movement during transient experiments.

The experiments are planned to include selected irradiated fuel elements which are representative of varying degrees of swelling. This

*Spalle, L. et al., Thermal Conductivity of Bulk Oxide Fuels, WAPD-TM-586 (1967).

will allow observing the effect of overpower conditions on the dimensional stability of the element for several different entrapping conditions of the sodium, and possibly the redistribution of fuel material within the fuel clad. The experiments planned are:

A. "High swelling" fuel:

1. Dry Transparent--Plan so as to obtain fuel centerline-to-surface temperature differences of ~70°C during transient. Instrument with (i) high-speed cameras to detect failure times, modes, and locations, (ii) fast-response cladding thermocouples, and (if possible) (iii) fuel-motion detectors. The following runs are planned:

(a) 1 pin, 2 transients, max fuel temperature ~700-800°C;
(b) 1 pin, 2 transients, max fuel temperature ~800°C; then just over estimated failure threshold;
(c) repeat (b).

2. Loop (single pin inside ring of 6 dummies, in Mark-I package loop):

(a) 1 pin, "flattop" transient ~10-15 sec, power at about 125% of design, constant flow;
(b) 1 pin, "flattop" at design power and flow, then simulate flow decay with scram.

B. "Low swelling" fuel:

1. Repeat 1(b) and 1(c) of "high swelling" fuel.

2. Repeat more of the experiments described in A, if necessary.

The main effort has been in preparation for the first transient TREAT irradiations of "high swelling" EBR-II Mark-IA fuel irradiated to 1.2 a/o max burnup in EBR-II. Sample capsules for a calibration run and for actual transients have been prepared.* Bench-top tests have been performed to check out preheating techniques. Current settings have been established for adequate preheating in a capsule mockup to melt the long sodium plug in the plenum above the fuel. Electrical connections (to the sample pin) suitable for remote attachment with manipulators have been made and tested, and a variable step-down transformer matched to the low-voltage high-current load has been assembled. Two slot liners, the

*Reactor Development Progress Report for November 1967, ANL-7399, p. 162.

sealed steel boxes which hold the capsules proper in the TREAT viewing slot, have been partially disassembled for modification of the slot liner electrical leads.

f. Mark-II Driver Fuel Element Development (M. A. Pugacz)

Last Reported: ANL-7403, p. 60 (Dec 1967).

The XO29 Subassembly containing fuel elements of Mark-II design, of 24- and 26-in. lengths, have been installed in EBR-II.

The redesign of the stagnant sodium TREAT capsule for irradiations of fuel elements of Mark-II design has recently been completed and is in the process of being reviewed for acceptability in the TREAT reactor before being released for manufacture.

g. Equipment--Fuel Related (E. Hutter)

(i) Improved Gripper and Holddown Force-limit Device

Last Reported: ANL-7403, pp. 60-61 (Dec 1967).

In the continuing tests of the prototype improved gripper and holddown force-limit device, the drive motor was mounted on the test rig and operated using the speed controller. The test rig performed satisfactorily, producing several thousand pounds of push and pull forces with no difficulty. The force could not be measured accurately because the new force gauge read erroneously; the readings were low by a factor of three or four. The gauge has been returned to the manufacturer for correction.

High-frequency (above 30 kHz) spurious oscillations in the prototype electronic control system were eliminated by decreasing the bandwidth of the amplifiers, but the resulting bandwidth still exceeds minimum requirements.

The servomechanisms used to store packing-gland-friction values tended to oscillate 60 cps between adjacent wires of the wire-wound feedback potentiometers. The amplitude of this oscillation represents approximately 12 lb of force, well within the acceptable tolerance of 50 lb. However, the oscillations occasionally produce an indicated force correction greater than 50 lb when power is turned off at the end of a calibration period. The manufacturer has indicated that servo hunting of this nature should not occur and that the units may be defective. However, a fail-safe brake that would lock the servo in position before power is shut off might ensure operation within tolerance. The control circuits are being revised to include control for such a brake and to provide a way to check the position of the servos immediately after power is removed.

(ii) New Control-rod Subassemblies

Last Reported: ANL-7403, p. 61 (Dec 1967).

(a) Control Rod of Greater Worth. A design technique proposed for the alternate-type absorber-follower control rod would use fuel elements similar to those now in use in the EBR-II control rods and would add seven boron carbide elements at the top of the control rod. The boron carbide elements would be suspended from a grid-support assembly and would be either welded in place or hung with T-bar grid-type element tips immediately below the top adapter. The proposed poison element would be approximately 34 in. long. The top 14 in. would be gas space to accommodate the released helium; the middle 10 in. would contain stainless steel shielding; the bottom 10 in. would contain ten 1-in. of boron carbide pellets. The boron carbide elements would be assembled as part of the upper preassembly (the fuel elements are assembled as part of the lower preassembly). This packaging technique would simplify disassembly and enable the boron carbide element bundle to be reused with a second control-rod fuel-element loading.

(iii) Oscillator Rod Mark II

Last Reported: ANL-7403, pp. 61-63 (Dec 1967).

Approval has been received to fabricate the following components for the Mark-IIA oscillator: bearing-carrier assembly, special guide tube, storage-basket adapter sleeve, and sleeve-handling tool. A Type-4 oscillator rod section is being designed to be used with these.

(iv) Engineering Consultation

Last Reported: ANL-7403, p. 63 (Dec 1967).

(a) Power Coefficient. Since the improved version of the BOW code* for calculating thermally induced subassembly movements became operational, about 30 problems have been solved in which various combinations of temperature distributions, subassembly bending stiffnesses, subassembly squashing stiffnesses, nominal subassembly spacer-dimple gaps, and subassembly zero-power leans were employed. The object was to find a combination of parameters that would make the calculations agree well with observed reactivity changes. Only then would it be meaningful to evaluate possible reactor modifications that might improve the power coefficient.

*Bump, T. R., Effect of Reactor Temperatures on Bowing of EBR-II Subassemblies, Trans. Am. Nucl. Soc. 10(2): 661-662 (Nov 1967).

Among the combinations tried, the best agreement with observed data was obtained with (1) temperature distributions similar to those used for many months in these studies,* (2) bending stiffnesses uniform throughout the reactor and based on the stiffness of the subassembly hexagonal tube alone (apparently the stainless steel reflector subassemblies act no more stiffly than any of the other subassemblies), (3) squashing stiffnesses at the low end of the calculable range, and (4) zero zero-power lean. With this combination, the calculated values of reactivity caused by subassembly movements are as shown by the curves in Fig. I.E.12; the data points indicate the nonlinear reactivity component derived from experiment (see Progress Report for September 1967, ANL-7382, p. 21). The calculated values were obtained by applying suitable reactivity coefficients ($\Delta k/\Delta r$) to the calculated movements of the subassemblies in Rows 6, 7, 8, and 9. Row 6 represented the core outer diameter; Rows 7 and 8 consisted of blanket subassemblies during Run 24 and reflector subassemblies during Run 25; Row 9 consisted of blanket subassemblies.

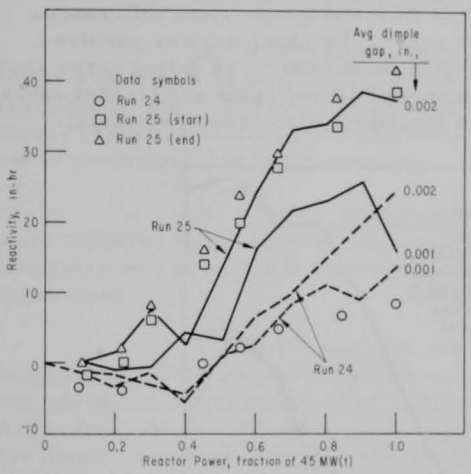

Fig. I.E.12. Top and Bottom Curves Show How Well BOW-code Calculations Using Best Combination of Parameters Agree with Experimental Data. Two middle curves show calculated effect of dimple gap on reactivity.

As Fig. I.E.12 shows, we obtained good agreement with the experiment by using average dimple gaps of 0.001 in. during Run 24 and 0.002 in. during Run 25. This is consistent with experimental evidence (see Progress Report for November 1967, ANL-7399, pp. 55-56) that the dimensions across the dimples are continuously decreasing with time, apparently because of loads exerted on the dimples by the bowing subassemblies. The calculated load on each core dimple during Run 25 at MWt is 23 lb, which is potentially high enough to cause the dimpled regions of the subassembly hex tubes to yield. Additional experimental evidence that the dimple dimensions decrease (gaps increase) with time is the increase of the positive reactivity component from Runs 25 to 26.

Calculated values of reactivity caused by subassembly movements are shown in Fig. I.E.13 for various reactor modifications that might improve the power coefficient. The heavy solid curve, which is for

*Cushman, R. A., The Effect of Radial Heat Transfer on the Temperature Distribution in EBR-II Stainless Steel Reflector Subassemblies, Trans. Am. Nucl. Soc. 10(2), 661 (Nov 1967).

reference, is the same as in Fig. I.E.12 for Run 25 with 0.002-in. dimple gaps. The light solid and long-dash curves represent cases in which there are reflector subassemblies in three and four rows, respectively, instead of the two rows employed in Run 25; the calculations assume that the top of the outboard row of reflector subassemblies (either Row 9 or 10) bows inward in much the same manner as the top of Row 8 is believed to have acted during Run 25. Although the addition of one or two rows of reflector subassemblies apparently would reduce positive reactivity somewhat, the other modifications considered appear more promising. For instance, the heavy-dash curve is for a case in which the reflector subassemblies in Rows 7 and 8 are reorificed to reduce flow and temperature differences across flats. Apparently this would practically eliminate any positive-reactivity component from subassembly movement. The dotted curve shows the case in which the bending stiffnesses of all reflector and blanket subassemblies are reduced by a factor of ten, which also seems beneficial.

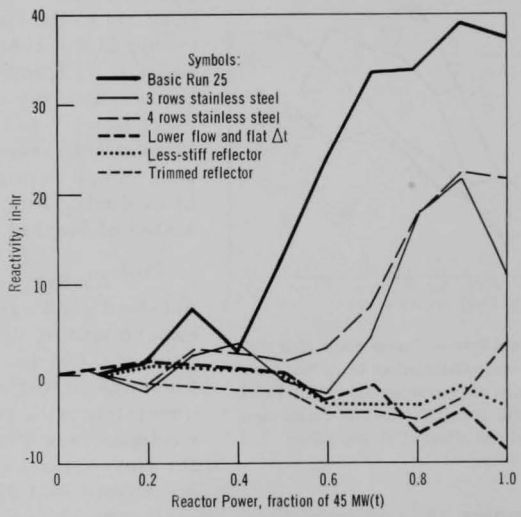

Fig. I.E.13. How Various Modifications to Reflector Subassemblies Would Have Affected Reactivity during Run 25 (as calculated by BOW code at 0.1 power fraction increments)

The light-dash curve is for the case in which enough material (0.065 in. on the radius) is removed from the tops of all reflector and blanket subassemblies that their tops do not touch until a power fraction of 0.5 is reached; although this would be beneficial at low powers, a positive reactivity component is introduced when power rises above 0.8. Thus, if material is removed to improve the power coefficient, the maximum power the reactor can reach, even during abnormalities, must be considered.

Other possible modifications are being studied to help determine whether reorificing, stiffness reduction, or material removal, or a combination of the three, should be used to improve the power coefficient.

h. Equipment--Reactor and Primary Coolant System (B. C. Cerutti)

Last Reported: ANL-7403, pp. 63-64 (Dec 1967).

(i) General Improvements

(a) FERD Loop Plugging Meter and Sampler. A new power supply for the pump in the FERD loop sampling system is being fabricated. The pump is designed to operate on 600 Amp. The power supply presently in use provides 200 Amp. The new power supply should aid in promoting flow in the system.

(b) Reactor Argon-supply System. Two argon totalizers were installed in the reactor argon-supply system. The addition of these totalizers will greatly aid in locating leaks and minimizing the amount of argon used.

The sources of reactor argon are the liquid argon supply in the FCF and the manifold of compressed-argon bottles in the reactor-building basement. The latter source is for emergency use only. Argon from these sources is piped to two lines in the reactor building: the mezzanine argon manifold and the reactor-floor service line. These two lines have now been made completely independent by the installation of a pressure regulator and argon totalizer in each line.

Two NaK vapor traps and a NaK scrubber were removed from the system because they are not needed. The original design assumed that the source of argon would be gas bottles which contain traces of moisture, but the argon supplied in liquid form has no moisture.

(ii) Sodium Sampling Pump and Filter. Initial tests of the pump and filter (without the filter screen) in the water loop were successful and confirmed the original hydrodynamic calculations for sizing the valve components in the removable pump. These calculations had established (1) the valve opening that would produce satisfactory flow past the filter valve and (2) the leakage past the pump piston. A 30-mesh stainless steel filter of 0.013-in.-dia wire will be installed in the filter assembly, and various minor improvements will be made to the pump drive. A short endurance test will be conducted in the water loop.

(iii) Intermediate Heat Exchanger Seal

Last Reported: ANL-7391, p. 85 (Oct 1967).

The new set of baffles has been completed and installed in the test fixture. We are studying whether the reliability of a single continuous-strip baffle would be an improvement over many individual baffles. The strip of Inconel-X baffle would be formed and partially slit to produce the same effect as many individual baffles.

i. Secondary Sodium and Power Systems (B. C. Cerutti)

Last Reported: ANL-7403, p. 64 (Dec 1967).

(i) General Improvements

(a) Servo-actuated Systems. The secondary sodium and power plant systems were reviewed to identify those components employing servo-actuated (recorder-actuated) devices for control and/or alarm functions. More than 30 systems were identified in the review. Conceptual redesigns of the systems were prepared for review by the Operating and Engineering Group and for budgetary purposes.

The boiler-water-level system is the system most dependent on servo-actuated functions. Action was initiated to eliminate the servo functions by replacement with separate static devices.

j. New Subassemblies Design and Experimental Support (E. Hutter)

(i) Mark-II Core Development

Last Reported: ANL-7403, p. 65 (Dec 1967).

(a) Fuel Subassembly. Detailed information on the Mark-IIA (26-in. element) fuel subassembly is being compiled for the AEC before the first group of subassemblies to be placed in the reactor is fabricated.

A major problem may be the long time (1 yr) involved in obtaining Vycor fuel molds and fuel-element jacket tubing, and in modifying assembly-line inspection devices to accept the longer elements. The time required to procure hardware for the fuel elements and subassemblies may further complicate the situation.

Hydraulic tests of the Mark-IIA blanket-region core subassembly have been completed. As predicted, the results were identical to those of previous tests on the original blanket-region core subassembly.

(ii) Irradiation Subassemblies

Last Reported: ANL-7399, p. 70 (Nov 1967).

(a) Mark F. A new subassembly, Mark F37, has been designed to meet the needs of experimenters for an irradiation subassembly that has 37 fuel elements, each of which is 0.250 in. in outside diameter. The center-to-center pitch between elements is 1.25 times the outside diameter of the elements. The external structure of this subassembly is of the standard-size hexagonal configuration. After the design is reviewed and approved, a dummy will be built for hydraulic tests to confirm that the flow and pressure-drop characteristics match those of the standard EBR-II core subassemblies. If experimenters desire to irradiate the Mark-F37 subassembly in blanket locations, additional units will be tested.

k. Instrumented Subassembly (E. Hutter)

Last Reported: ANL-7403, pp. 65-66 (Dec 1967).

(i) Design

(a) Subassembly Attachment and Lead Severance. Uncoupling tests of the top-end-fixture test gripper have been performed in both room-temperature air and hot sodium. For the tests, a subassembly top-end-fixture adapter was fastened to the bottom of a sodium test pot, and the test gripper was installed through the cover by means of packing glands. A dynamometer determined the force needed to uncouple the adapter. Initially, the test gripper was uncoupled a number of times in room-temperature air; the uncoupling force was 15 lb, with little variation between uncouplings.

Uncoupling tests were then performed in sodium at 500 to 900°F in steps of 100°F. The force required for 25 uncoupling operations varied between 6 and 10 lb, probably because of variation in the packing-gland pressure during each uncoupling. A second type of sodium test was performed in which the top end fixture was purposely misaligned from the gripper by 1/16 in. (the radial clearance between the coupling and the drywell liner). Results of these tests, which were conducted in 700°F sodium, were identical to those obtained without the misalignment.

l. Packaged Loop (B. C. Cerutti)

Last Reported: ANL-7403, p. 66 (Dec 1967).

An interim report concerning the feasibility of the package loop is being prepared.

m. Process Chemistry (D. W. Cissel)

Last Reported: ANL-7403, pp. 67-68 (Dec 1967).

(i) Sodium Coolant Quality Monitoring and Control

(a) Primary Sodium

(1) Studies of Cesium Segregation. A sample of primary sodium taken in an extrusion vessel was stirred electromagnetically as it was cooled and frozen. The sample was partitioned and analyzed by the method reported in Progress Report for June 1967, ANL-7349, pp. 37-39. Despite the fact that the electric current through the sodium was approximately 40 times greater than in a previous, stirred sample, the cesium segregation was nearly identical (see Progress Report for Oct 1967, ANL-7391, p. 91).

No further cesium segregation studies are planned. Future efforts will be directed toward sampling methods which will circumvent segregation problems by analysis of the total sample.

(2) Trace-metal Impurities. Two primary sodium samples were analyzed for trace-metal impurities by atomic absorption, with the following results:

	Sample Date			Sample Date	
Metal Impurity	10/24/67	11/17/67	Metal Impurity	10/24/67	11/17/67
Co	<0.7 ppm	<0.7 ppm	Cr	<2.0 ppm	<2.0 ppm
Mn	<0.3	<0.3	Bi	2.5	3.5
Ni	<0.3	<0.3	Ca	<2.0	<2.0
Fe	6.0	3.0	Sn	13.0	15.6
Cu	0.4	0.4	Al	<4.0	<4.0
Mg	1.4	1.1			

(b) Expanded Sampling Capabilities for Primary and Secondary Sodium

(1) Primary Sodium. Design was completed and fabrication started of a cup-and-spigot sampler for the sampling system in the FERD loop. The preliminary design of a sampler which will facilitate taking ~1-g samples in quartz vials was completed. If samples can be taken without contamination, this method should circumvent problems associated with carbon segregation by permitting analysis of the total sample.

n. Experimental Irradiation and Testing

Last Reported: ANL-7403, pp. 68-75 (Dec 1967).

(i) Experimental Irradiations (D. W. Cissel)

(a) Status of Experiments in EBR-II. No exposure time was added during January. Experimental Subassemblies XO29 and XO33 were loaded as planned into grid positions 4-E-3 and 5-E-2, respectively.

(b) Status of Irradiation Experiment Proposals Given Administrative Approval-in-Principle (AIP). There has been no change from that given in Table II.E.14, p. 71 of ANL-7403, Dec 1967.

(c) Other Work. In a continuing study of the use of melt wires for temperature measurements, a Type 304 stainless steel capsule containing seven melt-wire specimens was heated at 1100°F for 129 hr. A metallurgical examination showed that extensive interaction had occurred between the stainless steel and all melt-wire materials except silver-antimony.

A capsule with tantalum liner cups to contain the melt wires will be prepared and tested, upon the procurement of the necessary cups. A stainless steel capsule similar to the one previously tested will be prepared and heated at a lower temperature for further observation of interaction effects.

(ii) Nondestructive Testing (D. W. Cissel)

(a) Capsule Examination. At the request of General Electric, its structural irradiation Capsule OB from Group L-15 was rewelded at the lower end fitting to correct a faulty weld.

(b) Other Nondestructive Testing. The eddy-current flaw detector was completed, and tests are being conducted to relate natural tubing flaws with signal amplitude.

A specification was prepared for the setup and calibration of test equipment, and the ultrasonic testing of stainless steel tubing. Specifications for the ultrasonic equipment required were prepared for submittal to prospective vendors.

(c) Antimony-Beryllium Neutron Source. A document was prepared and submitted for criticality safety approval for installation of the antimony-beryllium source in the FCF argon cell.

(iii) Handling and Examination (D. W. Cissel)

Irradiated Capsules from XO11

(1) Capsules HOV-15, SOV-3, and TVOV-1. Mixed-oxide Capsules HOV-15, SOV-3, and TVOV-1 from experimental Subassembly XO11 were returned to ANL-MET for destructive analysis. Nondestructive inspection had indicated all three capsules to be in satisfactory condition.

(2) Capsules HOV-10, HOV-4, and F4F. Capsules HOV-10, HOV-4, and F4F from experimental Subassembly XO11 contained failed elements. All were returned to their sponsors. An interim inspection report for HOV-10 and HOV-4 was issued by ANL-MET. It is reported that HOV-4 had lost most, if not all, of the bond sodium (about 10 g). The HOV-4 capsule had failed and probably expelled fission products to the reactor primary sodium. HOV-10 showed no indications of failure of its capsule wall. The location of the failure in the capsule wall or welds of HOV-4 has not yet been determined.

Arrangements to check Capsule F4F at high temperature and vacuum and/or pressure are still pending at General Electric. Weight measurements are also planned. During preparation to examine the capsule wall of F4D, GE discovered fission gas between the element and capsule wall in the gas plenum above the bond sodium. Although the nondestructive inspection on this capsule (primarily neutron radiography) showed no signs of any internal failure, the discovery of the fission gas indicated that the element cladding had failed at some point. The location of the failure of F4D is still under investigation.

(b) Testing of Subassembly Sodium Removal Procedures

(1) Cyclical Testing of Types 304L and 304 Stainless Steel Tubing Exposed at 1100°F, Washed in Water, and Stored in Air. The samples of tubing exposed to the sodium, water wash, and storage cycles were mounted for microprobe examination and examined. The sensitivity of the microprobe was inadequate, however, to arrive at conclusive results in detecting sodium in the grain boundaries. Some sodium was detected, but it could not be determined whether it was located in grain boundaries or matrix, or was carried over from surface cleaning.

(2) Cyclical Testing of Stressed Capsules (Type 304 Stainless Steel) at EBR-II. Experimental Subassembly X900 containing the pressure-stressed tubing samples completed its fourth and final soaking cycle in the primary-tank storage basket. The subassembly will be reinserted into the primary sodium after the requested approval for irradiation in a Row-7 grid position has been received. Action is being delayed until the evaluation of the previous cycles is available.

(iv) Safety Review of Experiments (D. W. Cissel)

The irradiation of five driver subassemblies containing Mark-1B fuel elements, and a program for their surveillance, was recommended for approval by the EBR-II Irradiations Review Committee and was approved as irradiation experiments.

(v) Electromagnetic Test Equipment for the In-cave Testing of Sodium Bonds in Irradiated Capsules (C. J. Renken)

Last Reported: ANL-7403, pp. 74-75 (Dec 1967).

Electromagnetic test equipment will be used to check the sodium bonds in capsules that have been temporarily removed from EBR-II for inspection. Considerable development work is required because of the thickness of sodium annuli in the various types of irradiation capsules, up to 2 mm in some cases. The 22.9 m of cable required between the transducer and the rest of the test system in the argon cell of the FCF created another serious problem.

The prototype model of the electromagnetic test system has now been completed. Preliminary tests indicate that the cable-distance problem has been solved. The sensitivity of the system to defects at various depths in the bond layer and its ability to properly indicate how deep a defect lies in the annulus are now being checked with the Mark-A-type capsule. This test system probably will be applied first to the Mark-A capsules in Subassembly XO11. Later, it will be applied to capsules of the B-19, B-37, and B-61 types. All three of these latter types are equipped with an exterior spacer wire that can be expected to degrade the sensitivity of any type of sodium-bond quality test.

o. FCF Process Analysis and Testing (M. J. Feldman)

Last Reported: ANL-7403, pp. 75-76 (Dec 1967).

(i) Test and Analytical Methods. A need exists for the development of satisfactory test methods which can be used to identify possible defective irradiated driver fuel elements returned to the FCF from the EBR-II. One proposed method of identifying the leaking element(s) would be to reirradiate the elements in a controlled atmosphere. This can be done in TREAT. In order to test this procedure, two unirradiated elements with intentional leaks in the top plenum were irradiated in a container in TREAT.

Data obtained from a fuel element with a leak rate equivalent to 7×10^{-6} standard cc of air/sec at 1 atm differential pressure showed that both activated argon and fission gases could be detected in a liquid nitrogen cold trap connected to an evacuated capsule which contained the defected fuel element. Two hours after irradiation at 90 kW for one hour, the principal activity in the cold trap was argon-41, along with an easily detectable amount of xenon-135. Material collected in the cold trap during the period from 2 to 4 hr after reactor shutdown showed an increase in fission gas content relative to argon-41 content. Since the test capsule had been evacuated and filled with helium prior to the irradiation, the only source of argon other than trace amounts was the argon in the gas plenum of the fuel element. Therefore, detection of significant argon-41 after irradiation of the suspect driver fuel pins should be a positive indication of a leak in a pin. However, it cannot be assumed that a leaky pin which has been in the air cell for an extended period of time would contain a detectable amount of argon-41 following the TREAT irradiation.

Data obtained from the two new pins with known defects show that the fission gas release to the gas plenum is time and temperature dependent. In one case, a sudden increase in trap activity was detected after the pin had been held at 250°C for 2 hr after the irradiation. Data from the second pin showed that a temperature well in excess of 300°C was required for several hours to bring about a significant release of fission gas. Since this release was not detected until one hour after the capsule reached a temperature of 400°C, it is believed that the threshold temperature for this pin is about 400°C. It is interesting to note that the operating temperature of the upper plenum region of the elements in EBR-II at 25 MW is about 400°C.

Based on these tests, the following procedure will be used to test the suspect EBR-II driver fuel elements in TREAT:

(1) A group of 10 to 20 fuel elements will be loaded into a test capsule in the air cell at the FCF and transported to TREAT in the EBR-II source coffin.

(2) The group of elements will be irradiated in TREAT to produce fresh fission products and activate the argon in the gas plenums. Prior to the irradiation in TREAT the test capsule will be evacuated and backfilled with helium. The TREAT power level will be limited to a value which does not produce an element-cladding temperature greater than 500°C as indicated by a thermocouple spot-welded to the cladding of a cold-line pin. The first group of pins will be the only group which will contain an element with an attached thermocouple.

(3) Following the irradiation in TREAT the test capsule will be transferred to a shielded furnace in the TREAT reactor building. The capsule will be evacuated and heated to 500°C for a period of several hours. During this time, the effluent from the capsule will be passed through a liquid nitrogen-cooled trap. One cold trap will be removed for counting after one hour. The second trap will be removed for counting about one hour later.

(4) If and when a release of argon or fission gas is detected from a group of elements, the number in the group will be divided in the FCF and one-half returned to TREAT for irradiation. This process will be continued until the leaking element has been isolated.

(5) The above procedure may be modified after testing of the first group of suspect elements if excessive surface contamination or unforeseen conditions are encountered.

p. FCF Equipment Improvements (M. J. Feldman)

Last Reported: ANL-7403, p. 77 (Dec 1967).

(i) Auxiliary Equipment. An air-cooled, bottom-loading and -unloading cask is being designed for the interim subassembly-storage area. For the loading and unloading steps, the cask will utilize an in-cask subassembly grapple. As reported in ANL-7403, a model of one proposed grapple system was constructed and tested. This model utilized two stranded-wire cables, one for hoisting and the other for triggering the grapple. Test results disclosed cable-twisting problems which could not be overcome readily. Design work is now about 70% complete on a single-cable grapple; this grapple will utilize most of the pneumatic and mechanical features of the model tested.

q. Superheater and EM Pump Study and Test (R. A. Jaross)

(i) Superheater Vibration Study

Last Reported: ANL-7403, pp. 78-81 (Dec 1967).

In addition to the potential for a resonance condition resulting from the coincidence of a natural frequency of a tube with the vortex-shedding frequency associated with crossflow, fluid elastic instabilities due to parallel flow (both external and internal to the tubes) are being investigated.

(a) External Flow. Although the secondary pattern of fluid flow is primarily one of crossflow (due to the introduction of baffles), a predominantly parallel-flow component can be expected in the vicinity of the tubes in the outer rows (nearest the shell). Paidoussis* has derived an expression to allow computation of a dimensionless complex frequency of vibration, ω, of a slender cylinder in an axial flow field. The response is stable or unstable accordingly as the imaginary part of ω is positive or negative; $IM(\omega) = 0 \rightarrow$ neutral stability.

The dimensionless frequency, as well as being a function of other nondimensional parameters, is a function of a dimensionless flow velocity defined as

$$u = \left(\frac{M}{EI}\right)^{1/2} U\ell, \tag{1}$$

where M is the added mass of fluid per unit length, EI is flexural rigidity of the cylinder, ℓ is length of cylinder, and U is mean axial flow velocity. If u_{CR} is defined as the value of u at which $Im(\omega) = 0$, a critical flow velocity is defined as $U_{CR} = U(u = u_{CR})$.

Paidoussis has plotted the dimensionless complex frequencies of the three lowest modes of pinned-pinned, clamped-clamped, and clamped-free cylinders as a function of u for a set of nondimensional parameters closely approximating those associated with the superheater tubes. From his results we have constructed Table I.E.11. For the tubes of the superheater unit we have from Eq. (1)

$$U_{CR} = 169\ u_{CR}\ (\text{ft/sec}). \tag{2}$$

Equation (2), together with Table I.E.11, allows us to conclude that fluid elastic instability due to external parallel flow is not a problem because the critical flow velocities are not practical.

*Paidoussis, M. P., Dynamics of Flexible Slender Cylinders in Axial Flow, Part I, Theory, J. Fluid Mech. 26(4), 717-736 (1966).

TABLE I.E.11. Critical Dimensionless Flow Velocity

Mode	u_{CR} Pinned-pinned	Clamped-clamped	Clamped-free
1	3.13[a]	-	2.62[a]
2	5.55	8.4	4.7
3	8.25	11.2	7.4

[a]Buckling instability.

(b) Internal Flow. In regard to instabilities resulting from fluid flowing in a tube, it has been shown* that unless the fluid is very dense and is flowing at very high velocities, the fluid flow will not appreciably affect the vibration or stability of the tube. Therefore, for the case of steam flowing in the superheater tubes (low density and velocity), no problem is anticipated from this mechanism.

r. Reactor Improvements, Nuclear Instrument Test Facility Study (B. C. Cerutti)

Last Reported: ANL-7403, p. 81 (Dec 1967).

The study of an out-of-reactor test facility for the "01" thimble modification is in progress.

(i) "01" Thimble Modification To Provide a Facility for Tests at 650/700°F, Phase I. The gamma chamber (Type WL 23152) was received from the manufacturer. The detector was checked and found to be within specifications. The gamma chamber was installed in the "01" thimble, and a gamma plot made of the usable thimble area with the thimble cooled and the reactor shut down. This plot was made primarily to check plotting procedures and to give the personnel experience in use of the equipment. The fission-chamber holder was checked for fit to assure that all necessary modifications had been performed.

Because the reactor had been shut down for more than 22 days, the gamma level measured was low (maximum 6 R/hr), but there was sufficient spread in the level measured to define an area of gamma-flux deviation. A vertical length of thimble of 24 in. (-4 to +20 in. with core centerline as reference) exhibited an essentially flat profile of gamma flux. For each additional 10 in. of distance away from the core centerline, starting at 20 in. above the core centerline, the gamma flux decreased approximately 20% in level to a minimum reading of 1 R/hr. A complete

*Housner, G. W., Bending Vibrations of a Pipe Line Containing Flowing Fluid, Trans. ASME, J. Appl. Mech., pp. 205-208 (June 1952).

gamma-flux plot can be made in an 8-hr period. For an equipment check, two plots were made on consecutive days. The agreement of the measurements was well within 1% between the consecutive days.

The gamma chamber was left mounted in the thimble for gamma-flux plotting at saturated activity conditions in the sodium.

(ii) "01" Thimble Modifications To Provide a Facility for Tests from 700 to 1200°F, Phase II. Except for the insert-actuating mechanism and the prototype test facility, the conceptual mechanical design sketches of the items needed for this subtask are complete.

s. Feasibility Study of Fuel Failure Detection

(i) Trace Elements Analytical Techniques (C. E. Crouthamel)

Last Reported: ANL-7403, p. 82 (Dec 1967).

Matrix isolation techniques are being used to study the distribution of tellurium (dissolved in sodium) between the metal phase and a fused salt phase (see Progress Report for October 1967, ANL-7391, pp. 106-107). With a favorable distribution coefficient, concentration of the tag element in the fused salt phase should occur. The most significant feature of a recent experiment was the finding that most of the tellurium had adsorbed on the container material (alumina). These data have initiated an interest in the use of adsorption techniques as a quick and reliable method for tag-element collection. Further studies will examine the adsorption of tellurium and other tag elements on various substrate materials, including alumina. The Associated Electronics Industries spark-source mass spectrometer has been received and is being assembled. Completion of the laboratory facility for tagged-element study has been delayed because funds for equipment are unavailable.

(ii) Mechanical Failed-fuel Locator (E. Hutter)

Last Reported: ANL-7399, pp. 87-88 (Nov 1967).

Layout drawings have been prepared for a failed-fuel detector that would incorporate continuous fission-gas sampling and dip sampling of sodium. Quartz windows in the prototype detector will enable visual observation of the internal components during operation. A suitable method of attaching the windows is being studied, and drawings are being made for a test rig to measure the performance of the proposed fuel detector in sodium and at the actual service temperature and pressure conditions.

t. Hot Fuel Examination Facility (HFEF)--Engineering and Design (N. J. Swanson)

Last Reported: ANL-7403, p. 85 (Dec 1967).

The ANL contributions for the Feasibility and Cost Study report and technical coordination of the corresponding facilities engineering work performed by Norman Engineering Co. (NECO) are being prepared. The cost estimate will be based on a new reference design that will provide the same general functional capabilities as the design used for the Preliminary Cost Estimate, and will cost the same although many refinements and optimizations have been made. The refinements include (a) an increase in the handling capabilities in the basement cell (an increase in head room permits the use of the same materials-handling equipment as is planned for the main cell), (b) better ability to transfer large items in and out of the shielded environs of the facility by use of a vertical transfer lock, and (c) placement of building equipment on top of the main cell as a method for efficient utilization of available space.

Conceptual engineering work for the various systems for which ANL has maintained principal design responsibility continued. Prime emphasis has been placed on establishing reference cell-penetration designs (for estimating purposes) and on defining interfaces between the ANL and NECO efforts.

Technical meetings between NECO and ANL project personnel were held to establish preliminary design criteria on which to base the cost estimate and to review NECO progress on the Feasibility and Cost Study, particularly in the area of drawings.

Preparations began on the Conceptual System Design Description (CSDD) which will constitute Volume I (of three volumes) of the Feasibility and Cost Study report.

The cost breakdown for the facility will be organized according to systems rather than by the Schedule-44 pattern which was previously used for design and construction cost estimates.

Effort was also directed toward the establishment of a PERT monitoring system for ANL-engineered equipment. However, this system will not be activated until after the release of the Feasibility and Cost Study report.

2. Outside Fuel Procurement (C. E. Stevenson)

a. Mark-IA-IB Fuel Procurement

Last Reported: ANL-7403, pp. 86-87 (Dec 1967).

Aerojet-General Corp. has made seven 10-kg ingots in its alloy-preparation furnace, by melting under vacuum as compared to the procedure of melting under argon at subatmospheric pressure as used at the FCF. This resulted in good appearance of the ingot surface and a lower-than-normal amount of crucible residue. It was found possible to reuse the zirconia crucibles several times, although in one case a crucible cracked during its second use.

In connection with a proposed modification of the fuel-element tubing specification which would substitute a microhardness test requirement for a Rockwell B hardness requirement, preliminary results were reported for the Rockwell B hardness of a series of Type 304 stainless steel plate samples which had been annealed and then cold reduced to varying degrees. Vickers hardness measurements were also made on these samples, but it is now believed that these data cannot be used satisfactorily for correlation of the two hardness scales because of inhomogeneity of the samples and differences in the depths of penetration which are effective in these two hardness tests. Tests are now underway to determine the effect of cold work on the hardening by drawing of annealed tubing specimens.

3. Operations--Reactor Plant (G. K. Whitham)

Last Reported: ANL-7403, pp. 87-91 (Dec 1967).

a. Operations. No reactor operation was conducted during the month of January because of problems associated with diagnosis and replacement of a damaged control-rod thimble (see Sect. I.E.1.c.(iii)), and checks and measurements on the balance of the control rods to assure that they were in satisfactory condition. Fuel handling performed at the start of the month was interrupted because of this difficulty and because of a malfunction of the core-holddown drive mechanism which required some maintenance work.

The problem with the control-rod thimble appeared during loading changes for Run 27. During removal of control Subassembly L-446 from control-rod position No. 12 (grid position 5-C-3), interference was detected at the 52- and 69-in. elevations. This control subassembly was removed from the core with some difficulty. The installation of the replacement control rod was attempted, but interference was detected at 69.8 in., so the replacement control rod was returned to the storage basket.

In order to accomplish the tests and checks of the top of the reactor core and the control rods, it was necessary to remove the reactor-cover auxiliary gripper plug to allow access. This was done after reducing the bulk sodium temperature to 450°F. Measurement of the activity of the plug indicated a radiation level of 40 R/hr at 4 in. from the bottom surface of the plug. A guide fixture, which extends below the surface of the bulk sodium, was installed in the auxiliary gripper hole. Verification of damage to the control-rod thimble in position 5-C-3 was made with gauging tools made special for the purpose. An obstruction at the top of the thimble flat adjacent to core position 5-C-4, with possible deformation of the corners adjacent to the flat, was verified.

Results of the gauging indicated that a special thimble-removal tool, which had been fabricated for the job, could be locked in the damaged thimble and this operation was performed without incident. To define further the extent and type of deformation, each of the six subassemblies adjacent to the thimble was lifted about 1/2 in., and the lifting forces were measured. The average pulling force required for lifting a subassembly and the pulling tool was about 175 lb, except for Subassembly C-2039 in core position 5-C-4 for which a force of 315 lb was needed. This test verified, however, that this subassembly could be removed in the normal manner with the core gripper within the allowable force limits. Six control rods which had not been changed during the post-Run-26 fuel handling were manually raised 12 in. with no evidence of binding.

The primary tank bulk sodium was heated to 600°F to permit fuel handling associated with the thimble removal. Difficulties which were experienced with rotation of the small seal plug were resolved by readjustment of the settings for the seal temperature controller.

Special scalloped dummy subassemblies were substituted for the six subassemblies adjacent to the control-rod thimble in position 5-C-3 to permit unlocking and removing the thimble. The thimble was unlocked with the manual gripper through the auxiliary gripper hole, removed with the main core gripper by normal fuel-handling procedures, and placed in the IBC for an alcohol wash. A new control-rod thimble was installed through the auxiliary gripper hole by use of the special insertion tool. The new thimble was locked in the grid, and fuel handling to remove the six dummy subassemblies was begun.

This handling was interrupted for removal of the guide sleeve from the auxiliary gripper hole and installation of the cleaned auxiliary-gripper shield plug. Reinsertion of the plug was in progress when a chemical reaction occurred in the auxiliary plug hole. Sodium which ignited on contact with the air was expelled around the plug shaft up through the hole. The plug was lowered and seated, after which possible damage was assessed.

Investigation showed the probable cause of the sodium expulsion to be the result of reaction with the residual alcohol-water cleaning solution in the clearance between the labyrinth seal and shaft on the auxiliary gripper plug. Because of the use of protective clothing and special breathing-air supply to the technician who was installing the plug, only superficial skin burns were incurred. Since the reactor had been shut down for some time, the activity of the sodium was very low and contamination was minor. Damage to equipment due to the burning sodium was insignificant, and the sodium and sodium oxide were readily cleaned from the structure by the temporary removal of two control-rod upper assemblies.

Fuel handling was resumed after cleanup of the sodium had been accomplished. Following replacement of the scalloped dummy subassemblies, six control rods were individually lifted to the full-up position of the core gripper and then lowered again. These control rods had not been changed during normal fuel handling and had been lifted 12 in. manually through the auxiliary gripper plug hole. Only normal forces were required to raise or lower them. This confirmed that there was no rubbing in any control rod.

The decision was made to inspect the lower end of the auxiliary gripper plug to ensure that the labyrinth and lower retaining cap had not been damaged. The bulk sodium in the primary tank was cooled to 400°F, and the auxiliary gripper plug pulling pipe was modified by installing a viewing window in the lower part of the pipe to permit maintaining the plug under an inert gas atmosphere while viewing it. Visual inspection of the labyrinth and retaining cap revealed no damage, and the plug was lowered directly back into the primary tank.

The bulk sodium in the primary tank was then heated to 700°F for the start of Run 27. Among the driver-fuel surveillance subassemblies installed for this run, one subassembly including nineteen 70% enriched fuel pins (see Sect. I.E.1.d) was installed in Row 4 as an irradiation experiment related to the increase-in-power program. An approach to criticality on January 29 was terminated in order to adjust reactivity by substitution of two half-worth for full-worth subassemblies. The reactor was then brought critical on January 30 for rod-drop measurements and control-rod calibrations.

The following table summarizes loading changes in EBR-II during January:

Date	Grid Position	Removed	Installed[a]	Comment
1/6/68	9-D-5	U-1495	U-1110	Removed for surveillance (15,550 MWd)
1/6/68	4-F-2	XA08	C-2007	Removed because of suspected capsule-wall failure.

Date	Grid Position	Removed	Installed[a]	Comment
1/6/68	5-D-3	L-442	L-455	
1/6/68	5-F-3	L-443	L-456	
1/6/68	3-A-1	S-612	S-606	
1/18/68 1/26/68	4-C-2	XG05	C-2003	Removed because of suspected capsule-wall failure.
1/18/68 1/20/68	5-C-4	C-2039	C-2046	
1/19/68	5-C-3	Vacant	L-458	Control-rod thimble replaced.
1/26/68	4-B-1	C-299	C-2138	Installed S/A includes nineteen 70% enriched fuel pins.
1/30/68	3-E-2	C-2049	C-2008	Half-worth S/A installed for reactivity adjustment.
1/30/68	6-A-1	B-372	B-3000	

[a]U--Depleted uranium blanket subassembly
X--Experimental subassembly
L--Control rod subassembly
S--Safety rod subassembly
C--Driver fuel subassembly
B--Row-6-type driver fuel subassembly

b. Operational Support and Maintenance

(i) Plant Maintenance

(a) Fuel-handling Core Holddown. The upper drive system for the core holddown unit was completely disassembled for maintenance and for some minor modifications to promote smoother, more reliable operation of the elevation drive and force-limit setting system. The three elevation drive plates on the main shaft were machined for increased clearance on the orientation keyway inside the shroud tube. The guide rollers for these plates were realigned and doweled to prevent dragging of the plates inside of the shroud tube. This condition had caused many false push-force trips of the holddown in the past. The force-limit setting system was rebuilt, and several worn parts were replaced. A new shaft, new bearings, and a large roll pin were installed in the friction compensator. The push-force switch was calibrated to trip at 400 lb, and the elevation slip clutch was set at 25 lb-ft. A general realignment of the entire unit was completed.

(b) Purification System for Primary Sodium. Installation of couplings on the spare cold trap for the purification system for primary sodium was completed except for the drain line. Another fitting was ordered for completing the work on the drain line.

(c) Control Rod Drive No. 6. A replacement lower drive assembly was installed in control-rod position No. 6. The unit was operated satisfactorily.

(d) Steam Drum--West Gauge Glass. The west gauge glass on the steam drum was removed. New micas, glasses and cushions were installed, and the unit was placed in service.

(e) Primary Tank Transfer Port. The sodium oxide build-up in the guide tube for the primary tank transfer port was "rodded out" to ensure adequate clearance for the FUM gripper. The rotating port was cleaned and new O-rings were installed.

(f) Fuel Unloading Machine (FUM). In the course of cleaning the FUM rotating port, the shaft adapter for rotating the port failed. The port was removed for the installation of a new adapter on the shaft and was reassembled.

(g) Reactor-building Equipment Air Lock. The annual leak-rate test of the reactor-building equipment air lock was satisfactorily completed. Leakage was within allowable, previously established, limits.

(h) System for Sampling Secondary Sodium. The beaker in the system for sampling secondary sodium broke, allowing particles of glass to plug the discharge-sample valve upstream to the in-line filter. In order to minimize any future plugging, a new 1/2-in. Nupro bellows seal valve was installed to replace the original 1/4-in. valve.

(i) Secondary Sodium Recirculation Pump No. 2. The cooling jacket on the secondary sodium recirculation pump No. 2 had become partially plugged with fine sediment from the plant cooling-water system. The unit was backflushed and returned to service.

(j) Secondary Sodium Plugging Meter. The plugging valve thermocouple in the secondary sodium plugging meter was broken off. The thermocouple and a heating circuit were repaired.

(k) No. 2 Feedwater Heater. The upper two sections of the lower gauge glass on the No. 2 feedwater heater developed leaks. The glass was repaired and returned to service.

4. Operations--Fuel Cycle Facility (M. J. Feldman)

Last Reported: ANL-7403, pp. 92-96 (Dec 1967).

a. Hot Line Operation. Normal production operations were curtailed. Subassembly fabrication was limited because of insufficient storage space. In an effort to reduce the reactor storage-basket inventory to

facilitate the forthcoming exchange of the Rows 7 and 8 blanket subassemblies with depleted uranium, spent subassemblies were received from the reactor, but no refabricated subassemblies were sent to the reactor.

Loading of pins into jackets and closure welding of jackets have been temporarily stopped because analytical data indicate that the restrainers are not of uniform composition. A more detailed chemical analysis of the restrainers is being obtained, and metallographic examination of the welds obtained with these restrainers is underway.

Because of the decreased normal-production work load, surveillance activities were emphasized. In addition to driver-fuel surveillance, control rod L-446 was examined as well as elements from the second of two subassemblies (C-2111) which had been suspected of leaking.

Table I.E.12 summarizes the production activities.

TABLE I.E.12. Production Summary for Hot Line

		1/1/68 through 1/31/68
1.	Subassemblies Received:	
	Core, Control, Safety	15
	Other	0
2.	Subassemblies Dismantled (for processing)	13
3.	Subassemblies Dismantled (for examination, etc.)	0
4.	Subassemblies Fabricated	3
5.	Subassemblies Transferred to Reactor:	2
	Subassemblies Stored in L&O Vault and Interbuilding Corridor	0
6.	Elements Decanned:	
	From Irradiated Subassemblies	884
	Rejects	122
	Other	0
	Total Decanned	1,006

Melt Refining

		Irradiated Fuel	Recycle Material	New Fuel
7.	Number of Runs	6	3	0
8.	Average Pour Yield, %	89.7	93.6	-

TABLE I.E.12 (Contd.)

Processing	1/1/68 through 1/31/68
9. Injection Casting Runs (Total Number)	8
10. Elements Processed:	
Accepted	618
Rejected	94
11. Elements Welded	399
Rewelded	0
12. Elements Leak-tested:	
Accepted	396
Rejected	3
13. Elements Bonded (including recycle)	311
14. Elements Bond-tested:	
Accepted	284
Rejected	27
15. Elements to Surveillance	502
Number of Subassemblies	10
Waste Shipments	
16. Cans to Burial Ground	6
17. Oxide and Glass Scrap to ICPP	16

b. Cold Line Operation. A summary of the month's production data is given in Table I.E.13. As reported last month, metallic silicon has been added to the ingots made in the alloy-preparation furnace. Based on analysis of injection-cast pins, the results for 10 ingots show silicon contents of 230 to 450 ppm. Six runs with remelted heels and shards from injection casting have yielded a higher range of values, 330 to 585 ppm.

Another run with depleted uranium and 2 w/o silicon was made in the alloy-preparation furnace, but this time the melt was poured into a new leaf-type graphite mold that produced thin plates of metal. The run was quite successful and several samples from the plates indicated a very uniform dispersion of the silicon. Small quantities of this material can be added to alloy-preparation runs or possibly even injection-casting runs to provide a uniform dispersion of silicon in the alloy.

TABLE I.E.13. Production Summary for Cold Line

	1/1/68 through 1/31/68
1. Alloy Preparation Run	
New Fuel	2
Remelts	4
Total	6
2. Injection-casting Runs[a]	14
3. Fuel Pins Processed	
Accepted	1,047
Rejected	82
4. Elements Welded	915
Elements Rewelded	13
5. Elements Leak Tested	
Accepted	917
Rejected	11
6. Elements Bond Tested	
Accepted	775
Rejected	23
7. Subassemblies Fabricated	9

[a]Includes four runs made with vendor ingots.

Analysis of silicon content in pins cast from a melt containing 2 w/o silicon showed that many pins had a higher silicon concentration at the top of the pin than at the bottom. Samples taken in pins at 1-in. intervals showed a relatively uniform concentration of silicon in the lower half of the pins, and then a slight but uniform increase in concentration from the center to the top of the pin.

Typical values are shown in Table I.E.14.

TABLE I.E.14. Silicon Content in Injection-cast Pins

Sample Location (in. from bottom)	Silicon Content (w/o)	
	Water Washed	HF Washed
1	1.77	1.77
3	1.81	1.85
5	1.81	1.81
7	1.76	1.76
9	1.91	1.88
11	2.10	2.10
12	2.26	2.19

The pins were washed with water in one case to remove any surface contamination, and washed with hydrofluoric acid in the other case to remove a surface layer. The fact that the results are essentially identical indicates that the change in silicon concentration is not a result of reaction of the molten metal with the Vycor molds. Also, if this were the case, the lower ends of the pins would be expected to have a higher silicon content, since the lower ends of the molds are hotter and should have a higher reaction rate. A possible cause of the segregation could be a higher silicon concentration in the slag or dross that floats on the top of the melt. As the Vycor molds penetrated this layer, they would entrap metal with a higher silicon concentration, which would be carried to the top of the castings.

The first four uranium-5 w/o fissium ingots manufactured by a commercial vendor have been received by ANL. They were used in the cold-line injection-casting furnace, and samples of pins are being analyzed for alloying elements.

Two other special injection-casting runs were completed. One was a depleted uranium-6 w/o fissium run and the other a depleted uranium-3 w/o fissium run. Ten pins from each run are to be used as standards for spectrographic analysis of alloying elements in vendor fuel.

Final plans are being made to test the top-loading and -unloading cask to be used in the transfer of irradiated subassemblies to the Idaho Chemical Processing Plant (ICPP). The cask utilizes water to cool the contained subassembly. Pretesting of the equipment to be used in the test was completed, employing an irradiated subassembly for obtaining temperature data for the circulating coolant. The actual test will be conducted soon. Plans have been completed for testing unloading procedures with a dummy subassembly at the ICPP.

c. Maintenance and Repair. A new system for changing tongs and fingers on master slaves was instituted this month, and should save considerable time and decrease the inventory of tongs in the cell.

Some problems were experienced with the sequence latches on the new set of PAR telescoping tubes which have been installed on one of the operating manipulators. New latch-dogs are being installed; it is believed this will solve the problem, since the latches in this set of tubes were not made to specifications.

d. Product Analysis

(i) Chemical Analyses. The numbers of fuel production analyses on hot- and cold-line samples, together with the average values and range, are as follows:

Production Fuel

Analyzed for	Number	Average Value	Range
U (total and isotopic)	21	94.78 w/o	94.35-95.25
^{235}U		52.19 w/o	51.97-52.29
Pu (total and isotopic)	6	888 ppm	59-1517
Mo[a]	32	2.53 w/o	2.36-2.64
Ru	31	1.91 w/o	1.70-2.13
Pd	21	0.190 w/o	0.171-0.211
Rh	18	0.275 w/o	0.252-0.286
Zr	38	0.054 w/o	0.024-0.074
Nb	20	0.012 w/o	0.010-0.022
Fe	55	245 ppm	80-750
Al	21	233 ppm	194-330
Si	30	345 ppm	40-780
C	11	310 ppm	202-397
Total Analyses	304		

[a]The higher-than-normal molybdenum values reported last month were found to be in error. Corrected values (all within specifications) have been obtained.

Analyses for surveillance of irradiated pins from the reactor were as follows:

Surveillance Pins

Analyzed for	Number	Average Value (ppm)	Range
Fe	21	285	125-905
Al	12	205	70-430
Tc	16	382	248-518
C	11	270	115-325
Total Analyses	60		

In addition to the above analyses, samples from the top, center, and bottom of cast pins made from depleted uranium-3 w/o fissium alloy and depleted uranium-6 w/o fissium alloy were analyzed to determine homogeneity. These alloys are to be used as standards for emission spectrographic analysis of vendor fuel. The results of the analyses are as follows:

Depleted U-3 w/o Fissium Alloy

Pin	Element	Top (w/o)	Center (w/o)	Bottom (w/o)	Average (w/o)
1	Mo	1.48	1.48	1.47	
2		1.51	1.51	1.50	1.49
1	Ru	1.34	1.37	1.36	
2		1.38	1.39	1.36	1.37
1	Pd	0.122	0.121	0.125	
2		0.123	0.122	0.124	0.123
1	Rh	0.187	0.181	0.174	
2		0.174	0.181	0.177	0.179
1	Zr	0.065	0.056	0.056	
2		0.061	0.056	0.056	0.058
1	Fe	99 ppm	105 ppm	115 ppm	
2		103 ppm	108 ppm	106 ppm	106 ppm

Depleted U-6 w/o Fissium Alloy

Pin	Element	Top (w/o)	Center (w/o)	Bottom (w/o)	Average (w/o)
1	Mo	3.02	-	3.07	
2		3.02	3.13	-	3.06
1	Ru	2.54	-	2.54	
2		2.51	2.52	-	2.53
1	Pd	0.242	-	0.246	
2		0.242	0.249	-	0.245
1	Rh	0.358	-	0.357	
2		0.350	0.357	-	0.356
1	Zr	0.101	-	0.102	
2		0.100	0.096	-	0.100
1	Fe	90 ppm	-	100 ppm	
2		104 ppm	110 ppm	-	101 ppm

No significant variation in homogeneity was observed.

(ii) Postirradiation Analysis of EBR-II Fuel. EBR-II Subassembly No. C-2111, one of two driver subassemblies suspected of containing one or more defective fuel elements, was received from the reactor and subjected to visual examinations, closure-weld leak tests, and eddy-current bond tests in an attempt to locate leaking elements. No leakers were found. All elements from C-2111, along with those from the other suspect subassembly, C-2113, which were tested previously, are being held in storage in the FCF Argon Cell. Further tests will be conducted in the FCF and in TREAT in an attempt to identify leaking elements. These tests will involve the attempted identification of elements which release fission product gases when subjected to thermal treatments, to reirradiation in TREAT, or to a combination of the methods.

A total of 147 Mark-I and Mark-IA driver-fuel elements from 14 spent subassemblies representing 45 casting batches of FCF-produced fuel were subjected to postirradiation examinations in the FCF. These examinations were conducted in order to obtain irradiation swelling data for the U-5 w/o Fs alloy on a batch-to-batch basis. Included in the examination procedures were element dimensional surveys, sodium rebonding, sodium bond and level testing, and gamma spectrometry. Data from these examinations are now being assembled for analysis and reporting in conjunction with the EBR-II Driver Fuel Anomalous Swelling Investigation.

In addition, and as another part of this same program, similar postirradiation examinations have been completed for 445 driver-fuel elements representing 21 casting batches; these elements were irradiated in five special driver-fuel subassembly experiments which were designed to identify and aid in correcting the causes of anomalous

driver-fuel irradiation swelling. These subassemblies, Nos. C-283, C-292, C-296, C-297, and C-2035, are identified in ANL-7317 (March 1967), pp. 8-12. Postirradiation data are being assembled and swelling calculations are presently being made.

The Idaho Chemical Processing Plant (ICPP) is continuing its two testing programs concerned with underwater storage at ICPP of EBR-II fuel elements. Further results are reported for both programs. In one program, an evaluation is being made of the cladding integrity of stainless steel-clad EBR-II fuel which has been exposed to in-reactor sodium and then stored in the ICPP basin. Five irradiated EBR-II fuel elements have been exposed for seven months in the storage basin. Tests of these elements did not show any significant release of fission products. In the other program, the leachability of a declad segment of an irradiated fuel pin is being determined in storage-basin water. After 84 days of exposure to this environment, a slightly higher leach rate (0.35 $\mu Ci/cm^2$-day) than that previously reported (0.20 $\mu Ci/cm^2$-day) for cesium-137 was found. However, the higher rate is still only about 1/1200 of the leach rate obtained from a uranium-aluminum alloy fuel previously measured by Idaho Nuclear during storage in the ICPP basin.

PUBLICATIONS

LIQUID-METAL FAST BREEDER REACTORS--CIVILIAN

Remote Balance for Accurate Weighing in High Radiation Environment
D. N. Eggenberger and A. B. Shuck
Nucl. Instr. Methods 57, 89-92 (1967)

A Prototype Portable Pump and Oxide-cleanup System for EBR-II Rotating Shield Plug Seals
P. Elias and G. Goldfuss
ANL-7379 (Aug 1967)

Time Invariance of the Elementary Charge
R. Gold
Phys. Rev. Letters 20, 219-220 (Jan. 29, 1968)

Zero Power Plutonium Reactor Facility
H. Lawroski
Nucl. News 11, 46-49 (Feb 1968)

Low-Flux Measurement of ^{235}U Epicadmium Capture-to-Fission Ratio
W. C. Redman and M. M. Bretscher
Nucl. Sci. Eng. 31, 247-253 (Feb 1968)

The Development of a Design and Fabrication Method for Plutonium-bearing Zero-power Reactor Fuel Elements
A. B. Shuck, H. F. Jelinek, A. G. Hins, N. J. Carson, Jr., A. A. Denst, and T. A. Steele
ANL-7313 (Aug 1967)

Proceedings of the Symposium on Liquid Metal Instrumentation and Control, Idaho Falls, Idaho, March 1-2, 1967
ANL-7380

II. GENERAL REACTOR TECHNOLOGY

A. Applied and Reactor Physics Development--Research and Development

1. Theoretical Reactor Physics

a. Cross Section Data Evaluation (C. N. Kelber)

Last Reported: ANL-7403, p. 98 (Dec 1967).

Revisions have been made in the plotting program for the MC^2 library tape in order to conform to the present format of the tape. Some changes had been made in the format since the plotting program was last used. Also some improvements are being made in the program.

The codes CODILLI and CURVEPLOT developed by F. T. Adler and D. B. Adler for the analysis of low-energy neutron cross sections of fissile elements have been acquired and are being adapted to FORTRAN IV. When this is completed, an analysis of the data for the fission cross sections of ^{239}Pu, as measured with the nuclear explosion "Petrel," will be undertaken.

b. General Reactor Theory Studies (C. N. Kelber)

Last Reported: ANL-7403, pp. 98-101 (Dec 1967).

(i) Coherence Effects in Super Prompt Critical Excursions. To investigate the effects of randomness, Eqs. (1-4) given on p. 99 of ANL-7403 were programmed for the IBM 360/50-75 with a time step τ_n chosen from a normal distribution with preassigned mean and variance. The results are given in Table II.A.1 for n = 5. The conclusion is that the variance in the time between additions is significant only when $\tau > 1$.

TABLE II.A.1. Effect of Random Variations in Length of Time Step on Final Energy Release

τ/τ_0	$\sigma(\tau)/\tau$ [a]	W/W_0	$\sigma(W)/W$ [a]
0.0234	0	1.0	0
0.0234	1.0	1.0	0
0.234	0.1	0.9999	0
0.234	1.0	0.9999	0
2.34	0.1	0.29	0.13 ± 0.4
2.34	1.0	0.57 [b]	0.45 ± 0.04

[a] σ = standard deviation.
[b] Samples with a negative time were discarded.

When τ is greater than 1, the dispersion in τ about its mean appears to be about the same as the dispersion of W about its mean. For the case of n very large, some care must be used in relating this study to particular cases. Although the equations are in dimensionless form, the amount of reactivity increment, ρ_0, should be large compared with the delayed-neutron fraction β for the equations to be useful; of course, the underlying assumption is that the system starts at prompt critical.

c. Reactor Computations and Code Development (B. J. Toppel)

Last Reported: ANL-7403, pp. 101-102 (Dec 1967).

(i) Current Status of Phase-1 Fuel-cycle Package. Further test runs are being made on the system, which now includes the output edits described in Progress Report for November 1967, ANL-7399, pp. 105-107. Output is being checked against a CDC-3600 one-dimensional burn code which was developed from CYCLE 2 for 1000-MWe evaluation studies. Current problems are mainly in interaction with the neutronics modules.

An input preparation writeup was issued describing the preliminary formats, so that general usage of the system is now possible.

(ii) ARC System Development. Initial production-problem testing of the ARC system is being initiated for standard paths in the one-dimensional diffusion and transport theories. Experience has shown that such a user-testing program is most profitably undertaken with actual production problems rather than artificial test cases. Users will submit production problems in duplicate to the ARC system standard path and to the comparative CDC-3600 production code. It is expected that critical comments resulting from this effort will influence the ARC system development with regard to module and path organization, user-input formats, and the procedural and clerical details of problem submission.

A nearly completed revision of the ARC system utilities will increase the flexibility of module linkages and simplify development and extension of standard paths. Under the present system, each path is a load module in the IBM sense and requires construction by the linkage editor before use. This has the disadvantage of engendering module duplication in various standard paths and presents the problem of avoidance of duplication of control sections within the standard-path load module.

With the new system the individual computational modules and standard-path control programs are linkage edited to produce load modules. The construction of the standard paths is accomplished by linkages at run time using ARC utilities.

Figure II.A.1 shows a schematic illustration for a hypothetical ARC run showing core-storage allocation at various moments in time. The ARC system utility codes are marked with an asterisk. As shown in the figure, one standard path may call another standard path so that there is no formal limit to the possible algorithmic complexity of the system.

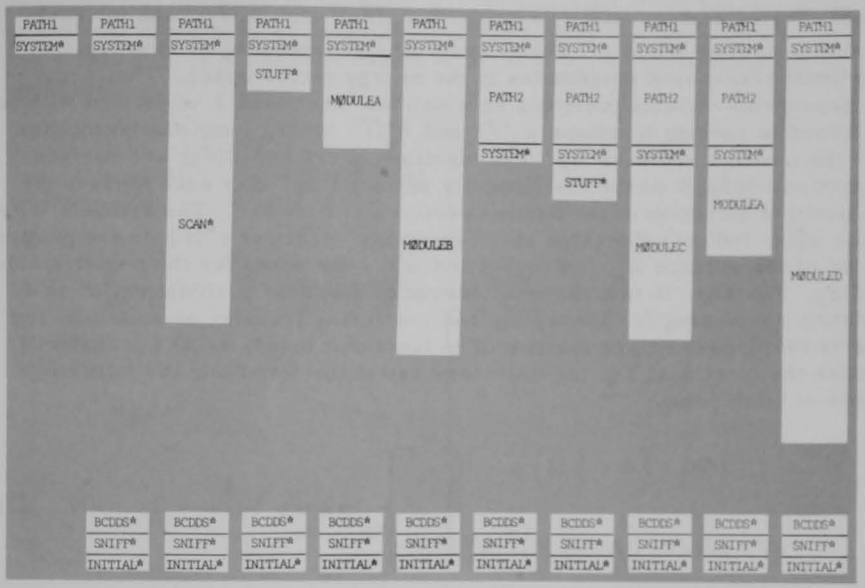

Fig. II.A.1. Core-storage Allocation for Hypothetical ARC Run

The new system is being tested with various input modules. When thoroughly debugged, the present standard paths will be converted to conform to the more flexible system. This conversion will be invisible to the user.

(iii) Variational Flux Synthesis. A scheme for variational flux synthesis using sets of discontinuous trial functions based on a variational principle proposed by Buslik† has been formulated. The functional used as a basis for the method is

$$J[u, u^*, \alpha, \beta] = \sum_{k=1}^{K} \int_{V_k} \left\{ \nabla u^{*T}(\vec{r}) \cdot D \nabla u(\vec{r}) + u^{*T}(r) \left[A - \frac{M}{\lambda} \right] u(\vec{r}) \right\} dV$$

$$+ \sum_{\ell=1}^{L} \int_{S_\ell} \left\{ \alpha^T(r_\ell) \left[u_\ell(+) - u_\ell(-) \right] + \left[u^*_\ell(+) - u^*_\ell(-) \right]^T \cdot \beta(\vec{r}_\ell) \right\} dS_\ell \qquad (1)$$

$$+ \frac{1}{2} \int_{S_0} u^{*T}(\vec{r}_0) \cdot u(\vec{r}_0)\, dS_0 .$$

†Buslik, A. J., WAPD-TM-610 (Oct 1966).

It is defined over the volume V occupied by the reactor system. This volume V is divided into a number K of partial volumes V_k separated by L internal surfaces S_ℓ. The outside surface of the reactor is S_0. The functions $u(r)$, $u^*(\vec{r})$, $\alpha(\vec{r}_\ell)$, and $\beta(\vec{r}_\ell)$ are the independent-variable functions of the functional, and are defined as column vectors in the energy dimension, having components $u_g(\vec{r})$, $u_g^*(\vec{r})$, $\alpha_g(\vec{r}_\ell)$, and $\beta_g(\vec{r}_\ell)$, one for each neutron energy group g. The quantity $u^{*T}(\vec{r})$ and similar expressions indicate transposed magnitudes in the energy vector space. The family of independent-variable functions on which the functional J is defined will be allowed to contain functions $u_g(\vec{r})$ and $u_g^*(\vec{r})$ having jump discontinuities at the internal surfaces S_ℓ. The functions $\alpha(\vec{r}_\ell)$ and $\beta(\vec{r}_\ell)$ are surface functions defined on the discontinuity surfaces S_ℓ. For each surface S_ℓ a positive direction of the normal vector $\vec{n}_\ell$ is chosen. The symbols $u_\ell(+)$ and $u_\ell^*(+)$ indicate the value of the functions $u(\vec{r})$ and $u^*(\vec{r})$ on the positive side of the surface S_ℓ, and $u_\ell(-)$ and $u_\ell^*(-)$ the same for the negative side of S_ℓ. Further, D is a diagonal matrix of diffusion coefficients, A is a matrix accounting for absorption and scattering transfer of neutrons, and M is the fission source matrix. The functions u, u*, α, and β that will make the functional Eq. (1) stationary are those satisfying the following sets of conditions:

$$\left.\begin{aligned} -\nabla \cdot D\nabla u + \left(A - \frac{1}{\lambda} M\right) u &= 0 \\ -\nabla \cdot D\nabla u^* + \left(A - \frac{1}{\lambda} M\right)^T u^* &= 0 \end{aligned}\right\} \text{ in each } V_k,\ k = 1, \ldots, K \tag{2}$$

$$\left.\begin{aligned} D\nabla u(-) \cdot \vec{n}_\ell - \beta(\vec{r}_\ell) &= 0 \\ -D\nabla u(+) \cdot \vec{n}_\ell + \beta(\vec{r}_\ell) &= 0 \\ D\nabla u^*(-) \cdot \vec{n}_\ell - \alpha(\vec{r}_\ell) &= 0 \\ -D\nabla u^*(+) \cdot \vec{n}_\ell + \alpha &= 0 \end{aligned}\right\} \text{ at every } S_\ell,\ \ell = 1, \ldots, L \tag{3}$$

$$\left.\begin{aligned} u_\ell(+) - u_\ell(-) &= 0 \\ u_\ell^*(+) - u_\ell^*(-) &= 0 \end{aligned}\right\} \text{ at every } S_\ell,\ \ell = 1, \ldots, L \tag{4}$$

$$\left.\begin{aligned} D\nabla u \cdot \vec{n}_0 + \tfrac{1}{2} u(\vec{r}_0) &= 0 \\ D\nabla u^* \cdot \vec{n}_0 + \tfrac{1}{2} u^*(\vec{r}_0) &= 0 \end{aligned}\right\} \begin{array}{l}\text{at the external surface } S_0, \\ \vec{n}_0 \text{ being its normal vector.}\end{array} \tag{5}$$

The conditions in Eq. (2) identify u and u* as the neutron flux and its adjoint, with the usual conditions for continuity in Eqs. (3) and (4), and a

condition for zero return current at the external boundary of the reactor in Eq. (5). The functions α and β are identified by Eq. (3) as the values of neutron and adjoint normal currents at the surfaces S_ℓ. The general principle in Eq. (1) has been developed in detail for the case of a reactor with cylindrical symmetry, divided into several radial zones V_k separated by cylindrical surfaces S_k of radii R_k. The outside of the reactor is the cylindrical surface S_0 of radius R, and the bottom and top planes at z = 0, z = h (see Fig. II.A.2 for the case k = 3). The synthesis assumption is made that

$$\left.\begin{aligned} u_{gk}(r,z) &= \sum_{n=1}^{N_{gk}} H^n_{gk}(z)T^n_{gk}(r) \\ u^*_{gk}(r,z) &= \sum_{n=1}^{N_{gk}} H^{*n}_{gk}(z)T^{*n}_{gk}(r) \\ \alpha_{gk}(z) &= \sum_{n=1}^{N'_{gk}} A^n_{gk}(z)a^n_{gk} \\ \beta_{gk}(z) &= \sum_{n=1}^{N'_{gk}} B^n_{gk}(z)b^n_{gk} \end{aligned}\right\} \quad \begin{aligned} k &= 1, \ldots, K \\ n &= 1, \ldots, N_{gk} \\ g &= 1, \ldots, G \end{aligned} \qquad (6)$$

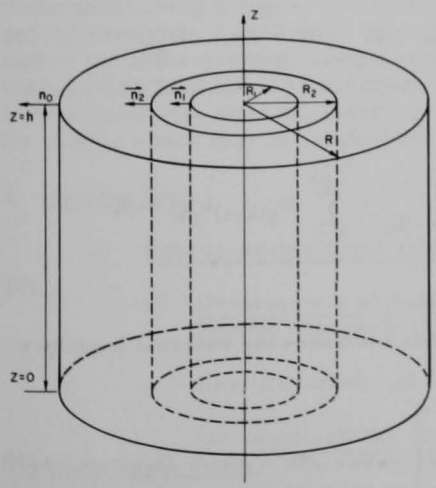

Fig. II.A.2. Schematic Representation of the Reactor

Here the trial functions $H^n_{gk}(z)$, $H^{*z}_{gk}(z)$, $A^n_{gk}(z)$, and $B^n_{gk}(z)$ are known functions of z defined per region and group. As the number N_{gk} indicates, their number is fixed for each region V_k and group g, but can change with both. The number N'_{gk} of trial functions for the surface current and adjoint surface current can also vary with g and k, and is in general different from N_{gk}.

Introduction of the forms in Eq. (6) into the functional in Eq. (1), and then integration over the z dimension produces a reduced functional for which the independent-variable functions are the $T^n_{gk}(r)$, $T^{*n}_{gk}(r)$, and the parameters a^n_{gk} and

b^n_{gk}. If we impose on this reduced functional the condition of remaining stationary for arbitrary variations of the $T^{*n}_{gk}(r)$'s and a^k_{gn}'s, the following system of differential equations and boundary conditions in the $T^n_{gk}(r)$ and b^k_{gn} is obtained:

In region V_k, having boundaries at R_k and R_{k+1},

$$\sum_{n=1}^{N_{gk}} \left[-\frac{d}{dr}\left(r D^{mn}_{gk} \frac{dT^n_{gk}}{dr} \right) + r\left(D'^{mn}_{gk} + \Sigma^{mn}_{rgk} \right) T^n_{gk} \right]$$

$$- \sum_{n=1}^{N_{g'k}} \left[\sum_{g'=1}^{g-1} \Sigma^{mn}_{g'gk} T^n_{g'k} + \frac{1}{\lambda} \sum_{g'=1}^{G} (\nu\chi_g \Sigma_{fg'})^{mn}_k T^n_{g'k} \right] = 0; \qquad m = 1, \ldots, N_{gk}; \tag{7}$$

at the surface with radius R_k,

$$\sum_{n=1}^{N_{gk}} A^{mn}_{gk} T^n_{gk}(R_k) - \sum_{n=1}^{N_{g(k+1)}} A^{mn}_{g(k+1)} T^n_{g(k+1)}(R_k) = 0; \qquad m = 1, \ldots, N'_{gk}; \tag{8}$$

also,

$$\sum_{n=1}^{N_{gk}} D^{mn}_{gk}(R_k) \left. \frac{dT^n_{gk}}{dr} \right|_{r=R_k} - \sum_{n=1}^{N'_{gk}} B^{mn}_{gk} b^n_{gk} = 0; \qquad m = 1, \ldots, N_{gk}; \tag{9}$$

and finally,

$$\sum_{n=1}^{N_{g(k+1)}} - D^{mn}_{g(k+1)}(R_k) \left. \frac{dT^n_{g(k+1)}}{dr} \right|_{r=R_k} + \sum_{n=1}^{N'_{gk}} B_{g(k+1)} b^n_{gk} = 0;$$

$$m = 1, \ldots, N_{g(k+1)}. \tag{10}$$

The principle also yields the following external boundary conditions:

$$\sum_{n=1}^{N_{gk}} \left[D^{mn}_{gk}(R) \left. \frac{dT^n_{gk}}{dr} \right|_{r=R} + \tfrac{1}{2} W^{mn}_{gk} T^n_{gk}(R) \right] = 0; \qquad m = 1, \ldots, N_{gk}. \tag{11}$$

A similar system of equations and boundary conditions for the T^{*n}_{gk}'s and a^{n}_{gk}'s is obtained by imposing stationarity with respect to variations in the T^{n}_{gk}'s and b^{n}_{gk}'s.

Most of the coefficients appearing in Eqs. (7) to (11) are bilinear averages of the parameters in Eq. (1). For example,

$$D^{mn}_{gk}(r) = \int_0^h D_g(r, z)\, H^{*m}_{gk}(z)\, H^{n}_{gk}(z)\, dz. \tag{12}$$

The coefficients W^{mn}_{gk} and D'^{mn}_{gk} are given by

$$W^{mn}_{gk} = \int_0^h H^{*m}_{gk}(z)\, H^{n}_{gk}(z)\, dr \tag{13}$$

and

$$D'^{mn}_{gk}(r) = \int_0^h D_g(r, z)\, \frac{dH^{*m}_{gk}}{dz} \cdot \frac{dH^{n}_{gk}}{dz}\, dz. \tag{14}$$

The next step in the development of the variational synthesis scheme will be to solve the system of Eq. (7) by finite-difference techniques, using a digital computer, and then to test the method by comparing results in a particular case with those obtained with an exact solution of the same problem using a two-dimensional multigroup diffusion code such as CANDID-2D. The synthesis technique chosen will ultimately be incorporated into the ARC system in a standard path and as a general utility module which may be invoked by other paths in the system.

2. Nuclear Data

a. Burnup Analysis and Fission Yields for Fast Reactors

(i) Development of Analytical Procedures for Fission-product Burnup Monitors (R. P. Larsen)

Last Reported: ANL-7399, pp. 108-111 (Nov 1967).

(a) Applicability of Technetium as a Burnup Monitor for Uranium Oxide Fuels. The reasons for evaluating a fission product as a burnup monitor were discussed previously (see Progress Report for November 1967, ANL-7399, pp. 108-109). That report described an evaluation

method which was successfully tested on an irradiated UO_2 fuel using cerium-144, a fission product that does not migrate. The method was then used to evaluate molybdenum as a monitor for oxide fuels.

Technetium has now been evaluated as a monitor by the same technique and the same samples of irradiated UO_2 test fuel. The concentration of technetium was determined spectrophotometrically as the thiocyanate complex* and compared with the burnup values previously calculated from pre- and postirradiation mass-spectrometric data. The actual technetium concentrations in all three samples were significantly lower than the values predicted. It is therefore apparent that technetium is not a satisfactory burnup monitor for oxide fuels.

(b) Photometric Titration of Total Rare Earths. A method of determining burnup by photometric titration of total rare earths is being developed. A modification in the separation procedure to optimize the separation of rare earths from yttrium was reported previously (see Progress Report for November 1967, ANL-7399, pp. 110-111). This modified procedure has been tested with two mixtures of rare earths and yttrium. One mixture simulated that which would be produced by uranium-235 fission, the other mixture simulated that produced by plutonium-239 fission. Three rare earth determinations were carried out on each mixture. Recoveries for the ^{235}U mixture were 100.5, 100.5, and 101.0%; for the ^{239}Pu mixture, 99.9, 100.4, and 100.6%.

Because the constituents of stainless steel interfered slightly in previous procedures, the effect of stainless steel was retested using the latest procedure. No interference was observed.

An evaluation of the present rare earth procedure was made by analyzing two samples of irradiated UO_2. One sample was declad prior to the dissolution; the other was not. The rare earth (R.E.) content and the cerium-144 count rate of each solution were determined. A comparison of the results obtained with the two solutions was made by means of the ratio (μmoles R.E./ml)/(^{144}Ce γ counts/ml). Ratios of 1.597×10^{-5} and 1.613×10^{-5} were obtained for the declad and clad samples, respectively.

The determined R.E. content of each sample differs by 6% from the value calculated from pre- and postirradiation mass-spectrometric uranium analysis and the best available fission-yield data. Uncertainties in both the mass-spectrometric burnup analysis and the fission-yield data could easily account for this difference.

The agreement in the analyses of the clad and declad samples is a further substantiation that stainless steel constituents no longer interfere in the total R.E. determination.

*Foster, R. E., Maeck, W. J., and Rein, J. E., Anal. Chem. 39, 563 (1967).

(c) X-ray Spectrometric Determination of Rare Earth Fission Products. Measurement of burnup in fast reactor fuels by an X-ray spectrometric assay of the rare earth fission products is under development. An X-ray spectrometer has been constructed that is capable of generating satisfactory X-ray intensities of individual rare earths using 50- to 100-μg samples of mixed rare earths. From a radiation point of view, this is an amount that can be managed without remote handling.

The general analytical procedure was described previously (see Progress Report for July 1967, ANL-7357, pp. 70-71). An internal standard (a rare earth not produced in fission) is added to the sample; the rare earth fraction is separated from interferences, mounted on a metal plate, and assayed X-ray spectrometrically.

Terbium is the element that has been selected for use as an internal standard. It is attractive because it is the lightest rare earth element not produced in a significant amount in fission and because its principal emission lines do not interfere with the emission lines of the fission-product rare earths of interest. Because the chemical properties of terbium are nearly identical to those of the fission-product rare earths, no separation is expected to occur in the isolation step. It is currently planned to incorporate about 8 μg of terbium into each sample. The $TbL\beta_1$ emission line will be used in the assay.

The separated rare earth solutions are prepared for analysis by evaporation to dryness on high-purity aluminum (99.999%) discs, 23 mm in diameter by 0.75 mm thick. Aluminum has been selected because the aluminum X rays that are generated will not traverse the helium atmosphere of the instrument and will not, therefore, complicate the spectra of interest. The use of high-purity aluminum was necessary to minimize the generation of X rays from iron impurities present in less pure aluminum.

Mounting the rare earth fission products as a solid on a metal plate provides increased sensitivity, but a high degree of geometric reproducibility of the sample mount is difficult to achieve. This variability can be overcome by use of an internal standard. The increase in precision achieved by this technique is demonstrated by the results obtained in the following experiment.

Six aluminum plates, each containing 58 μg of inactive fission product rare earths and 8 μg of terbium internal standard, were prepared and assayed by measuring the $LaL\alpha_1$, $CeL\alpha_1$, $PrL\alpha_1$, $NdL\alpha_1$ $SmL\alpha_1$, and $TbL\beta_1$ line intensities. Line-intensity ratios (rare earth/internal standard) were then calculated from these line-intensity data.

TABLE II.A.2. A Comparison of Absolute and Relative Line Intensities in X-ray Spectrometric Rare Earth Analysis Emission Lines: Nd = $L\alpha_1$; Tb = $L\beta_1$

	Nd (counts/sec)	Tb (counts/sec)	Nd/Tb
	159.9	61.5	2.60
	172.6	69.7	2.48
	176.8	66.8	2.65
	164.2	65.1	2.52
	125.7	48.9	2.57
	149.9	58.2	2.58
Average	158.2	61.7	2.57
Rel. Std. Dev.	11%	8%	2.3%

A comparison of the precision obtainable from absolute intensity data with the precision obtainable by use of an internal standard is in Table II.A.2. For simplicity only the neodymium and terbium data are presented.

The precisions of the line-intensity ratios for the other rare earths were similar to that shown for neodymium in Table II.A.2. Relative standard deviations of the ratios for the $L\alpha_1$ lines were as follows: lanthanum, 4.3%; cerium, 2.9%; praseodymium, 2.8%; neodymium, 2.3%; samarium, 2.3%. The poorer precision for lanthanum is the result of a line intensity that is significantly lower than that of the other rare earths.

The results of these preliminary experiments indicate that the internal-standard technique is capable of producing data of the desired precision. A calibration curve will next be prepared and its application to unknowns will be studied.

b. Cross-section Measurements (A. B. Smith)

Last Reported: ANL-7403, pp. 105-107 (Dec 1967).

(i) Fast Neutron Cross Sections

(a) Vanadium. Principal attention has been given to elastic neutron scattering and total cross sections of vanadium;* the measurements are now nearing completion and the analysis and interpretation are well along. An extensive effort has been made to compare the present experimental results with the evaluated data contained in ENDF-B. It was found that ENDF-B, although based upon limited information, gives a remarkably good description of the recent measurements. Examples of this agreement are shown in Figs. II.A.3 and II.A.4.

The capabilities of the present Van de Graaff generator limit the present experiments to neutron energies of ~1500 keV. However, detailed optical-model fits to the data up to 1500 keV provide potentials that should permit a good extrapolation of these vanadium results to ~3000 keV. By such a mechanism it is probable that the needs of the reactor program are met to incident neutron energies of 3.0 MeV. Extension of the measurements to the requested upper limit of 14 MeV will be made when the new Fast Neutron Generator becomes operational.

*Work is pertinent to the RDT request for basic data as defined in request #82 and #83 of WASH-1078

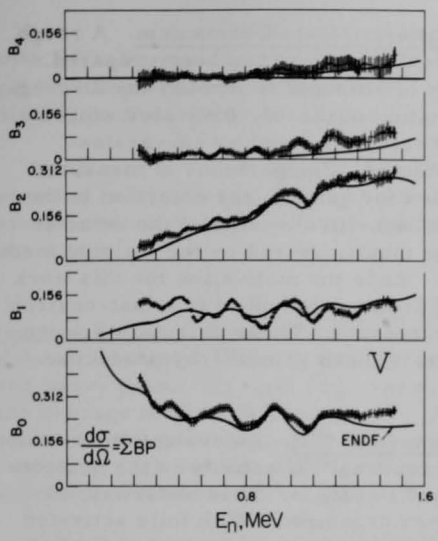

Fig. II.A.3

Differential Elastic-scattering Cross Sections of Vanadium. Data points represent the experimental result; the curve was derived from the ENDF-B file.

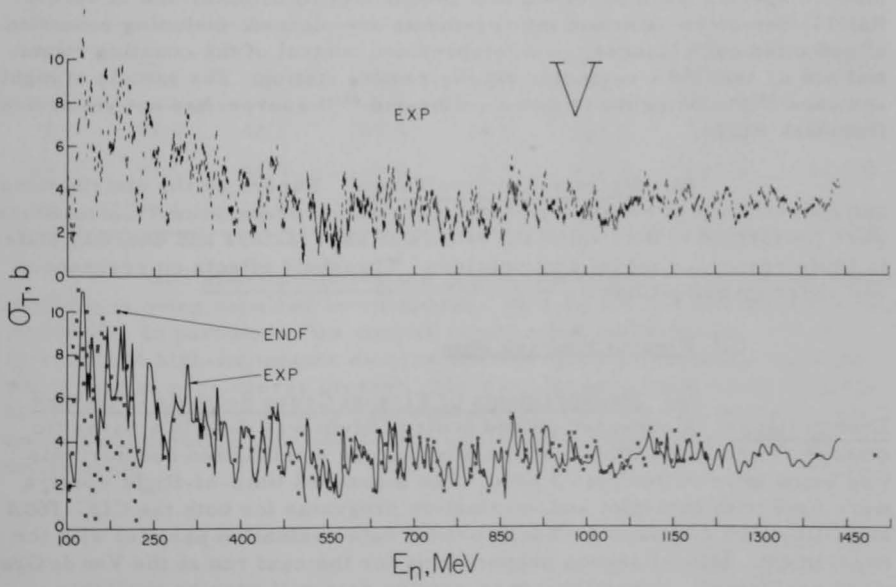

Fig. II.A.4. Total Neutron Cross Sections of Vanadium. The upper curve is the experimental result. The lower portion of the figure indicates the ENDF-B values (boxes) and the experimental result (curve).

(b) Fast-neutron Scattering from Germanium. A rough draft of several sections of a paper on this subject has been prepared. Completion of the draft awaits results of attempts to identify the discrepancy between cross sections for excitation of the 0^+, 0.69-MeV state in ^{72}Ge as measured by time-of-flight spectroscopy and by conversion-electron self-detection in a Ge(Li) detector. Comparisons of measured and theoretically calculated efficiencies for gamma-ray detection in the Ge(Li) detector indicate that the actual sensitive volume of the detector may have been somewhat smaller than that measured by the staining method during preparation of the detector. Since the motivation for this work was accurate determination of Ge(Li) detector response in a fast-neutron environment, this is an important discrepancy. These detectors are the crux of determinations of important (n; n'γ) and gamma-ray production cross sections.

(c) Fast-neutron Capture in ^{236}U. An evaluation of various possible methods for measuring the resulting ^{237}U activity in the neutron-irradiated uranium metal foils enriched to 82% in ^{236}U is underway. A counting room for this purpose has been organized. With foils activated in a reactor and ^{241}Pu (α-decay to ^{237}U) as sources, both singles and coincidence spectra were observed in a 24-cm^3 Ge(Li) detector and in several NaI(Tl) detectors. Certain improvements are planned, including reduction of unwanted coincidences, good temperature control of the counting room, and use of the 160A computer via the remote station. The sample of highly enriched ^{241}Pu, being made into a calibrated ^{237}U source, has not yet arrived from Oak Ridge.

(d) Nuclear Reaction Theory. Papers on the distributions and correlations of resonance parameters are in preparation. Calculations were performed to determine the effects of shift factors and doorway states in finite resonance model computations. Threshold effects on resonances are under investigation.

(ii) Fission Process Data

(a) Measurements of Fission Cross Sections in the keV Energy Range. A one-nsec pulsed neutron beam was used in a parasitic manner to check the time resolution of the gas scintillation counter; this was found to be better than 3 nsec. The measured time-of-flight spectra were used with data-plot and -evaluation programs for both the CDC-160A and CDC-3600 computers. These permit data evaluation parallel with the experiment. Miscellaneous preparations for the next run at the Van de Graaff were performed. Hopefully, cross-section data will soon be available.

A fission counter for measurements of fission cross sections of various fissile materials at 30 keV using 3 surface barrier detectors was designed and constructed. Test measurements will be performed soon.

The measurement of a fission cross section at ~900 keV with a Na-Be radioactive source was considered. This will be performed to get an independent value in case the measurements in the keV range give discrepancies to previous measurements.

A second gas scintillation fission counter was constructed to bypass the recovery time after gas refilling and to allow ratio measurements between several fissile nuclei and $^{10}B(n,\alpha)$ and $^{6}Li(n,\alpha)$ reactions.

(b) Correlation of Mass, Energy, and Angle in Neutron-induced Fission. Measurements have been made for 5.6-MeV-neutron-induced fission of ^{238}U. Table II.A.3 lists the average masses of the light and heavy peaks ($\overline{M}_L$ and $\overline{M}_H$, respectively) as well as their variances σ, the average total kinetic energy $\overline{E}_T$ after neutron emission and its variance, and the peak-to-valley ratio of the mass distribution. These may be compared with similar data for 6-MeV fission of ^{235}U.* No significant dependence of the mass or energy distribution on angle was observed.

TABLE II.A.3. Summary of Mass-Energy-Angle Data for ^{238}U Fission by 5.6-MeV Neutrons

Angle (deg)	$\overline{M}_L$	σ_L^2	$\overline{M}_H$	σ_H^2	$\overline{E}_T$	$\sigma^2(E)$	Peak/Valley
0	99.9	42.3	139.5	44.5	167.8	120.2	57 ± 6
45	99.6	41.7	139.0	44.0	168.0	115.9	63 ± 8
90	99.6	42.9	139.2	42.7	166.9	118.6	48 ± 5

(iii) Instrumentation and Digital Techniques. The Van de Graaff machine is being repaired and modified. This device has run for more than 30,000 hr. In particular, the control circuits had deteriorated. These circuits are high-impedance devices and had developed leakage currents which lead to poor energy control. The circuits have been completely rebuilt. The resulting greatly improved energy stability will save a large amount of operating time and lead to appreciably better experimental information.

*Fission Process Data, ANL-7391, p. 124 (Oct 1967).

B. Reactor Fuels and Materials Development

1. Fuels and Claddings--Behavior of Reactor Materials

a. Irradiation Behavior of Advanced Ceramic Materials (L. C. Michels)

Last Reported: ANL-7403, p. 108 (Dec 1967).

Capsule ANL-56-11 was removed from MTR at the end of Cycle 270 because of a capsule malfunction. The capsule contains four US pellet specimens and two specimens of vibratorily-compacted UC-20 w/o PuC powders. The last remaining thermocouple in the capsule gave erratic temperature readings shortly before shutdown. The cause of this thermocouple behavior is not known.

Irradiation of Capsule ANL-56-8 continues in MTR. This capsule also contains four US pellet specimens and two specimens of vibratorily compacted UC-20 w/o PuC powders.

Pertinent irradiation data for both capsules are given in Table II.B.1.

TABLE II.B.1. Status of Ceramic-fuel[a] Irradiations in Progress in MTR

		Design Parameters		Operating Conditions		
					Estimated Burnup to Date	
Capsule No.	Specimen No.	Fuel Composition (w/o)	Effective Density (%)	Max Cladding Temp (°C)	a/o (U+Pu)	fiss/cc x 10^{-20}[b]
56-11[c]	MV-2	UC-20 PuC	79	470	9.3	25
56-8	MV-3	UC-20 PuC	81	715	9.7	27
56-8	MV-5	UC-20 PuC	80	705	9.4	26
56-11[c]	MV-6	UC-20 PuC	80	480	9.8	25
56-8	S-7	US	80	535	7.8	15
56-8	S-8	US	89	725	10.0	20
56-8	S-9	US	76[d]	750	10.0	19
56-8	S-10	US	91	690	10.0	22
56-11[c]	S-15	US	82	380	6.7	13
56-11[c]	S-16	US	90	510	9.1	20
56-11[c]	S-17	US	88	500	7.6	17
56-11[c]	S-18	US	77[d]	610	9.6	18

[a]All cladding of fuel is Nb-1 w/o Zr alloy of 0.281-in. OD and 0.012-in. thickness.
[b]Based on effective density.
[c]Removed from MTR at the end of Cycle 270.
[d]Partially annular pellets with center thermocouple.

Postirradiation examination of fuel specimens irradiated in Capsules ANL-56-12 and ANL-56-13 continues. Capsule ANL-56-12 contained one specimen of vibratorily-compacted PuC powder and three specimens of vibratorily-compacted UC-20 w/o PuC powders and had achieved

an estimated burnup of 0.3 a/o at a maximum cladding surface temperature of 860°C. Capsule ANL-56-13 also contained one specimen of vibratorily-compacted PuC powder and three specimens of vibratorily-compacted UC-20 w/o PuC powders and had achieved an estimated burnup of 5.0 a/o at a maximum cladding surface temperature of 700°C.

b. Fundamentals of Corrosion in Liquid Metals

(i) Corrosion Mechanisms (D. L. Smith and R. H. Lee)

Last Reported: ANL-7382, pp. 100-101 (Sept 1967).

The results of calculations on the solution of oxygen in tantalum and niobium exposed to a liquid sodium environment have been published.*

Preliminary results have been obtained in the study of the effects of nonmetallic impurities (O, N, C, and H) on vanadium exposed to liquid sodium. Vanadium wires have been equilibrated in sodium under various conditions and the concentrations of the impurities in vanadium have been determined. Oxygen appears to have the largest effect on the vanadium exposed to 700°C cold-trapped sodium. Large increases in the oxygen concentration of the vanadium wires were measured, and the samples became very brittle. Internal-friction measurements of the wires indicated that the oxygen concentrations were generally above the limit that can be determined by this technique. The results of vacuum-fusion analyses for the oxygen concentration in the vanadium wires are given in Fig. II.B.1 as a function of the sodium cold-trap temperature. The oxygen concentrations range from 0.75 w/o at 114°C cold-trap temperature to 1.39 w/o at 175°C. Samples exposed to higher cold-trap temperatures (>175°C) tended to disintegrate or lose weight rapidly. The results are tentatively interpreted to mean that the solubility of oxygen in vanadium is reached (~1.4 w/o at 700°C). Therefore, the phase in equilibrium

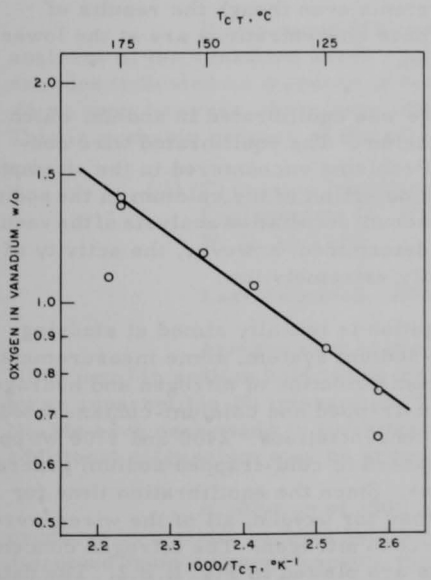

Fig. II.B.1. Oxygen in Vanadium Wires Equilibrated in 700°C Sodium at Cold-trap Temperature T_{CT}

* Kassner, T. F., and Smith, D. L., ANL-7335 (1967).

with oxygen in sodium changes from oxygen in solution in vanadium to vanadium oxide. Present data on the solubility of oxygen in vanadium are inadequate to substantiate this. (The Bureau of Mines is reported to be initiating an investigation of the solubility of oxygen in vanadium.)

The oxygen concentrations in the sodium, as determined by vacuum distillation, compare favorably with the equation used by Kassner and Smith. These values give a distribution coefficient for oxygen between vanadium and sodium that decreases with increasing oxygen concentrations: 1.4×10^4 at 114°C cold-trap temperature to 2.9×10^3 at 175°C. If the solutions of oxygen in sodium and oxygen in vanadium obey Raoult's Law ($a_0 = N_0$),* the distribution coefficient would not change with oxygen concentration.

The oxygen concentration was also measured in vanadium wires equilibrated in sodium that had been hot trapped. The oxygen concentration of the vanadium was only about 600 wt ppm, which is much lower than obtained from the cold-trapped sodium. Vacuum distillation analyses of the sodium indicated oxygen concentrations of the order of 1 to 2 wt ppm, which is about the same as attained from the sodium cold trapped at ~125°C. It is obvious that the activity of oxygen in the sodium is considerably different in the hot- and cold-trapped systems even though the results of distillation analyses were similar. These concentrations are at the lower limit of detection by vacuum distillation.

Another vanadium wire was equilibrated in sodium which inadvertently contained 200 wt ppm calcium. The equilibrated wire contained less than 100 wt ppm oxygen. Problems encountered in the attempted vacuum distillation analyses led to the detection of the calcium in the sodium. Since the calcium interferred with the vacuum distillation analysis of the vacuum sodium, no oxygen concentration was determined; however, the activity of the oxygen in the sodium was apparently extremely low.

Although this investigation is initially aimed at studying the effects of oxygen on the vanadium-sodium system, some measurements were simultaneously obtained on the redistribution of nitrogen and hydrogen. The vanadium wires exposed to the hot-trapped and calcium-contaminated sodium indicated significant nitrogen concentrations: 2400 and 1700 wt ppm, respectively. The vanadium wires exposed to cold-trapped sodium generally indicated lower nitrogen concentrations. Since the equilibration time for nitrogen in vanadium is much longer than for oxygen, all of the wires were not completely equilibrated with respect to nitrogen. The nitrogen concentrations adjusted to equilibrium values are plotted in Fig. II.B.2. The data show that the nitrogen concentration changes with a change in cold-trap temperature. Longer-term data (closer to equilibrium) also indicate that the nitrogen concentration in the vanadium varies with the system cold-trap

* This law states that the activity equals the fractional concentration at low temperatures.

temperature. This result is significant because the solubility of nitrogen in sodium is believed to be extremely low (<1 wt ppm).

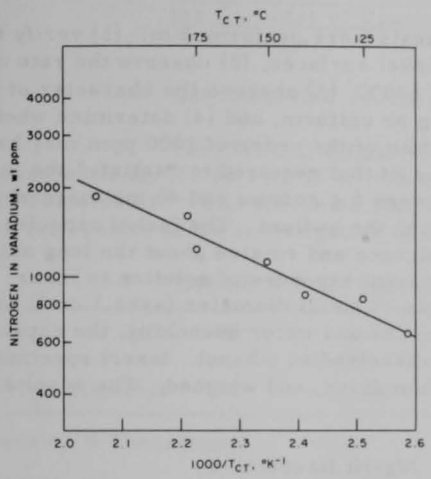

Fig. II.B.2

Nitrogen in Vanadium Wires Exposed in 700°C Sodium at Cold-trap Temperature T_{CT}

It was more difficult to interpret the results of the hydrogen analyses of the vanadium wires equilibrated in the cold-trapped sodium. All samples indicated an increase in hydrogen from the pre-exposed value of <6 wt ppm; however, there is no discernible effect of cold-trap temperature. This is probably because of the relatively high error in the hydrogen analysis.

(ii) Corrosion Inhibition by Dissolved Getters in Liquid-sodium Environment (C. A. Youngdahl, S. Greenberg, and W. D. McFall)

Last Reported: ANL-7399, p. 117 (Nov 1967).*

Achievement of the desired concentration of magnesium (1000 ppm) in sodium held in the nickel loop at 650°C has been complicated by an apparent Mg-Ni interaction.** Tests with nickel capsules loaded with Na-Mg have been made to investigate the effect and to determine whether additional magnesium may be properly added to the loop.

A solution of 1000 ppm magnesium in sodium was readily produced in a static capsule held several hours at 400°C. However, sodium dissolved from a second capsule that had been treated similarly, then held

*Erratum in ANL-7399, p. 117. Fifth sentence of second paragraph should read, "Possibilities considered are (1) that the sampling temperature was too low, (2) that there is interaction of magnesium with nickel present, and (3) that the analysis did not reveal all of the magnesium that was present."

**See Progress Report for November 1967, ANL-7399, p. 117.

overnight at 650°C, contained only 160 ppm of the original 1000 ppm of magnesium loaded into it.

Additional capsule tests were performed to: (1) verify that interaction product is retained on nickel surfaces, (2) observe the rate of the interaction process with time at 650°C, (3) observe the character of the interaction, i.e., whether penetrating or uniform, and (4) determine whether sodium solutions containing magnesium of the order of 1000 ppm may be obtained by adding amounts in excess of that required to "satisfy" the interaction process. Quantities used were 5 g sodium and 46 mg magnesium for 63 cm^2 of nickel surface contacting the sodium. The nickel capsules were held horizontally in a muffle furnace and rotated about the long axis at 1 rpm to promote stirring and uniform exposure of solution to inner surfaces. A nickel-rod insert sample of small diameter (area 1 cm^2) was present in each capsule. After exposure and water quenching, the capsules were sectioned and the sodium was dissolved in ethanol. Insert specimens were recovered, water rinsed, vacuum dried, and weighed. The results are given in Table II.B.2.

TABLE II.B.2. Mg-Ni Interaction

Sample	Time at 650°C (cum) (hr)	Weight Gain (mg/cm^2)	Appearance
a	17	0.551	Gray, adherent
b	108	0.597	Silver, adherent
c	175	0.840	Silver, adherent; dark patches, less adherent

The results of microhardness analyses of the inserts and capsule walls are not yet available. The ethanol solutions have been submitted for analysis for sodium, magnesium, and nickel. A precipitate was present in the ethanol, suggesting the presence of significant amounts of magnesium not incorporated by the solid surfaces. A few larger particles of dark product were also present in the ethanol solution associated with sample c. The weight gain of sample c is anomalous, being in excess of that expected if all the magnesium had been uniformly distributed over the available nickel area. Layer thicknesses revealed during microhardness study and identification of the surface-product composition may contribute to understanding this result.

Conclusions relating to the addition of more magnesium to loop sodium will be drawn when the results of the microhardness and chemical analyses are available. The results may be of more general interest in connection with the behavior to be expected of transmutation-product magnesium in LMFBR sodium.

c. Structure and Properties of Advanced Fuel Materials

(i) Properties of Prospective Fuels: Thermal Diffusivity of the Carbides of Uranium and Plutonium (J. B. Moser and O. L. Kruger)

Last Reported: ANL-7399, pp. 115-116 (Nov 1967).

The thermal diffusivities of UC, $(U_{0.8}Pu_{0.2})C$, and PuC were measured from 500 to 1500°C by means of the flash technique with a lead sulfide detector.* The specimen characteristics are given in Table II.B.3, and the results of the investigation are shown in Fig. II.B.3.

TABLE II.B.3. Specimen Characteristics

Material	UC Arc-cast	UC Sintered (1800°C)	$U_{0.8}Pu_{0.2}C$ Sintered (1800°C)	PuC Sintered (1400°C)
Density, % Theoretical	99.0	78.8	74.8	83.8
Carbon, w/o	4.93	4.69	4.66	4.12
Oxygen, w/o	0.0117	0.106	0.202	0.567
Nitrogen, w/o	0.0021	0.0228	0.0206	0.0440
Equivalent Carbon, w/o[a]	4.94	4.79	4.83	4.58
Equivalent Carbon, a/o	50.8	49.9	50.2	48.9

[a]Equivalent carbon: w/o = w/o C + 12/16 w/o O + 12/14 w/o N.

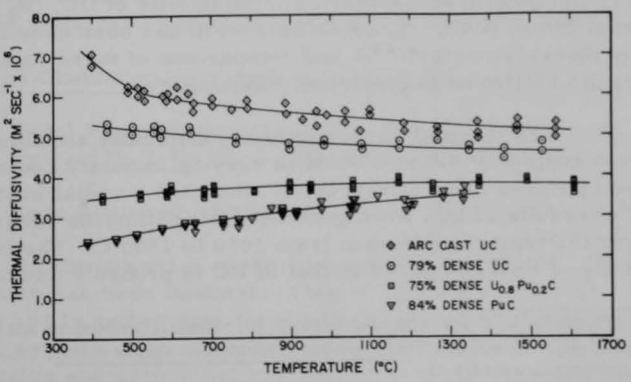

Fig. II.B.3. Thermal Diffusivity of Uranium and Plutonium Monocarbides

*Moser, J. B., and Kruger, O. L., Annual Report for 1966, Metallurgy Division, ANL-7299.

The major impurities, oxygen and nitrogen, were converted to equivalent carbon content since they dissolve in the monocarbides to a considerable extent. Uranium monocarbide and mixed monocarbide of U/Pu ratio 4:1 can be obtained as single-phase material only if the nonmetal atom content does not exceed 50 a/o; for PuC the upper limit for single phase material is 46.5 a/o.

The arc-cast uranium carbide had an equivalent carbon content of 50.8 a/o carbon; a small amount of a second phase consisting of UC_2 was observed in the microstructure. The sintered uranium carbide specimen contained more oxygen but less carbon than the arc-cast material and had an equivalent carbon content of 49.9 a/o. No second phase was observed.

Compounds containing plutonium generally have a greater affinity for oxygen, and the increase in oxygen pickup with increasing plutonium content is shown in Table II.B.3. The mixed carbide of nominal U/Pu ratio of 4:1 contained 0.2 w/o oxygen. The calculated equivalent carbon content of this material was 50.2 a/o carbon. No significant amounts of any second phase were observed. The equivalent carbon content of the plutonium monocarbide was 48.9 a/o carbon with approximately 10% plutonium sesquicarbide (Pu_2C_3) phase present.

Since the values for the heat capacity of carbides containing appreciable oxygen and nitrogen are not available, a calculation of the thermal conductivity is unrealistic. For this reason, the data were analyzed directly in terms of the experimentally determined diffusivity. The rank of the curves in Fig. II.B.3 has been found previously by Leary and coworkers,* who measured the thermal conductivity of UC, $(U_{0.8}Pu_{0.2})C$, and PuC from 200 to 400°C. Considerable work has been done in electrical-conductivity measurements,*,**,† and comparison of these data show that the same rank is followed in electrical conductivity.

The thermal conductivity of chemically stoichiometric UC, with a carbon content of 4.8 w/o but with varying impurity contents, was investigated by Hayes and DeCrescente,† who used a radial heat-flow method. The results of this work generally fall within the range of ANL UC data over the temperature span from 1000 to 1500°C. The lower thermal diffusivity of PuC compared to that of UC is probably due to the fact

---

* Leary, J. A., Thomas, R. L., Ogard, A. E., and Wonn, G. C., "Thermal Conductivity and Electrical Resistivity of UC, (U,Pu)C, and PuC," in Symposium of Carbides in Nuclear Energy, Vol. 1, p. 365, Macmillan Company, London (1964).

** Kruger, O. L., and Moser, J. B., The Electrical Properties and Electronic Configuration of the Monocarbide, Monophosphide and Monosulfide of Plutonium, J. Chem. Phys. 46, 891 (1967).

† Hayes, B. A., and DeCrescente, M. A., Thermal Conductivity and Electrical Resistivity of Uranium Monocarbide, Report PWAC-480, Pratt & Whitney (1965).

that PuC is a defect structure. The difference in thermal diffusivity between the three compounds studied decreases as the temperature increases. At 1300°C the diffusivity of PuC becomes approximately equal to that of $(U_{0.8}Pu_{0.2})C$.

2. Fuels and Claddings--Chemistry of Irradiated Materials

a. Development of Analytical Facilities, Microstructure Sampling Techniques, and Analytical Procedures for Analysis of Irradiated Fuels (C. E. Crouthamel)

Last Reported: ANL-7403, pp. 108-109 (Dec 1967).

Construction and testing of equipment for an analytical facility for the study of irradiated fuels continues.

A spark-source mass spectrometer, Model MS-7, has been received. Assembly is nearly complete; it is expected that the instrument will be operational by about the end of February.

Construction of a shielded fuel-evaluation facility is proceeding. Electrical work is about 95% complete. A jib crane has been installed and preliminary tests of its operation have been made. Final testing will be done upon installation of flexible power cables. Five sets of manipulators are being installed. The installation of a periscope and cell windows will follow the completion of the work on the manipulators.

Design work has been completed for the metallograph enclosure and shielding. Installation of the pneumatic tube is awaiting receipt of the motor-drive units, which were recently shipped from the factory.

3. Fuels and Claddings--Thermodynamics of Fuel Materials

a. Total Vapor Pressures and Carbon Potentials in the Ternary System U-C-Pu (P. E. Blackburn, M. Tetenbaum)

Last Reported: ANL-7391, p. 135 (Oct 1967).

An investigation of the vaporization behavior of the uranium-carbon system has been initiated. This is a preliminary study to test procedures and to gather data for the U-C system before starting work on the U-Pu-C system. Measurements of the total pressure of uranium-bearing species and carbon activity will be made as functions of temperature and composition by means of the transpiration method. Hydrogen-methane mixtures will be used to fix the carbon activity in the carrier gases. The carrier gases will be monitored for methane by means of a total-hydrocarbon analyzer (flame ionization principle). The total pressure

of uranium-bearing species will be obtained by collection of the vapor in the condenser tube and assaying the sublimate for uranium.

Activity measurements over a wide range of temperatures and with well-defined compositions are needed in order to establish reliable partial thermodynamic quantities as well as to define phase-boundary compositions. Direct measurements of carbon activities at high temperatures have not been made with the uranium-carbon system except for some recent studies at GE-NMPO.* Storms** at Los Alamos derived carbon activities from mass-spectrometric measurements of vapor-pressure ratios of UC_2 to U as functions of composition at 2100 and 2300°K. At GE, gas-solid studies were made with uranium monocarbide compositions at 1773 and 1873°K with H_2-CH_4 mixtures. However, the monocarbide specimens used in these measurements were highly contaminated with oxygen, e.g., ~6300 ppm. The total pressures of uranium-bearing species were not measured by the GE investigators because the specimens were encapsulated in rhenium capsules that served as a membrane permeable to carbon. Reaction of the monocarbide specimen with the rhenium container was also observed.†

The transpiration equipment which was used previously to investigate the vaporization behavior of the uranium-oxygen system has been modified for the uranium-carbide study. Preliminary measurements for the total pressure of uranium-bearing species have been initiated; activity measurements await installation of a hydrocarbon analyzer.

4. Radiation Damage of Structural Materials--Research and Development

a. Electron Microscopy of Cladding and Structural Materials (L. C. Michels and R. Natesh)

Not Previously Reported.

Preparations are being made to examine irradiated cladding and structural materials by transmission electron microscopy. Specimens of Type 304L stainless steel tubing and of Type 304 stainless steel rod have been successfully thinned. A simple single-step electropolishing procedure is used to thin the tubing specimens. In the case of rod specimens, 0.020-in.-thick, 0.12-in.-dia wafers are cut from the rod for use as starting specimens in a two-step thinning procedure. An electrolytic jet-machining technique is first employed to remove material rapidly from the central areas on both sides of the wafer. Final thinning is accomplished by use of an electropolishing technique similar to that used for the tubing specimens.

---

* AEC Fuels and Materials Development Program Progress Report No. 69, GEMP-69 (Sept. 29, 1967), pp. 128-133.

** Storms, E. K., Thermodynamics of Nuclear Materials, Vol. 1, IAEA, Vienna (1966), p. 327.

† High Temperature Materials Programs. Part A. Annual Report No. 6, January 31, 1966-January 31, 1967, GEMP-475A (March 31, 1967), pp. 280-283.

5. Techniques of Fabrication and Testing--Basic Fabricability--Research and Development

a. Development of Nondestructive Testing Techniques (H. Berger)

Last Reported: ANL-7403, pp. 110-111 (Dec 1967).

(i) Neutron Techniques. Tests of detail visibility show that the optimum separation between object and imaging screen for radiography through different thicknesses of highly scattering material (plastic and tissue-equivalent gel) should, because of the beam divergence, be zero. Larger separations may improve contrast, and they may be recommended for more highly collimated neutron beams.

Studies continue of the possibilities of a small isotopic neutron source for neutron radiography. A larger-yield Am-Cm-Be source is now available for experimental work. Indium foils have been used to check the previously reported* gold-foil flux measurements. An error in calculation methods of previously quoted neutron fluxes has been revealed. Correcting for this, the peak thermal flux in the water assembly measured by the gold foil should read 0.89×10^5 n/cm^2-sec, and 0.69×10^5 n/cm^2-sec for the BeO assembly with the same (Am-Cm-Be) neutron source (1.2×10^7 n/sec, January 1, 1968).

The importance of using foils within a narrow range of weights has also been indicated. One-square-centimeter indium foils weighing about 185 mg measure fluxes only 50% of those with gold foils when the 2π counter calibration factors are used. Indium foils weighing 93 mg, however, measure fluxes which agree to within 5% of those obtained with gold foils weighing 46 mg. Subsequent foil intercalibration, performed by spinning different foils simultaneously in the Juggernaut beam of nominal intensity 1.9×10^7 n/cm^2-sec, indicate that gold foils weighing 59 mg give the correct flux. Foils weighing about 46 mg, used with the previously accepted formulas, overestimate the neutron fluxes by 25%. Investigation of these inconsistencies is continuing.

The difference between the experimental thermal-neutron fluxes for water and the BeO moderator assemblies compared with the theoretical predictions (by D. Cutforth, Idaho) may be due to the 2.5-cm-square air gap existing above the source in the experimental BeO setup. The importance of moderator displacement near the source is now being checked theoretically and experimentally for the water system.

Further tests indicate that the new cellulose nitrate layers used as neutron track-etch detectors are superior to other cellulose

*See Progress Report for October 1967, ANL-7391, pp. 136-137.

nitrate tested. The new cellulose nitrate layers are 8 μ in thickness; layers used formerly were three times thicker. It is not clear whether the improved results are due to the smaller thickness or to better material. The new layers yield useful neutron images with neutron exposures about one-fourth the 2×10^9-n/cm^2 exposures required for the old cellulose nitrate material. Much better contrast in neutron images of 0.5-mm steps in natural uranium test pieces 1 to 2 mm in thickness can be observed readily. With the old cellulose nitrate material, it was difficult to detect the neutron shadow of 2 mm of uranium.

(ii) Passive Ultrasonic Techniques. A high-temperature transducer probe for acoustic-emission tests in reactors is being developed. Several attempts to attach gold-plated piezoelectric elements to Type 304 stainless steel plates were unsuccessful. Quartz and tourmaline elements were used in this evaluation of bonding methods. The thermal properties of these materials are believed to be the cause of bonding failure (quartz undergoes a large volume change at 575°C and tourmaline cracks and outgasses at about 1025°C). A temperature of 1100°C is utilized in the bonding sequence.

A lithium niobate element has been bonded to a Type 304 stainless steel capsule with a wall thickness of 0.159 cm. Basically, the procedure consists of (1) placing gold foil between the element and the capsule window, (2) heating the assembly in a helium atmosphere to 1100°C, and (3) cooling the assembly slowly. This assembly, with signal leads attached, shows sensitivity to ultrasonic energy over a wide frequency range.

(iii) Scatter X-radiography

Not Previously Reported.

The intensity of X radiation scattered from known types of inspection samples is being studied. Initial studies are being made with a 1.27-cm-dia aluminum rod containing holes of various sizes drilled into the end face to simulate internal voids. A collimated (0.95-cm-diameter) X-ray beam is directed along the axis of the sample, and detection is accomplished with film wrapped around the circumference of the rod sample. Several hole sizes at depths of 0.38 to 1.65 mm have been resolved on these scatter radiographs.

113

C. Engineering Development--Research and Development

113

C. Engineering Development--Research and Development

113

C. Engineering Development--Research and Development

113

C. Engineering Development--Research and Development

113

C. Engineering Development--Research and Development

113

C. Engineering Development--Research and Development

113

C. Engineering Development--Research and Development

113

C. Engineering Development--Research and Development

113

C. Engineering Development--Research and Development

113

C. Engineering Development--Research and Development

113

C. Engineering Development--Research and Development

b. Study of Remote Handling for LMFBR Facilities. We continued to study the remote-handling problems of the FFTF to establish what general types of advanced manipulator systems would be beneficial. It appears that improvements could be made in design and operation if one or more of three manipulator systems were available and used: (1) an existing system consisting of a pair of electric master-slaves (Mark E4A of 50-lb capacity), with slave TV, Mark TV1 or TV2 (two-dimensional); (2) a near-future system, consisting of electric master-slaves (100-lb capacity and medium fidelity), also with slave TV, Mark TV1 or TV2; (3) a system for a little more distant future--electric master-slaves (100- to 150-lb capacity and with better grasping ability, better handle, and somewhat higher fidelity), with improved slave TV (with greater picture quality, at least in the center, and possibly also incorporating stereo). It is also assumed that the master arms, slave arms, and TV systems would be mounted on suitable support systems that can readily move them to all desired locations and that these support systems would have compatible cranes to work with the slave arms. Also, a variety of tools compatible with the manipulators is assumed to be provided (some of these would have to be designed and/or developed).

Studies to date indicate that there are several handling problems that could be greatly eased if one of the above systems were used.

The present design of FFTF provides for extensive compartmentation to separate the operations of fuel handling, loading, disposal, and experiment examination. This concept permits continued operation in one area while cleanup or contact maintenance is carried out elsewhere. However, such direct operations can only be carried out in the absence of fuel or fixed radioactive contamination. In the event of breakdown during fuel-handling operations, an entire machine or major component must be uncoupled remotely, and moved to the repair and maintenance facility. Operation, modification, and adjustment of in-core loops is also a problem which could be helped with one of the manipulator systems. The capability to perform intricate repairs and adjustments (to these machines while they are in place) without the need for removal of these units would reduce downtime and radiation danger to personnel, for example.

In all, or nearly all, places where unilateral electric manipulators are shown, electric master-slaves would improve operation, and, in many cases, simplify some of the equipment.

In most cases, the better the manipulator system, the better would the operations be and the simpler the other equipment. In many of the places the first manipulator system listed (E4A and TV1 or TV2) would be quite helpful, but the second (near-future) system would be considerably better. The third system listed would be still better, but the time schedule of this latter one may preclude its consideration except for this study.

2. Instrumentation and Control

a. Boiling Detector (T. T. Anderson)

Last Reported: ANL-7399, pp. 127-128 (Nov 1967).

(i) Prototype High-temperature Acoustic Sensor. To establish specifications for commercial acoustic sensors, prototype units are being designed and fabricated; the first series of units is half assembled. Critical to the design of a sensor is the method of bonding the piezoelectric crystal to the capsule. A gold-braze bonding method has been developed for high-temperature application; the crystals used were: (1) X-cut quartz (to perfect the method), (2) Z-cut tourmaline, and (3) Z-cut lithium niobate for prototype transducers. Tests of different brazing methods also gave information on the behavior of these crystals at 1100°C. For example, a 30-min cooldown from 1100°C to room temperature caused three quartz crystals to crack or fracture parallel to the bond surface; the crystals also lost the bond with their gold-over-chrome electrodes; these results may be indicative of the effects of a large volume change at 575°C. The Z-cut tourmaline, which was commercial-grade material, outgassed and formed a cinder, resulting in a loose bond to the gold, which had separated into small globules on the cinder surface; therefore, commercial-grade tourmaline is unacceptable for 1000°C transducers, although gem-quality tourmaline, which does not have the tiny fissures found in the commercial grade, might be suitable. A successful bond was made between a lithium niobate crystal and the Type 304 stainless steel capsule. Refinements are being made in the gold-braze method to bond other components within the sensor.

(ii) Geometrical Resonance Tests. An acoustic-boiling monitor must detect boiling wherever it occurs in a reactor core. Therefore, design of the monitor should include the effects of sound generation and transmission within the reactor vessel. To simulate boiling sounds in a vessel, we have measured the amplitude versus frequency spectra of sound pressure from boiling inside a water-filled cylindrical tank of 3-ft diameter. These spectra contain resonance peaks that correspond to standing waves of sound in the water tank. Vertical and horizontal scans of standing waves in the tank showed that the resonances do not correspond to the rigid-wall solution. Rather, the frequencies can be predicted by considering tank walls to be flexible, with inertia and elasticity. The same analysis shows that the flexible-wall boundary conditions apply for low-pressure, thin-wall containment vessels, such as the EBR-II primary tank. However, the resonance frequencies associated with the EBR-II primary tank should be lower by an order of magnitude than frequencies in the 3-ft tank.

The effect of flexible walls was included in boundary conditions for the wave equation by considering simple volume expansion of the tank. The reflection coefficient of reflected pressure wave over incident

pressure wave was calculated, using only dimensions and physical properties. From the reflection coefficient we calculated extrapolated boundaries of the tank corresponding to the free-boundary solution of the wave equation. In Table II.C.1, a comparison is made of the predicted and measured resonance frequencies. Spatial modes in diameter and water height are given to the third harmonic. At higher frequencies, the cross modes crowd the spectrum and cannot be resolved in a spatial scan, although discrete frequencies to the seventh harmonic can be observed in the spectra. By comparison with audio oscillator and digital frequency meter, the observed frequencies were resolved within 3%.

TABLE II.C.1. Comparison of Predicted and Measured Acoustic Resonance Frequencies[a]

Maxima of Standing Wave		Water Height = 0.95 diameter (EBR-II Ratio) Resonance Frequencies				Water Height = 1.25 diameter Resonance Frequencies		
			Measured (3 Runs)				Measured (2 Runs)	
Axis	Diameter	Predicted	Run 5	Run 7	Run 9	Predicted	Run 4	Run 4A
1	1	1.55		~1.5		1.45	1.475	1.40
3	1	2.78			>2.60	2.29	2.20	2.20
1	3	2.92	2.78	2.95	2.94	2.85	2.80	2.80
3	3	3.70	3.68	3.65	3.68	3.35	3.35	3.30

[a]Sound resonances caused by boiling in a water-filled tank, of 3-ft diameter and 0.125-in. wall, with the boiling source in the center of the tank.

Thus resonance measurements have been made for simple cylindrical geometry. Experiments are beginning on the ultrasonic portion of the sound spectrum in this geometry. Components scaled to those of the EBR-II vessel are being fabricated for measurements of resonances and sound absorption.

3. Heat Transfer, Fluid Flow, and Mechanics of Materials

a. High-temperature Boiling Sodium Experiments (J. V. Tokar)

Last Reported: ANL-7403, p. 114 (Dec 1967).

(i) Niobium-1% Zirconium Loop. Repairs and modifications to the power feedthrough, the shutter drive, and the liquid-nitrogen system were completed. Four additional boiling runs have been made. Interpretation of the data is not complete. Stable boiling was obtained in the last run under the following conditions: heat flux of 3×10^5 Btu/hr-ft^2, boiler-outlet pressure of 37 psia and temperature of 1830°F, and boiler-inlet liquid velocity of 2.2 ft/sec. The system was completely isolated from the free-surface area of the dump tank.

b. Heat Transfer to Liquid-metal Heat Exchangers (R. P. Stein)

Last Reported: ANL-7403, p. 114 (Dec 1967).

(i) Nonsymmetrical-duct Heat Exchangers. Final checking of the loop has begun. The initial attempt to fill with sodium could not be completed because of an unexplained plugging in the pressurization tubing to the 50-gal drum from which the sodium enters the loop. The line is being cleared.

(ii) Liquid-metal-heated Steam Generators. Loop construction continues. The first test section has been fabricated and is being assembled and placed in position. This section, a simple double-pipe configuration with mercury flow through the annular space, is 6 ft long and has an annulus of 0.75-in. OD and 0.50-in. ID. Freon-11 will flow through the tube side. The copper inner tube has a 0.5-in. OD and 0.035-in. wall.

To provide "engineering" predictions of vaporization rates for comparison with actual experimental data, a computer program based on empirical heat-transfer correlations as used in current design procedures is being prepared. These design procedures assume the liquid-metal-side heat-transfer coefficient to be independent of length and to be given by a suitable empirical formula. Analyses that eliminate this assumption by applying "first principles," rather than heat-transfer coefficients on the liquid-metal side, are being developed. The analysis receiving the most attention accounts for nucleate bulk boiling on the simulated steam side (Freon-11) by a Rohsenow-type empirical correlation for forced-convection boiling* based on actual Freon boiling data.** This results in a nonlinear problem for which special procedures of solution must be developed. An iteration method is being studied.

c. Heat Transfer in Liquid-metal-cooled Reactor Channels (R. P. Stein)

Last Reported: ANL-7399, p. 129 (Nov 1967).

The derivation of the engineering-type relationship to account for forced-convection heat transfer during flux transients (see Progress Report for July 1967, ANL-7357, pp. 116-117) is being written for publication. Also being studied are several examples of the use of the relationship when flux transients are specified.

*Rohsenow, W. H., and Choi, H., Heat, Mass, and Momentum Transfer, Prentice-Hall, New Jersey, pp. 226-228 (1961).

**Blatt, T. A., and Adt, R. R., Jr., An Experimental Investigation of Boiling Heat Transfer and Pressure Drop Characteristics of Freon-11 and Freon-113 Refrigerants, AIChE J. 10, 369 (1964).

d. Fog Flow Heat Transfer and Fluid Flow (R. P. Stein)

Last Reported: ANL-7403, p. 115 (Dec 1967).

Fabrication of the apparatus has begun. Fiber-optics probes that were developed at Rutgers University are being sent to the Laboratory. They will be used to measure local liquid-concentration profiles.

4. Liquid-metal Linear Generator

a. Effect of Interfacial Transport Process on Condensation (J. H. Linehan)

Last Reported: ANL-7403, p. 116 (Dec 1967).

The comparison of the condensing heat-transfer model with the data has shown excellent agreement. The results of this research are being compiled for a report.

5. Engineering Mechanics

a. Core Structural Dynamics Studies (M. W. Wambsganss)

Last Reported: ANL-7403, p. 117 (Dec 1967).

Data from parallel-flow-induced vibration of a pinned-pinned brass rod are being processed and analyzed. An attempt to use the mechanical-impedance computer to compute and plot frequency-response functions proved unsuccessful because of inherent noise levels in the signals; it was necessary to resort to hand calculation. The frequency-response functions so constructed exhibited the damping trend (viz., an increase in damping with increasing flow velocity) observed in earlier tests with a relatively flexible acrylic rod (see Progress Report for July 1967, ANL-7357, pp. 122-124), thus qualitatively verifying earlier interpretations.

The importance of knowledge and understanding of the energy-dissipative mechanisms has been discussed (see Progress Report for August 1967, ANL-7371, pp. 92-93). It appears to be difficult to construct the frequency-response function with sufficient accuracy to allow determination of damping factor (other than to gain qualitative insights into trends). Therefore, it would be desirable to determine an equivalent damping factor from the measured (experimental) random input and output.

If we neglect the spatial variance of the pressure field and assume that the integrated force exciting the rod can be approximated from a differential pressure measurement, the resulting differential equation for a single-mode approximation is one that can be simulated easily on an

analog computer. The suggested procedure for studying the damping with an analog simulation is: (1) input, to the analog circuit, a measured pressure-differential signal that has been recorded on magnetic tape, (2) process the analog-circuit output to read the mean-square value of the output, (3) monitor the mean-square output while adjusting the damping (potentiometer) to give a mean-square value equal to that obtained from the corresponding experimental response, (4) record that value of damping, and (5) repeat for each flow velocity to be tested. The usefulness of this method depends on the validity of (a) the single-mode approximation and (b) the assumptions used in the derivation of equations, as well as on the ability to make pressure measurements representative of the actual forcing function. The feasibility of this technique is being evaluated.

D. Chemistry and Chemical Separations

1. Aqueous and Volatility Processes--Research and Development--Fluoride Volatility Process

a. PuF_6 Chemistry and Purification Procedures (M. J. Steindler).

Last Reported: ANL-7399, pp. 130-131 (Nov 1967).

Experimental work has continued on testing of procedures to separate mixtures of plutonium and ruthenium fluorides. Recent work has shown that contacting mixtures of fluorine, PuF_6, and ruthenium fluorides with granulated LiF at 300-400°C results in preferential retention of ruthenium by LiF and a consequent decontamination of the PuF_6 (see ANL-7399). The present report describes (1) experiments in which two types of LiF not used in previous experiments were evaluated for plutonium purification and (2) a series of experiments to evaluate an alternative procedure of removing both plutonium and fission products from the gas stream by sorption on NaF, then leaching the NaF with anhydrous HF to dissolve fission products and NaF and obtain a purified PuF_4 product.

A satisfactory purification procedure must provide removal of contaminants and recovery of a high percentage of plutonium. Three purification experiments were performed in which retention of both ruthenium and plutonium by LiF was measured. In each experiment, a gaseous mixture of PuF_6, ruthenium fluoride, and fluorine, generated by fluorination of mixtures of PuF_4 and ruthenium metal spiked with ^{106}Ru, was passed through a bed of LiF.

In the first experiment (F121) a bed of broken, optical-grade LiF crystals was evaluated. With the LiF bed at 300°C for 7 hr, the decontamination factor (DF) corrected for the loss of ruthenium in the laboratory equipment was 1.1×10^2, and 1.2% of the plutonium was retained by the bed.

In the second experiment (F125) a bed of LiF pellet fragments (-6 +10 mesh fraction) pressed from reagent-grade powder was evaluated. The bed was held at 300°C for 7 hr and at 400°C for 2 hr. The corrected DF was 2.0×10^2, and 3.2% of the plutonium was retained by the bed.

In the third experiment (F131) a bed of LiF pellet fragments at 400°C only was examined. The results were a corrected DF of 4.9×10^2 and a retention of 2% of the plutonium by the bed.

Six experiments were performed utilizing the alternative procedure of sorption on NaF at 100°C, followed by solvolysis with HF at room temperature. In one experiment, NaF containing plutonium (prepared by sorbing PuF_6 on NaF) and tracer quantities of ruthenium, antimony, and niobium was contacted with liquid anhydrous HF, and the distribution of the tracer elements between the solid PuF_4 and the liquid phase was measured. Moderate decontamination factors were achieved for antimony and niobium, that for ruthenium being <4. The low DF for ruthenium may have been due to the interaction of ruthenium fluoride with atmospheric moisture to form an insoluble ruthenium compound that accompanied the plutonium.

Three laboratory-scale experiments were performed to determine conditions that yield maximum decontamination. In a typical experiment, a mixture consisting of PuF_4 and ruthenium metal containing ^{106}Ru was fluorinated with fluorine at 350°C in a boat contained in a tube furnace. The gas-stream effluent was passed through a U-tube trap containing NaF pellets at about 100°C to form a complex. Atmospheric moisture was not allowed to come in contact with the sorbed ruthenium. After the trap was cooled, HF was added in three successive portions, each being allowed to remain in contact with the solid for 1 hr, to produce solid PuF_4 and an HF solution of NaF and ruthenium fluoride. Recovery of the solid was by filtration. In one experiment (F25), treatment of the complex with HF as described above yielded a DF for ruthenium of 59. In the second experiment (F45), treatment with HF was followed by washing with liquid BrF_3, which gave a DF of 53. Treatment of the sample from the third experiment (F49) with HF was followed by washing with liquid BrF_5, and gave a DF of 200.

Two other experiments were performed with the same general procedure. In one experiment (F63), the procedure was varied by digesting the plutonium- and ruthenium-containing bed in anhydrous HF at 40°C for 16 hr; a DF of 38 was obtained. In the other experiment (F75), fluorine was passed over the ruthenium-plutonium-NaF bed for 2 hr at 400°C before solvolysis with HF; the DF for the run was 59. The best plutonium purification utilizing NaF (DF of 200) was obtained in experiment F49, which included a BrF_5 wash.

b. Fission Product Fluoride Chemistry (R. L. Jarry)

Last Reported: ANL-7399, p. 131 (Nov 1967).

(i) Chemistry of Ruthenium. A series of experiments to determine the loading capacity of LiF for ruthenium at 300 and 400°C was performed in support of the work on PuF_6 chemistry and purification procedures. The experimental work involved the preparation of a mixture of UF_6 (as a stand-in for PuF_6) and ruthenium fluorides containing ^{106}Ru tracer followed by the transpiration of this mixture from a cold trap, using fluorine as the transporting gas. The fluoride mixture passed from the product cold trap through a trap containing LiF,* a backup trap containing NaF, and into an activated alumina trap.

In one experiment, fluorine gas was reacted with a mixture of tagged metallic ruthenium and UF_4 at 300°C to prepare the fluoride mixture. In two other experiments, fluorination was performed at 600°C using a 3:1 fluorine-oxygen mixture to favor the production of RuF_6 and possibly $RuOF_4$. The product cold trap was maintained at -78°C during the fluorination step, and the LiF trap was at 300°C in the first and second experiments and at 400°C in the third experiment. After 1 to 2 hr, fluorination of ruthenium and UF_4 was considered complete, and transpiration with a fluorine gas flow of 100 ml/min was started. The cold trap was heated to 0 or 50°C, and then to 100 or 150°C, to volatilize the compounds of ruthenium formed by fluorination (e.g., RuF_5, $RuOF_4$, RuF_6, and perhaps others). Gas flow was continued until the activity in the LiF trap reached a steady state. The results of the experiments suggest that less than 1% of the ruthenium volatilized from the trap as fluorides other than RuF_5. Additional experiments must be carried out to substantiate and refine these results, which are promising because RuF_5 is relatively easy to separate from PuF_6 by sublimation.

The experimental results also showed a ruthenium sorption capacity at 300°C of 12-13 mg ruthenium per gram of LiF, and a sorption capacity of 9 mg ruthenium per gram of LiF at 400°C.

c. Neptunium Fluoride Chemistry (L. E. Trevorrow)

Last Reported: ANL-7403, p. 119 (Dec 1967).

The removal of NpF_6 from a gas stream by reaction with particulate NaF contained in a fixed bed is being studied as a method of separating neptunium from uranium and plutonium. Additional work has confirmed that the reaction of NaF with an excess of NpF_6 is

$$3NaF + NpF_6 \rightleftharpoons 3NaF \cdot NpF_5 + \tfrac{1}{2}F_2. \qquad (1)$$

*The LiF consisted of reagent-grade powder that had been pelletized, then quartered.

The removal of neptunium from $3NaF \cdot NpF_5$ by fluorination with fluorine is being investigated. From the total amount of fluorine at 1 atm passed over the complex and the amount of NpF_6 produced, minimum values of the equilibrium constant

$$K_p = p_{NpF_6}/(p_{F_2})^{1/2}$$

for Eq. (1) were calculated. In five determinations, the values ranged from 1×10^{-4} to 4×10^{-4}.

d. Development of Decladding Procedures (R. L. Jarry)

Last Reported: ANL-7391, p. 148 (Oct 1967).

Examination of the literature on the fluoride-catalyzed destructive oxidation of stainless steel has been completed.

e. Engineering-scale Development for UO_2-PuO_2 Fuel (N. M. Levitz)

Last Reported: ANL-7403, pp. 119-121 (Dec 1967).

(i) Engineering-scale Alpha Facility. Additional data have been obtained for the third of three campaigns consisting of fluorination experiments* intended to demonstrate the feasibility of producing and transporting PuF_6 and collecting it quantitatively on an engineering scale. The campaign consisted of three successive fluorination runs performed in a 3-in.-dia fluorinator. A single bed consisting of 6500 g of 48-100 mesh prefluorinated alumina was used in the campaign. In each fluorination, ~200 g of plutonium (~260 g of -325 mesh PuF_4) was charged and the bed temperature was brought to 450°C. Enough fluorine was then added to the gas stream in a 30-min period to give a concentration of ~90 v/o fluorine. Fluorination was continued while the temperature was increased with time (approximately 25°C every 15 min) to 550°C; these runs were continued at 550°C for 2 hr for a total run time of 3 hr for each fluorination.

In the first two fluorination runs (Runs Pu-25 and -26) of Campaign 3, the PuF_6 produced during the first hour was sorbed directly on NaF that could later be sampled and analyzed to get reliable data on fluorination rates for PuF_4. The PuF_6-bearing off-gas stream from the fluorinator was passed through one NaF trap during the first 30 min, through a second NaF trap during the second 30 min, and was passed directly to cold traps during the final 2 hr of the run. Immediately after the third run in the campaign, a cleanup fluorination of the primary filter section was carried out by exposing the primary filters to a fluorine (~90 v/o) stream at 300°C

* See Progress Reports for September 1967, October 1967, November 1967, and December 1967 (ANL-7382, pp. 116-117; ANL-7391, pp. 149-150; ANL-7399, pp. 132-134; ANL-7403, pp. 119-121).

for 2 hr. In a separate cleanup-fluorination period, other portions of the equipment (e.g., cold traps) were also held at 300°C while exposed to ~90 v/o fluorine to recover any plutonium deposited by alpha-radiation decomposition.

The first two 30-min periods of Run Pu-25 showed fluorine utilization efficiencies* of 77 and 42%, whereas Run Pu-26 showed values of 98 and 51% for the two corresponding periods. The average efficiencies for the final 2-hr periods of the two runs were 17 and 20%. The higher values in Run Pu-26 are believed to be a result of a higher plutonium inventory--the bed contained the new PuF_4 charge plus the residue from Run Pu-25. The residue represented an interim holdup, not a loss, and was recovered in the subsequent fluorination run.

Production rates for PuF_6 were higher for the 3-hr fluorinations, 4.1 lb PuF_6/(hr)(sq ft), than in earlier 5-hr fluorination runs, 2.4 lb PuF_6/(hr)(sq ft). Rates as high as 6.5 lb PuF_6/(hr)(sq ft) were attained during the initial 30-min periods.

These results indicate that fluorination rates for plutonium, although substantially lower than for uranium, are adequate for practical applications. The results lend support to the feasibility of applying the fluoride volatility process to fast reactor fuels.

2. Closed Cycle Processes--Research and Development--Compact Pyrochemical Processes

a. Process Chemistry of Molten Salt Systems (I. Johnson)

Last Reported: ANL-7403, pp. 121-122 (Dec 1967).

The large differences in the solubilities of PuO_2 and UO_2 in $MgCl_2$-based salt mixtures may provide the basis for a process to separate uranium from plutonium. Uranium dioxide is only slightly soluble in $MgCl_2$-based salts, whereas PuO_2 reacts readily with $MgCl_2$ and is considerably more soluble in $MgCl_2$-based salts. Because an oxide fuel discharged from fast breeder reactors probably will be in the form of a high-fired solid solution of UO_2 and PuO_2, several experiments have been performed to determine how these oxides interact with the $MgCl_2$-based salt mixtures that are used in the current pyrochemical flowsheet.

An experiment was conducted in which a solid solution containing 80 w/o UO_2 and 20 w/o PuO_2 was added in the form of a powder to a 47.5 m/o $MgCl_2$-47.5 m/o $CaCl_2$-5 m/o MgF_2 salt mixture at 800 to 875°C.

---

*Fluorine utilization efficiency is defined as the ratio of the amount of PuF_6 produced to the maximum amount that could be produced as calculated from chemical equilibrium considerations ($K_{eq_{500°C}}$ = 100 moles fluorine/mole PuF_6).

Only about 20% of the plutonium reacted and dissolved in the salt after 24 hr. The relatively insoluble UO_2 appeared to prevent the salt mixture from making good contact with the PuO_2 in the solid solution.

Another experiment was performed in which the UO_2-PuO_2 powder was oxidized to U_3O_8-PuO_2 to break up the UO_2 structure and thereby allow better contact between the PuO_2 and the salt mixture. The oxidized powder was then added to a 50 m/o $MgCl_2$-30 m/o NaCl-20 m/o KCl eutectic salt mixture at 800°C. Samples taken after 6 and 22 hr showed that 42 and 71% of the plutonium, respectively, had dissolved in the salt mixture, while only 0.6% of the uranium had dissolved. Methods of further increasing the rate and extent of the PuO_2 reaction with the salt mixture are being investigated.

Kinetic studies of the reduction of uranium oxide in metal-salt systems could be simplified if a low-melting salt mixture containing $MgCl_2$ were used. One salt system that was evaluated contained varying proportions of $MgCl_2$ and MgF_2. A tentative phase diagram for this system is presented in Fig. II.D.1. A eutectic with a melting point of 646 ± 4°C was found at approximately 78 m/o $MgCl_2$-22 m/o MgF_2. The curve on the low $MgCl_2$ side of the eutectic is only approximate because of difficulties experienced with the evaporation of the $MgCl_2$ at the higher temperatures in this concentration range.

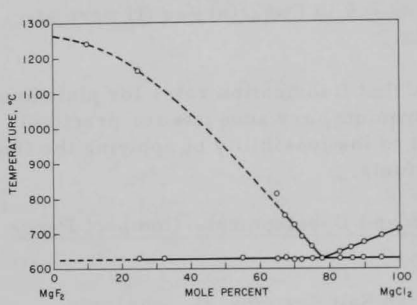

Fig. II.D.1. MgF_2-$MgCl_2$ Phase Diagram

b. Unit Operations Development (R. D. Pierce)

Last Reported: ANL-7403, pp. 122-123 (Dec 1967).

An initial series of experiments in the program for determining phase disengagement properties of various metal-salt systems has been completed. In these experiments, the metal alloy and salt mixture are stirred together to attain a steady-state dispersion of metal droplets in the salt phase. The melt is then allowed to settle for a fixed period of time (about one minute) and the bulk of the salt phase (~70%) is quickly poured into a receiver. The amount of metal remaining in the salt phase is then determined and compared with the amounts left in the salts in other tests with different salt compositions and alloys. The vessel geometry, mixing conditions, and salt-to-metal volume ratio (2 to 1) were the same in all tests. The salt and alloy compositions and the temperature were the variables.

A few typical results are presented in Table II.D.1. The observed entrainment levels varied over a range of approximately 10^4. The

data on the Wood's metal-water system are presented to provide a point of reference. The entrainment levels reported in these tests are not to be interpreted as those which would be expected in pyrochemical processes, since the experimental procedure was deliberately designed to produce measurable entrainment in the poured salt phases. These results indicate only the relative ease of phase disengagement for the various systems that were tested. Although no additional phase-disengagement experiments are planned at this time, further tests will be run as new metal-salt systems are proposed for pyrochemical applications.

TABLE II.D.1. Partial Results of Phase-disengagement Experiments

System	Application	Entrainment Level (w/o)
Wood's metal/water, 85°C	For reference only	0.0003
Cu-33 w/o Mg/ternary salt[a] + 5 w/o MgF_2, 600°C	Candidate plutonium transport donor system	0.01
Cd-18 w/o Mg/ternary salt,[a] 600°C	Candidate plutonium transport acceptor system	0.032
Zn-4 w/o Mg/ternary salt,[a] 600°C	Candidate plutonium transport acceptor system	0.11
Cu-33 w/o Mg/$CaCl_2$-15 m/o CaF_2 (CaO level of 12 w/o after a UO_2 reduction), 800°C	Current reference flowsheet reduction system	0.37
Cu-33 w/o Mg/ternary salt,[a] 600°C	Candidate plutonium transport donor system without 5 w/o MgF_2 (see second system above)	0.87

[a]Ternary salt = 50 m/o $MgCl_2$-30 m/o NaCl-20 m/o KCl.

c. Mass Transfer in Salt-Metal Systems (R. D. Pierce)

Last Reported: ANL-7391, pp. 151-152 (Oct. 1967).

The program to investigate mass transfer in salt-metal systems is continuing. Experimental determinations of the distribution of cerium between Mg-Cd alloys and a $MgCl_2$-30 m/o NaCl-20 m/o KCl salt mixture are almost complete, and the data are being correlated. The measurements are being made for alloy compositions ranging from 10 to 60 a/o Mg at temperatures of 441, 500, 527, 578, and 637°C. The results will be reported when all of the analytical data become available.

d. Laboratory Process Development (I. Johnson)

Last Reported: ANL-7391, pp. 152-153 (Oct 1967).

A method of decladding stainless steel-clad oxide fuel is being investigated in which the cladding is dissolved in molten zinc. As

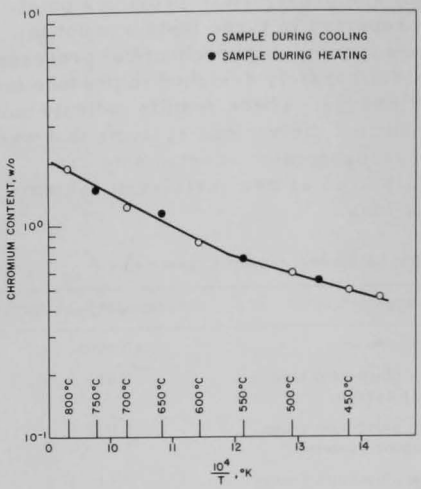

Fig. II.D.2. Solubility of Chromium in Zinc

a part of these investigations an experiment was conducted to determine the solubility of chromium in liquid zinc. A tantalum crucible was charged with 15 g of chromium and 500 g of zinc, and held at 800°C for 48 hr with agitation at 300 rpm. The melt was then thermally cycled between 400 and 800°C, and sampled during both the heating and cooling portions of the cycle. Duplicate filtered samples were taken at ten temperatures following a settling period of from 2.5 to 16 hr at each temperature. Analytical results from the samples are plotted in Fig. II.D.2. It appears that a phase change occurs at ~568°C, as indicated by the change in slope of the line in the figure. The compositions of the equilibrium solid phases have not yet been determined.

e. Materials Testing and Evaluation (R. D. Pierce)

Last Reported: ANL-7403, pp. 123-124 (Dec 1967)

A niobium crucible was exposed to a Cu-33 w/o Mg-0.1 w/o U/$MgCl_2$-30 m/o NaCl-20 m/o KCl system at 700°C for 962 hr to investigate the suitability of niobium as a container material for pyrochemical processes (see Progress Report for September 1967, ANL-7382, p. 122). Metallographic examination of the crucible revealed a 0.2-mm-thick reaction layer on the portion of the crucible that had been exposed to the metal phase. Although its composition has not been identified, the film appears to be the result of copper penetration into the niobium base material, and it has the appearance of an intermetallic compound. Portions of the crucible that had been exposed to the salt and vapor phases showed no evidence of corrosion, but physical tests indicated that some embrittlement had occurred. Further tests will be conducted with niobium to determine its compatibility with plutonium-bearing solutions.

3. General Chemistry and Chemical Engineering--Research and Development

a. Identification of Mechanism(s) of Carbon Transport in Sodium Systems (F. A. Cafasso)

Last Reported: ANL-7391, pp. 154-155 (Oct 1967).

The mechanism of carbon transport between structural materials in liquid sodium is not understood. The nature of the migrating

carbon-bearing species, if known, could provide insight into this mechanism. Therefore, experiments to detect, assay, and identify such species are being made. Materials labeled with beta-active ^{14}C are being used to differentiate between the carbon that is transported and the carbon that pre-exists in sodium.

Previously it was shown that the carbon from a Fe-^{14}C crucible (ferritic steel) containing liquid sodium at 650°C migrated to a Type 304 stainless steel coupon (austenitic steel) immersed in the sodium (see Progress Report for May 1967, ANL-7342, p. 68). A similar experiment has since been completed in which the sodium was sampled at temperature after ~67 hr at 650°C. Three samples, one unfiltered and two filtered through 5-μ-porosity nickel frits, were taken by pressurizing the sodium into nickel tubes. The ^{14}C content of the samples was determined by melting the sodium out of the tubes, followed by combustion of the sodium in oxygen and measurement of the $^{14}CO_2$ formed. The results--1.7 ppm C in the unfiltered sample, and 0.03 and 0.6 ppm C in the filtered samples--indicate that the bulk of the ^{14}C-bearing species in the sodium was particulate during the experiment. The discrepant analyses for the two filtered samples may, in fact, be due to the existence of very fine ^{14}C-bearing particles that can pass through a 5 μ filter.

These results are consistent with our earlier speculation that transport of carbon in sodium systems may involve particulates. Attempts are underway to identify the migrating carbon-bearing species by reaction of sodium samples with water and chemical identification of the ^{14}C-labeled products that appear in the off-gases, solutions, and residues.

b. Total Vapor Pressure and Oxygen Potentials in the Ternary System U-Pu-O (P. E. Blackburn and J. Reishus)

Last Reported: ANL-7391, pp. 155-156 (Oct 1967).

A high-temperature transpiration system is being assembled to study total pressures and oxygen potentials in the U-Pu-O system. The equipment consists of a gas-handling and monitoring system, balance chamber, pumping system, transpiration tubes, and resistance furnace. Except for the latter two items, the apparatus is contained in a glovebox mounted above the resistance furnace. The transpiration tubes, sealed to the bottom of the glovebox, protrude into the furnace. They may be removed from the furnace while maintaining glovebox integrity by raising the box and attached transpiration tubes with a winch. This procedure is required for replacement of furnace elements.

During the transpiration experiments, a H_2O-H_2 gas mixture is recirculated over the Pu-O or U-Pu-O sample until the mixture reaches a fixed composition in equilibrium with the sample. The H_2O/H_2 ratio

establishes the oxygen potential for the sample. Continued gas circulation transpires plutonium-oxide or uranium-plutonium oxide vapor. The rate of transpiration is monitored with a Cahn electrobalance which measures weight changes of the oxide sample. Alternatively, the overall rate of transpiration is obtained at the conclusion of the experiment by chemically analyzing the condensed oxide vapor. To change gas compositions, the gas-handling system, balance chamber, and transpiration tubes are evacuated with mechanical, vac-ion, and titanium sublimation pumps.

Components of the transpiration complex are in various stages of assembly and testing. The glovebox has been mounted over the vacuum furnace. All the components of the transpiration tube assembly, as well as the power feedthroughs for the glovebox, are on hand. The glovebox-lifting mechanism, the balance-chamber vacuum system, and the Cahn electrobalance have been checked out.

Remaining work on the complex will involve assembling the gas-flow system (moisture monitor, mass-flowmeters, etc.), connecting the glovebox to the system for helium purification, and final checking of the completely assembled apparatus.

c. Vapor Species Partial Pressures in the Ternary U-Pu-O System (P. E. Blackburn and J. E. Battles)

Last Reported: ANL-7391, p. 156 (Oct 1967).

The objective of this mass-spectrometric research is to obtain data from which the partial pressures of the vapor species may be calculated for any temperature and composition of the uranium-plutonium fluorite phase. The binary Pu-O system is being investigated first since no mass-spectrometric work has been done to establish the relationships between the Pu, PuO, and PuO_2 gaseous species and the condensed plutonia phase.

As previously reported (ANL-7391), visual examination of the rhenium and tungsten effusion cells from the initial experiments with plutonia revealed that a metallic deposit had formed on the inner surface of the top half of the cell and that the sample residue had apparently undergone melting. Further examination by mass spectrometry and metallography of the tungsten effusion cell indicated that the metallic deposit was tungsten; this deposit may have resulted from the high-temperature dissociation of gaseous WO_2 and WO_3 produced by the reaction of tungsten with the plutonia sample. Presumably, the metallic deposit is rhenium in the case of the rhenium effusion cell.

X-ray diffraction analysis of the sample residues from several experiments showed that the major phase was PuO_2 (or $PuO_{1.98}$). A minor phase, either fcc with a = 5.5 Å or bcc with a = 11.0 Å, was also detected.

It is most likely that the minor phase is bcc α-Pu_2O_3. Metallographic examination of the residue revealed a two-phase structure composed of $PuO_{1.98}$ and a eutectoid believed to be formed of α-Pu_2O_3 and $PuO_{1.98}$.

The temperature dependence of the plutonium-bearing vapor species in equilibrium with condensed plutonia has been determined in several measurements with both tungsten and rhenium effusion cells. The samples, initially $PuO_2(s)$, were heated at about 2025°C until the ion intensities of PuO^+ and PuO_2^+ reached constant values before measuring the temperature dependence. When the logarithm of the variation of the ion intensity-temperature product of Pu^+, PuO^+, and PuO_2^+ was plotted as a function of the temperature reciprocal (log IT vs 1/T), no difference was found between data taken as the temperature was systematically increased and those taken as the temperature was systematically decreased. The concurrence of the data regardless of the direction of temperature variation gives assurance that equilibrium among the phases was achieved. The partial heats of sublimation were determined from the slope of the lines with best fit drawn through the data points. Table II.D.2 summarizes the data from several runs.

TABLE II.D.2. Mass-spectrometrically Determined Partial Heats of Sublimation for the Vapor Species of Plutonia

Run No.	Cell Material	Ionizing Electron Energy (eV)	Partial Heat of Sublimation (kcal/mole)			Ratio of I_{PuO}/I_{PuO_2} at 2175°K	Atom Ratio O/Pu
			PuO_2	PuO	Pu		
P-2	W	13.0	136.8	124.8		2.2	1.85
P-5A	Re	13.0	137.8	124.4	136.4	2.6	1.83
P-5B	Re	13.0	137.4	122.9		2.8	1.81
P-5B	Re	17.0	137.2	129.1		2.2	1.81

Except for the run P-5B made with an ionizing electron energy of 17 eV, the partial heats of sublimation for $PuO_2(g)$ and PuO(g) from these experiments are essentially constant, with an average value of 137.3 kcal/mole for PuO_2 and of 124 kcal/mole for PuO. The larger value (129.1 kcal/mole) obtained for PuO(g) at an ionizing electron energy of 17 eV was probably caused by fragmentation of $PuO_2(g)$ at the higher energy. Fragmentation of $PuO_2(g)$ does not occur at 13 eV. Although Pu^+ was observed, it is believed to be a fragment of PuO.

Vacuum fusion analysis of the sample residues yielded O/Pu atom ratios ranging from 1.81 to 1.85 for the apparently congruently vaporizing composition. These values agree reasonably well with those obtained from

effusion experiments with tungsten cells by Ackermann et al.* (O/Pu = 1.83) and Ohse and Ciani** (O/Pu = 1.85). However, the fact that WO_2^+ and WO_3^+ or ReO_2^+ and ReO_3^+ are still observed mass spectrometrically suggests that the final composition may be controlled by the cell reaction rather than congruent vaporization.

The appearance potentials of the vapor species were determined by the linear extrapolation method. The values obtained for Pu(g), PuO(g), and PuO_2(g) are 6.2, 5.8, and 9.4 eV, respectively, with an uncertainty of ±0.5 eV.

d. Preparation of Nuclear Materials (P. A. Nelson)

Last Reported: ANL-7391, pp. 157-159 (Oct 1967).

A fluidized-bed process is being developed to convert UO_2 to UC. This process is also expected to be applicable for the preparation of (U,Pu)C. The preparation of UC and (U,Pu)C by this technique shows promise of being more economical than the classical carbothermic reduction procedure.

A fluidized-bed reactor for conversion of UO_2 to UC was constructed for operation at temperatures up to 2000°C and pressures up to 10 atm. Installation of the reactor is complete, and initial tests have been made; these have demonstrated that the equipment will operate at the designed conditions.

Initial experiments with this equipment will characterize the reaction of UO_2-carbon particles to form UC. Fluidizable particles suitable for this reaction are prepared by the following procedure:

(1) blending of the UO_2, carbon, and binders (e.g., polyvinyl alcohol or ethyl cellulose) powders in a V-blender;

(2) adding of solvent (distilled water or an organic liquid);

(3) agglomerating by tumbling in the V-blender;

(4) screening to obtain the desired particle size for fluidization (~300- to 1000-μ diameter);

(5) baking at a low temperature to remove the binder.

Calculations are being made to determine the UO_2-C particle size which will give good fluidization at high flow rates for efficient removal of the carbon monoxide reaction product.

*Ackermann, R. J., Faircloth, R. L., and Rand, M. H., J. Phys. Chem. 70, 3698 (1966).

**Ohse, R. W., and Ciani, V., presented at Third International Symposium on High Temperature Technology, Asilomar, California (Sept. 17-20, 1967).

To follow the progress of the reaction, the carbon monoxide content of the argon or helium off-gas will be measured by a continuously indicating thermal conductivity cell, as well as by a gas chromatograph with a 6-min cycle time. The gas chromatograph, due to its higher sensitivity, will give a more accurate record of the final portion of the runs when the CO concentration is very low. The thermal conductivity cell will give a continuous record which can be used to calculate instantaneous reaction rate data. The gas chromatograph has been installed and tested with a gas mixture which simulates expected process conditions. The thermal conductivity cell is being installed, and will be calibrated prior to the first runs which should begin in the near future.

PUBLICATIONS

GENERAL REACTOR TECHNOLOGY

Engineering Development of a Fluidized-bed Fluoride Volatility Process. III. Bench-scale Studies with Irradiated Uranium Alloy Fuels
A. A. Chilenskas and K. S. Turner
Nucl. Appl. 4, 6-16 (Jan 1967)

Polarization in the Elastic Scattering of Neutrons from Intermediate Weight Elements
S. A. Cox and E. E. D. Whiting
Bull. Am. Phys. Soc 13, 116 (Jan 1968) Abstract

An Induction Probe for Measuring Levels in Liquid Metals
T. R. Johnson, F. G. Teats, and R. D. Pierce
Nucl. Appl. 4(1), 47-53 (Jan 1968)

Calculations on the Kinetics of Oxygen Solution in Tantalum and Niobium in a Liquid-sodium Environment
T. F. Kassner and D. L. Smith
ANL-7335 (Sept 1967)

Direct Indication of Particle Size in Fluidized Beds
I. E. Knudsen and W. F. Olsen
Chem. Eng. 75, 190 (Jan. 15, 1968). Republication of an article in Chem. Eng. 74, 224 (April 10, 1967) in recognition of an award.

Preparation, Electronic Structure, and Conduction Processes of Actinide IVA-VIA Compounds
O. L. Kruger and J. B. Moser
Chem. Eng. Prog. Symp. Series--Amer. Inst. of Chem. Eng. (Series 80, 63, 1-10, 1967), Preparation of Nuclear Fuels

Vapor Pressure of Gd_2O_3 from 2350° to 2590°K
D. R. Messier
J. Am. Chem. Soc. 50, 665-668 (Dec 1967)

The EBR-II Skull Reclamation Process. Part III. Skull-oxidation Equipment
W. E. Miller, G. J. Bernstein, R. M. Fryer, R. F. Malecha, M. A. Slawecki, and R. C. Paul
ANL-7338 (Oct 1967)

Reduction of Electrical End Losses in MHD Generator Channels by Insulating Vanes
Jerzy R. Moszynski
ANL-7188 (Sept 1967)

MC^2, A Code to Calculate Multigroup Cross Sections
B. J. Toppel, A. L. Rago, and D. M. O'Shea
ANL-7318 (June 1967)

III. ADVANCED SYSTEMS RESEARCH AND DEVELOPMENT

A. Argonne Advanced Research Reactor--Research and Development

1. Instrumentation and Control (J. H. Tessier)

Last Reported: ANL-7403, pp. 128-131 (Dec 1967).

a. Loss-of-coolant Accidents. The FLASH computer code has been modified so that results of calculations can be plotted automatically by means of the Calcomp system. Values that can be graphed include net reactivity, normalized power, pressure in each control volume, coolant flow rate through the reactor core and in the primary loop, and coolant enthalpy at core inlet. Each quantity is represented as a function of time during a simulated loss-of-coolant accident.

The effort to modify the FLASH code to obtain acceptable solutions to simulated loss-of-coolant accidents for AARR continues. The FLASH subroutine that stores and determines the physical properties of water has been modified for pressures from 1 to 800 psia. Revised water-property data calculated by the methods in the 1967 Steam Tables are not markedly different from those stored in FLASH.

By changing the pressure-search increment from the 10 psia specified by the program to 1 psia, we were able to perform calculations that had previously diverged prior to completion. However, the calculated results still contain questionable oscillations of system variables. These and other possible modifications must be considered before FLASH can be confidently applied to AARR.

b. Performance of Automatic Control and Safety Systems. A mathematical model and appropriate analog computer program are being developed to provide design- and safety-related information. In general, the program will make calculations for these problem areas: (1) primary-system and core response to loss of utility electrical power, (2) primary-system and core response to inadvertent scram, (3) primary-system and core response to small ruptures, (4) overall reactor and coolant system response to nominal perturbations of normal operating parameters, and (5) accidents involving instrumentation and control malfunctions.

To demonstrate that the AARR design meets safety criteria for anticipated transients (problem areas 1 and 2), the calculational model must simulate the reactor, the primary coolant loop, and salient features of the automatic control and safety channels. Thus, a primary goal is to obtain information from which we can establish safety-system set points and performance specifications for components of the control and safety channels.

In providing data for other safety problems (problem areas 3, 4, and 5), we will avoid undue complexity in this code (and an associated large development effort) by limiting the model to physical representation of primary coolant conditions extending only to limited vapor production. For postulated accidents leading to conditions well beyond incipient vapor production, the model will provide initial conditions for computer codes designed to treat plant conditions following the development of two-phase conditions in the coolant.

Detailed consideration has been given to the specific studies to be performed with the analog program so as to establish the necessary capabilities of the program, to assign problem priorities, and to obtain a clear understanding of the interrelationships between these analyses and others planned for AARR. An appropriate mathematical model is being developed.

2. Core Research and Development

a. Heat Transfer Analysis (R. R. Rohde)

Last Reported: ANL-7403, pp. 131-133 (Dec 1967).

(i) Analysis of Core Structures. Preliminary estimates of temperature have been obtained in the study of thermal conditions in the reflector shroud and pedestal.

Figures III.A.1 and III.A.2 show the grid arrangement used in calculations in conjunction with the THTB code* for vertical cross sections through the structures with long and short gussets, respectively. The term "gusset" here refers to that part of the structure that is to the right of a vertical plane containing Face 2 and Nodes 16 and 156. However, Nodes 171 through 175 are not part of the gusset.

Calculations were made for the following cases: (1) the long-gusset integral with the reflector shroud and pedestal, (2) the long-gusset integral with the shroud and pedestal only at Nodes 16-17, 25-26, 126-127, 141-142, and 156-157, (3) the short-gusset integral with the shroud and pedestal, and (4) the short-gusset integral with the shroud and pedestal only at Nodes 66-67, 126-127, 141-142, and 156-157.

The small cubes shown in the figures represent a typical node. Face 1 of Nodes 169, 170, 175, and 241-246; Face 3 of Nodes 1-8; and Face 4 of Node 175 were considered to be insulated. For Cases 2 and 4, we assumed that the Faces 2 and 4 of the unattached nodes between the reflector shroud and pedestal and the gusset were cooled by natural convection. In all other cases, Faces 2 and 4 were assumed to be in perfect contact. Faces 5 and 6 on the gusset were considered to be cooled by natural

*Stephens, G. L., and Campbell, D. J., Program THTB, for Analysis of General Transient Heat Transfer Systems, General Electric #R60FPD647 (April 1961).

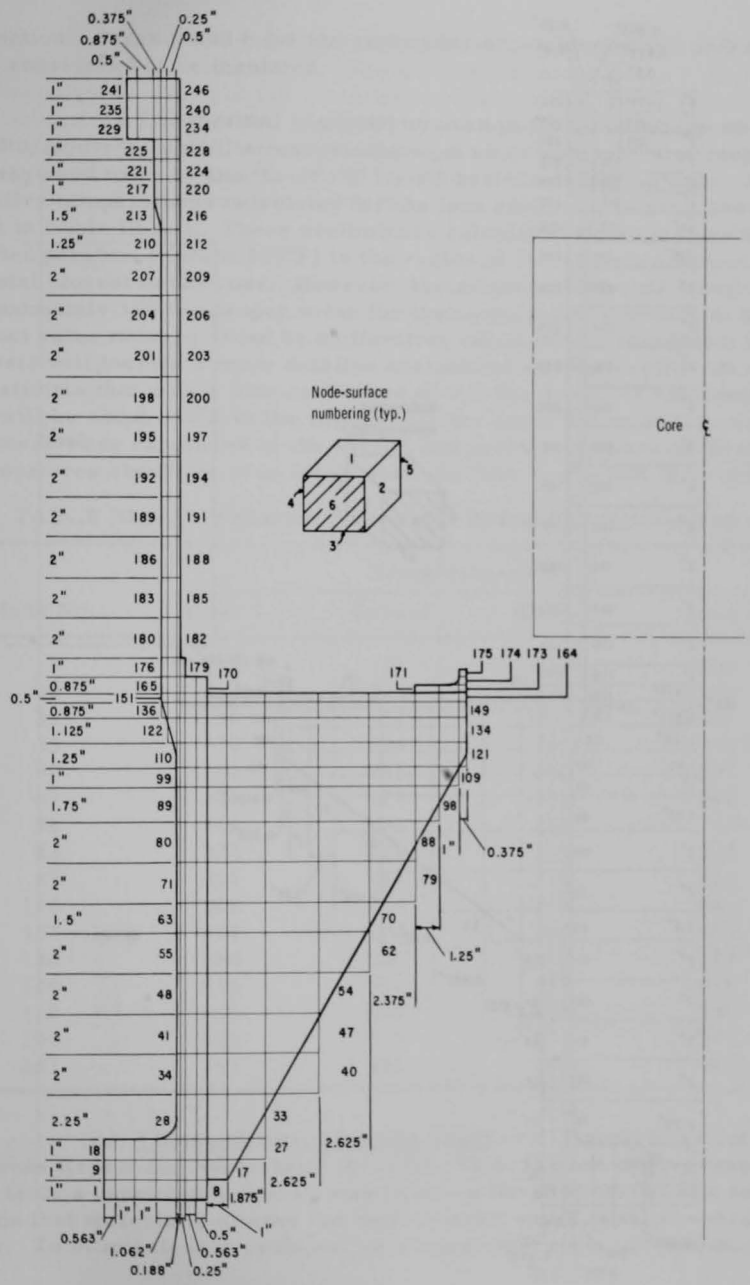

Fig. III.A.1. Cross Section of Reflector Shroud and Pedestal with Long Gusset

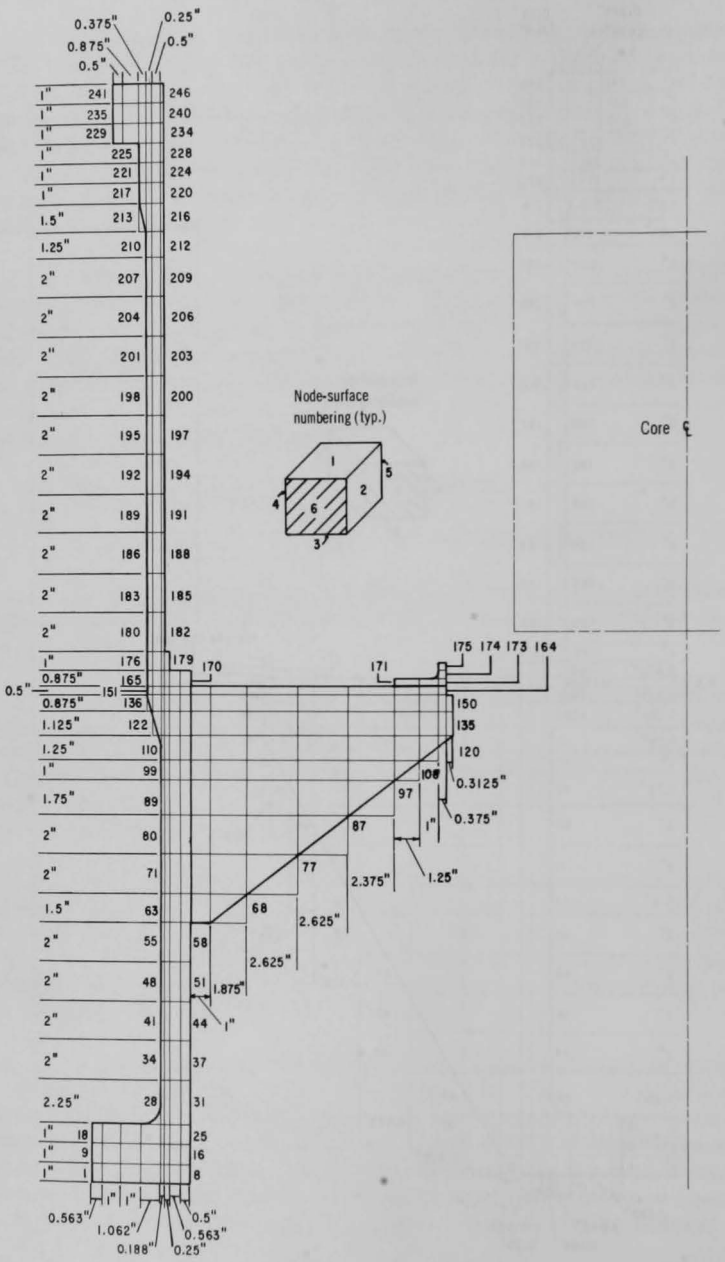

Fig. III.A.2. Cross Section of Reflector Shroud and Pedestal with Short Gusset

convection. Faces 5 and 6 for the remainder of the shroud and pedestal were considered to be insulated.

The thermal conductivity used in the calculations was 100 Btu/hr-ft-°F, which is representative of aluminum; the film coefficient was assumed to be 50 Btu/hr-ft^2-°F for all heat-transfer surfaces. Representative temperatures calculated for the four cases we investigated are given in Table III.A.1. These preliminary calculations indicated rather high temperatures (about 500°F) in the region of the reflector shroud and pedestal closest to the core. However, the assumed film coefficient was approximately 1/6 the proper value for the temperatures indicated; the correct value must be found by an iterative calculation. Therefore, future analysis will include a more detailed assignment of film-coefficient values. We estimate that with a film coefficient of 300 Btu/hr-ft^2-°F the temperature will be about 300°F in the region near the core. Much lower temperatures were calculated in the shroud and pedestal proper, so these temperatures should be even lower when the film coefficient is corrected.

TABLE III.A.1. Reflector Shroud and Pedestal Temperatures

	Temperature (°F)			
Node No.	Case 1	Case 2	Case 3	Case 4
5	170	172	192	191
22	168	171	190	190
33	158	152	NA	NA
36	170	184	191	191
50	184	203	200	201
65	204	219	205	207
76	210	202	205	197
83	226	224	224	241
87	286	284	265	263
112	260	274	258	269
120	474	474	462	462
140	280	285	279	280
149	518	518	507	507
175	556	556	555	549
199	373	373	373	373
243	353	354	353	353

(ii) Transient Heat-transfer Tests. As reported earlier (see Progress Report for November 1967, ANL-7399 p. 145), during steady-state tests a cupricoxide deposit was found on the walls of the fifth test section that materially altered the heat-transfer and fluid-flow characteristics. To eliminate this problem, we attempted to apply chromium plating

to the interior of the two remaining test sections. The plating attempts were unsuccessful, primarily because of restricted working space in the fabricated sections. New test sections will be plated during fabrication. The sample sections are being plated by two different techniques; they will be tested and compared to determine the plating system best suited for future test sections.

The X-ray power supply (Universal Voltronics) has been tested with the following results: (1) defective resistors were found in the high-voltage divider section and (2) low-frequency oscillations were evident in the current-regulator circuit. The defective resistors are being replaced and corrections are being made to the regulator circuit.

The final mounting system for the scintillation-crystal photomultiplier-tube assembly has been completed. Work continues on the mounting system for the X-ray tube.

b. Core Structure Development (W. J. Kann)

Last Reported: ANL-7403, p. 134 (Dec 1967).

(i) Test of Beryllium Reflector to Beam-tube Liner Seal. The liner seal was tested at room temperature and at about 150°F at various pressures up to 150 psig with the following results:

	Leakage (ml/hr)		
	Room Temp		
Pressure (psig)	Test 1	Test 2	150°F
50	0	6	-
100	50	18	-
150	575	600	0

These tests are continuing.

(ii) Test Fixture for Holddown of Outer-shroud Structure. Although the design of the outer shroud (surrounding the permanent reflector) is similar to that used for HFIR, in AARR a different method will be used to attach and hold down the outer shroud to the reflector support pedestal and to the upper shroud flange. The HFIR design employs captive T-bolts; the retainer rings must be loosened before the bolts can be removed. To permit removal of only one bolt at a time, we will use an independent swing-latch assembly for each bolt; it can be manipulated simply with a long-handled tool. A test fixture has been constructed that geometrically simulates restrictions that will exist in the reactor. In initial demonstrations, the swing-latch T-bolts are being installed and removed from

the test fixture from a distance of about 13 ft through a $2\frac{1}{2}$-in.-dia hole that simulates a vessel top-head nozzle. Latching operations and removal and replacement of bolts have been satisfactory; formal tests will begin soon.

(iii) Stress Analysis of Vessel Internals and Beam Tubes. Input data are being prepared for the analysis of the blind and through beam tubes and the Grayloc clamp.

Franklin Institute has found that existing mathematical techniques are inadequate for predicting the distribution of temperature and stress in the permanent reflector. A three-dimensional, finite-element approach is being prepared.

For the analysis of the vessel adapter, the reflector shroud and support pedestal, and the fuel and shield support assembly, Franklin Institute has started to review and evaluate the criteria and design of the components and to prepare mathematical models. Models have been developed for analyzing stresses under axisymmetric and thermal loadings.

c. Dummy Core Procurement (V. M. Kolba)

A dummy core and control plates that will provide the proper pressure drop in hydraulic tests are being obtained to ensure proper alignment and clearances in relation to prototype structures.

To prepare for procurement, detailed drawings are being made for a set of dummy control rods that will permit tests to be made without endangering the actual rods.

3. Component Development

a. Beam Tube Development (A. R. Jamrog)

Last Reported: ANL-7403, p. 135 (Dec 1967).

(i) Beam-tube Test Facility. Assembly of the beam-tube test facility has been completed. The fitting, welding, and leaktesting of the pipes and valves that connect the test facility to the general-purpose hydraulic loop have been completed. The pipe-section assemblies are being separated from the test facility and hydraulic loop for independent hydrostatic testing.

The clearance between the prototype beam tube and the simulated reflector liner is being established by critical measurements.

(ii) Beam-tube Handling Tool. A tool for handling the prototype blind and through beam tubes has been fabricated. The tool was attached

to the prototype blind tube, counterbalanced, and inserted in the test facility. The tool guide would not fit inside the beam-tube adapter, so the tool was removed and the guide plate was reworked. Then the beam tube and tool were again assembled, inserted in the facility, and seated; the breech lock was rotated and the locking bolts were secured; the tool was detached from the beam tube and removed. No difficulty was experienced. The tool was reinserted and attached to the prototype tube, the locking bolts were loosened, the breech-lock ring was rotated to the unlocked position, and the beam tube was removed from the test facility with no difficulty. The capability of the handling tool will be demonstrated by inserting and removing the beam tube through a simulated coffin.

(iii) Through-tube Guide Assembly. A guide assembly for the prototype through tube has been designed; fabrication is about 50% complete. This assembly will guide and protect the end of the through-tube connector while the beam tube is being inserted into the test facility.

4. Planning and Administration

a. Project Definition and Safety Analysis (M. Levenson)

Last Reported: ANL-7391, pp. 165-166 (Oct 1967).

The Advisory Committee on Reactor Safeguards (ACRS) has formally advised the Commission of its favorable conclusion that "there is reasonable assurance that a reactor facility of the type proposed can be constructed and operated at the Argonne National Laboratory site without undue hazard to the health and safety of the public."

The disagreement between ANL and the AEC Division of Reactor Licensing (DRL) regarding suitable seismic design criteria for the facility has been resolved by AEC criteria that are acceptable to DRL. Facility design will be reviewed in light of the new criteria, although a preliminary appraisal shows that the original ANL seismic design criteria, arrived at with the benefit of seismology and geology consultants, are generally more conservative. The AEC criteria are given in Table III.A.2.

TABLE III.A.2. Allowable Stress Limits for AARR Facility

Loading Condition	Liner Plate		Pipes, Tanks, Switchgear, etc.	Reinforcing Steel	Concrete
	P_m	$P_m + P_b$			
FOR REACTOR CONTAINMENT BUILDING					
Case III:DL + LL + PL + EL	S_m	1.5 S_m	-	0.5 f_y	0.60 f'_c
Case IIIA:DL + LL + PL + 2 EL	0.90 S_y	0.90 S_{cs}		0.90 f_y	0.85 f'_c
FOR ALL OTHER CLASS-I STRUCTURES, SYSTEMS, AND COMPONENTS					
Case III:DL + LL + PL + EL	-	-	0.90 of yield or equivalent[a]	0.90 f_y	0.85 f'_c
Case IIIA:DL + LL + PL + 2 EL	-	-	Generally not to exceed yield[b]		0.95 f'_c

[a]The "equivalent" value for austenitic pressure vessels remains to be defined.
[b]If yielding is to be permitted at local regions, analysis will be performed to determine failure modes; total deformation allowable will not exceed 50% of the deformation that would cause failure.

Symbols for Table III.A.2

DL = dead loads.
LL = live loads.
PL = design pressure load.
TL = design temperature load.
EL = design earthquake load (based on maximum horizontal ground acceleration of 0.1 g).
2 EL = maximum earthquake load (based on maximum horizontal ground acceleration of 0.2 g).
P_m = primary membrane stress.
P_b = primary bending stress.
f_y = yield stress (minimum guarantees for reinforcing bars).
f'_c = minimum ultimate compression strength of concrete.
S_y = yield strength at temperature as specified in Table N-424, Section III, ASME Nuclear Vessel Code.
S_{cs} = collapse stress as defined in Fig. 2 on p. 6 of Criteria of Section III, ASME Nuclear Vessel Codes (1964).
S_m = allowable membrane stress as specified in Section VIII, ASME Boiler and Pressure Vessel Code times a factor of 1.10.

IV. NUCLEAR SAFETY

A. Other Reactor Kinetics--Research and Development

1. Fuel Meltdown Studies with TREAT (C. E. Dickerman)

Last Reported: ANL-7403, pp. 140-143 (Dec 1967).

a. Meltdown Studies

(i) Development of Experimental Methods

(a) Mark-II Integral Sodium Loop Development. In order to obtain the highest practical degree of quality control of the high-pressure Mark-II integral loops, the loop design and specifications have been made in accordance with the ASME Boiler and Pressure Vessel Code as a Class A Nuclear Vessel. All loop material and welding rod is analyzed prior to use to insure proper chemical composition. With each component fully heat treated prior to welding, the design code neither "requires nor prohibits" postweld heat treatment in stationary systems not subject to rapidly changing internal pressures. However, as demonstrated in the TREAT loop experiments with metallic fuels, sharp transient pressure loadings can be encountered in fuel-failure experiments.

Thus, to optimize as far as possible the loop strength and ductility, it was specified that a final postweld heat treatment be given each loop body. This procedure consists of a 1950°F heat treatment in an inert gas, followed by a neutral water quench. This treatment is not a "full stress relief," but a full austenite normalization of the entire weldment.

After extensive discussions with consultants, the prototype loop was treated by a succession of methods to work out proper techniques. The technique finally adopted consists of supporting the weldment vertically from its top plate within a vertical-pit, radiant tube furnace purged with commercially pure argon. After a 2-hr "soak" at 1950°F, the weldment is withdrawn from the furnace into an inert gas-filled shroud of 20-gauge mild steel and transferred inside the shroud to the water tank where it is quenched. By this means, quenching distortions and scaling are minimized.

The prototype loop has been used as a trial loop in development of welding, radiographic, and heat-treatment techniques. The material is fully certified, it is fully radiographed, and it has been heat treated as per specifications to a ductile state. The loop has been returned from the plant of the heat-treatment vendor for cleanup of flange surfaces

and subsequent outfitting. Plans call for the loop to be fully outfitted and used for checkout, and for loop-design proof tests at temperature and at pressure. After proof tests, the prototype would be qualified for transient reactor use.

(b) Conversion of TREAT for Testing Fast Fuel Clusters. A continuing study to modify the TREAT reactor for carrying out satisfactory meltdown tests of fast reactor subassemblies is discussed in the following.

Since in its present arrangement TREAT supplies neutrons having the spectrum of a thermal reactor, it is not suitable to produce radially uniform heating in a highly enriched fast fuel subassembly. To avoid excessive surface heating in clusters of prototypical fast reactor fuel in the present TREAT reactor, the latter must be modified to minimize the number of low-energy neutrons reaching the test section, which consists of 0.29-in.-dia fuel pins consisting mainly of oxides of ^{235}U, ^{238}U, and ^{239}Pu in ratios of about 77:6:17. Use of a 0.635-cm Boral sheet to surround the test section does not sufficiently reduce the number of low-energy neutrons reaching the test section. As a result, there is an appreciable gradient in radial heating; furthermore, the fission heat energy available at the test section under these circumstances will not be as great as in a design using a converter described below.

A portion of the study was conducted with designs optimized to produce a relatively hard neutron spectrum inside the TREAT loop test section. The spectrum of neutrons in the test section was quite similar to that calculated for ZPR-3 Assembly 48.

The converter is located between the test section and the core of TREAT, occupying approximately 5.4% of TREAT core space. The ^{235}U isotopic density in the test section is $N^{25} \simeq 1.16 \times 10^{22}$, whereas in the core $N^{25} = 7.574 \times 10^{18}$, as a result, care had to be exercised to minimize hot spots at the interfaces. To achieve a radially uniform heating and reduced hot spots, the converter was made of four sections, with step-up concentrations of N^{25}, using no moderator in the two sections nearest to the test section. For a greater reduction of hot spots, thin sheets of Boral equivalent are used in the converter interface where hot spots might occur.

Important operational requirements of the converter are:

1) TREAT core temperature should not exceed 400°C;*

2) Temperature of the converter should not exceed 1800°C;

*Requests have been made of the AEC to raise the temperature limit to 600°C.

3) There should be a radially flat heating of the test section;

4) For a single-step adiabatic excursion, energy available at the test section should be greater than that required for melting UO_2.*

A design study of the proposed converter was made, taking into account the number of sections, and the composition of each section and localized poison, in order to best meet the above requirements. Design constants of a number of TREAT-converter systems studied are given in Table IV.A.1.

TABLE IV.A.1. Isotopic Densities N of Elements in the Various Regions of the Reactor and in the Different Designs of the Converter (Units of 10^{24})

TREAT Core	Reflector	Test Section
$N^{25} = 7.574 \times 10^{-6}$	$N^{C} = 7.602 \times 10^{-2}$	$N^{49} = 3.733 \times 10^{-3}$
$N^{28} = 5.543 \times 10^{-7}$	$N^{Nat\ B} = 1.6 \times 10^{-7}$	$N^{25} = 1.6614 \times 10^{-2}$
$N^{Nat\ B} = 5.047 \times 10^{-7}$	$N^{Al} = 2.605 \times 10^{-3}$	$N^{28} = 1.25 \times 10^{-3}$
$N^{C} = 7.602 \times 10^{-2}$		$N^{40} = 4.66 \times 10^{-4}$
$N^{Fe} = 3.343 \times 10^{-6}$	Instrument Loop Section	$N^{O} = 4.18 \times 10^{-2}$
		$N^{Na} = 2.18 \times 10^{-2}$
	$N^{Fe} = 1.051 \times 10^{-2}$	N^{Fe} (cladding) $= 7.62 \times 10^{-2}$
	$N^{Ni} = 1.116 \times 10^{-3}$	N^{Ni} (cladding) $= 8.05 \times 10^{-3}$

Design No.	Isotope	Converter: Inner Converter 1	Inner Converter 2	Outer Converter 1	Outer Converter 2
1	^{235}U	0.007935	0.00265	4×10^{-4}	2.5×10^{-4}
	^{238}U	0.0185	0.0070	2.8×10^{-6}	1.75×10^{-6}
	C			7.22×10^{-2}	7.22×10^{-2}
	Fe			3.34×10^{-5}	3.34×10^{-5}
2	^{235}U	0.0040	0.0020	4×10^{-4}	2.5×10^{-4}
	^{238}U	0.0224	0.0060	2.8×10^{-6}	1.75×10^{-6}
	C			7.22×10^{-2}	7.22×10^{-2}
	Fe			3.34×10^{-5}	3.34×10^{-5}
3	^{235}U	0.0020	0.0010	4×10^{-4}	2.5×10^{-4}
	^{238}U	0.02445	0.02545	2.8×10^{-6}	1.75×10^{-6}
	C			7.22×10^{-2}	7.22×10^{-2}
	Fe			3.34×10^{-5}	3.34×10^{-5}
4	^{235}U	0.0040	0.0020	4×10^{-4}	2×10^{-4}
	^{238}U	0.0224	0.0240	4×10^{-5}	2×10^{-5}
	C			7.22×10^{-2}	7.22×10^{-2}
	Fe			3.34×10^{-5}	3.34×10^{-5}
	B	0.004.....located at interface of converter and core, to a thickness of 0.15 cm.			
5	The same as No. 4 except $N^{B} = 0.001$.				
6	The same as No. 4 except $N^{B} = 0.007$.				

* This energy is denoted by ΔH_{melt}.

Reactivity and fission density data were obtained using the SNARG-1D* code, and the sixteen-group cross-section set No. 201.** The Westcott data† was used for the evaluation of the thermal cross sections at different core temperatures.

The maximum heat energy that can be made available at the test sample, without overheating of the converter or of the core, is determined from the SNARG-1D results and the analysis which follows.

For a one-step adiabatic-heating excursion,

$$(FD)_i \propto H_i = \overline{C_{pi}} T_i$$

where, FD_i and T_i are the fission density and temperature rise in region i, and $\overline{C_{pi}}$ is the average specific heat of that region. We define the following ratios in terms of maximum and center-line fission-density values:

$$\frac{(FD_{max})_{converter}}{(FD_{center\ line})_{test\ section}} \equiv a_{max}; \tag{1}$$

$$\frac{(FD_{center\ line})_{test\ section}}{(FD_{max})_{core}} \equiv b. \tag{2}$$

Assuming a maximum allowable temperature in the converter and in the core of 1800 and 400°C, respectively, we obtain

$$\frac{(\overline{C}_p)_{converter} T_{converter}}{(\Delta H_{center\ line})_{test\ section}} = a_{max},$$

or

$$(\Delta H_{center\ line})_{test\ section} = \frac{1345}{a_{max}}; \tag{3}$$

also,

$$(T_{max})_{core} = \frac{1345}{a_{max} b (\overline{C}_p)_{core}}. \tag{4}$$

In Eqs. (4) and (5), the number 1345 is the product $(\overline{C}_p T)_{converter}$, where $\overline{C}_p = 0.769$ and T is the temperature rise: (1800-50)°C. To allow for hot spots, the maximum value of a is taken.

* Duffy, G. F., et al., ANL-7221 (1966).

** "LASL 16-group Cross Sections," ANL-5800, pp. 568-576.

† Westcott, C. H., CRRP-960 (3rd Ed.).

It follows from the results that

a) Of the first three designs which do not use boron for reducing power peaks in the converter, $N^{25} = 0.004 \times 10^{24}$ and $N^{25} = 0.002 \times 10^{24}$ give best results;

b) Using $N^{B}_{(Boral)} = 0.001 \times 10^{24}$ to a thickness of 0.158 cm gives the highest energy available for melting of test samples;

c) Use of 1/4-in. Boral filter only results in lower available energy than obtainable with a converter design. It also yields appreciable radial heating, as already stated.

Our calculations were made for a maximum spectral hardening at the test section. By allowing some softening of this spectrum, the maximum energy available at the test section may be increased considerably.

Use of a converter operating at ~1800°C may result in oxidation unless proper precautions are taken by the use of some inert gas, such as helium, inside the converter cans.

2. Materials Behavior, Equation of State, and Energy Transfer

a. Materials Behavior and Energy Transfer

(i) Interactions of Fuel, Cladding, and Coolant (R. O. Ivins)

Last Reported: ANL-7399, pp. 162-165 (Nov 1967).

Studies relating to the possible physical or chemical interactions between reactor materials and the reactor coolant, sodium, have been continued. The initial studies were made of the interaction of molten fuel and cladding materials with liquid sodium where extensive fragmentation of the samples occurred, resulting in violent expulsion of some of the fragmented material (see Progress Report for May 1965, ANL-7046, p. 81). In an attempt to determine the cause of the fragmentation phenomenon, later experiments (see Progress Report for January 1966, ANL-7152, p. 90) were performed to compare the effects of dropping molten metals into sodium and into water; for example, molten silver dropped into water did not fragment, but did fragment when dropped into liquid sodium. It was hypothesized that the breakup results from violent formation and collapse of vapor bubbles in the nucleate and transition boiling regimes. Cladding metals are in a molten state in the violent boiling regime for sodium (900-2300°C) and thus fragment; however, they are not in a molten state in the violent boiling regime for water (100-373°C) and, therefore, do not fragment in that medium. Experiments in water using low-melting-point metals support this hypothesis (see ANL-7152, p. 95).

The experiments in water were extended to include a survey study of the dynamics of fragmentation in water, and a more extensive examination of the thermal effects on fragmentation (see ANL-7399, p. 162).

Recently an effort has been made to describe fragmentation quantitatively by the use of a photographic method to determine the surface area of the fragmented particles. Since the size of the fragments may vary considerably for any given experiment, a more descriptive method for determining the degree of fragmentation than simply considering the total number of fragments (see ANL-7399, p. 163) is necessary; the photographic method (described below) allows an estimation of the increase in the surface area of the particles after fragmentation.

A photograph of the fragments is analyzed by the CHLOE apparatus (computer-controlled film digitizer) by comparing the photograph of the sample to standards of known area. The output from CHLOE gives the total cross-sectional area of the fragments. If the fragments are assumed to be flat plates, the total smooth surface area would be twice the number obtained from CHLOE; if the fragments are assumed to be spheres, the total smooth surface area would be four times the photographic area. A visual examination of the fragments can often be used to decide which factor is more appropriate.

A reproducibility test of this method was made with a sample of fragmented bismuth containing over 500 fragments ranging in size from approximately 10 μ to 10 mm. The sample was divided in five portions and a photograph taken of each. This was done three times with the sample mixed and redivided before each set of photographs was made. The three trials gave areas of 2.99, 2.98, and 2.87 cm^2, with a maximum error of 4%.

Preliminary fragmentation experiments with the CHLOE apparatus to determine surface areas have been performed. Single drops of molten tin (at 255, 310, 385, 550, and 600°C) were dropped into room-temperature water at entrance velocities of 243 and 486 cm/sec (corresponding to drop heights of 1.0 and 4.0 ft). To commence a run, a sample (weight, ~0.4 g; spherical surface area, 0.6 cm^2) was heated in air or in argon to the desired temperature while positioned in a quartz dropper within a small furnace. A single drop was expelled by exerting a slight overpressure in the dropper.

Calculations have shown the heat loss of a falling metal drop to be negligibly small under the conditions of the experiment; therefore, the temperatures reported are the temperatures measured before falling. The initial area of the drop was calculated from the weight of the fragments by assuming the drop to be spherical. The fragments were assumed to be two-dimensional plates for the surface area calculations, i.e., the area as determined by CHLOE has been doubled.

Values of the ratio of the surface areas of the fragmented particles to the initial surface area of the molten drop were determined at different temperatures and entrance velocities. The resultant surface-area ratios of five runs under identical conditions were then averaged to obtain the values listed in Table IV.A.2.

TABLE IV.A.2. Comparison of Surface Areas (Determined by CHLOE) for Fragmented Tin under Various Conditions

Temperature (°C)	Entrance Velocity (cm/sec)	Atmosphere	Ratio of Fragmented Area to Initial Area
255	243	Air	0.88 ± 0.16
255	486	Air	3.04 ± 0.68
310	243	Air	2.79 ± 1.52
310	486	Air	5.87 ± 1.18
385	243	Air	5.02 ± 0.66
385	486	Air	5.25 ± 0.48
385	486	Argon	5.16 ± 0.64
550	243	Air	1.57 ± 0.48
550	486	Air	2.65 ± 0.30
600	243	Air	1.69 ± 0.16
600	486	Air	2.62 ± 0.56
600	486	Argon	2.16 ± 0.24
700	486	Air	2.57 ± 0.46
700	486	Argon	2.41 ± 0.67
800	486	Air	2.25 ± 0.66
800	486	Argon	1.32 ± 0.28
900	486	Air	1.78 ± 0.46
900	486	Argon	1.83 ± 0.49

The results of the experiments that were run at sample temperatures substantially above or below the critical temperature of water (373°C) show an increase in the surface area with increasing entrance velocity. This dynamic effect has been observed previously (see ANL-7399, p. 162). There does not appear to be a pronounced thermal effect at these temperatures. However, at 310 and 385°C (temperatures which bracket the critical temperature of water), there are significant increases in the surface areas. These observations indicate that a pronounced thermal contribution to the fragmentation process may be occurring near the critical temperature of water. This is in agreement with previous studies in which gallium fragmented in water (see ANL-7399, p. 162).

Some of the experiments were conducted using an inert atmosphere purge (argon) to keep the tin samples from oxidizing at high temperatures. The formation of an oxide coating on the molten drop might

result in a change in the surface tension of the drop, which in turn could affect the degree of fragmentation. The results of the inert-atmosphere experiments (see Table IV.A.2) indicate little deviation from those carried out in air. Thus, if an oxide film is formed, it does not significantly affect the degree of fragmentation of tin in room-temperature water.

(ii) Violently Sprayed Sodium-Air Reaction (R. O. Ivins)

Last Reported: ANL-7391, pp. 176-178 (Oct 1967).

Safety analyses for sodium-cooled reactors require knowledge of the temperatures and pressures generated during sodium combustion in air. A study of the reaction of sodium sprays in air is underway in which pressure-generation rates as well as peak pressures and temperatures are being determined as functions of the initial conditions.

Experiments are being performed to study the effect of varying the driving pressure on the piston spray injector (see Progress Report for January 1967, ANL-7302, p. 93) which, in turn, results in changes in the spray velocity and particle-size distribution. Preliminary results of these experiments have been described (see ANL-7391, p. 176).

A calculational attempt is also being made to predict mathematically the rate of pressure rise in a closed volume due to the sodium-air reaction. The method is based on a modification of a model proposed by Mouradian and Baker.* The first phase of the theoretical analysis has been completed. In this treatment, the burning rate and burning temperature are calculated for a single spherical particle of sodium moving through air or air depleted in oxygen.

If it is assumed that the sodium burning rate is controlled by the diffusion of oxygen to the combustion zone, then the following relationships** should be valid. The rate of diffusion of oxygen can be expressed as

$$N_{O_2} = \frac{k_y(Y_{O_2,A} - Y_{O_2,B})}{1 - Y_{O_2,A}}. \qquad (1)$$

(The symbols used in this equation and in those below are defined in Table IV.A.3.) By analogy to heat-transfer phenomena, the mass-transfer coefficient k_y can be predicted by defining a Nusselt number for mass transfer as

$$Nu_m = k_y d/(CD)_f. \qquad (2)$$

*Mouradian, E. M., and Baker, L., Nucl. Sci. Eng. 15, 388 (1963).

**Bird, R. B., Stewart, W. E., and Lightfoot, E. N., Transport Phenomena, Ch. 13 and 21, John Wiley and Sons, Inc., New York (1960).

For flow around a sphere, this Nusselt number is correlated by the following expression:

$$Nu_m = 2.0 + 0.6\ Re^{1/2}Sc^{1/3}, \tag{3}$$

where the Reynolds number Re and the Schmidt number Sc are defined as

$$Re = (dv\rho/\mu)_f; \quad Sc = (\mu/\rho D)_f. \tag{4}$$

TABLE IV.A.3. Definition of Symbols

C - molar density, g-mol/cm^3	Y - gaseous mole fraction
C_p - heat capacity, cal/g-°K	ρ - density, g/cm^3
d - sphere diameter, cm	μ - viscosity, centipoise
D - diffusion coefficient, cm^2/sec	σ - Maxwell-Boltzmann constant
ΔF - free energy change for reaction, cal/g-mol	ϵ - emissivity
h - heat-transfer coefficient, cal/(sec)(cm^2)(°K)	
k - thermal conductivity, cal/(sec)(cm)(°K)	Subscripts
k_y - mass-transfer coefficient, g-mol/(sec)(cm^2)	A - ambient conditions
K_p - equilibrium constant	B - burning-zone conditions
N - molar flux, g-mol/(sec)(cm^2)	f - diffusion film-zone conditions
P - pressure, atm	O_2 - oxygen
Q - heat of reaction, cal/g-mol O_2	Na - sodium
R - universal gas constant	N_2 - nitrogen
T - temperature, °K	t - total
v - velocity, cm/sec	

A heat balance is obtained by equating the heat-generation rate to the heat-loss rate by radiation and convection:

$$N_{O_2}Q = \sigma\epsilon(T_B^4 - T_A^4) + h(T_B - T_A). \tag{5}$$

The heat-transfer coefficient h is obtained in the usual fashion by introducing the Nusselt number:

$$Nu = (hd/k)_f. \tag{6}$$

The heat-transfer correlation for forced convection around a sphere is

$$Nu = 2.0 + 0.6\ Re^{1/2}Pr^{1/3}, \tag{7}$$

where the Prandtl number Pr is defined as

$$Pr = (C_p\mu/k)_f. \tag{8}$$

It is assumed that chemical equilibrium exists in the combustion zone. For the reaction

$$2Na(g) + \tfrac{1}{2}O_2(g) \rightleftharpoons Na_2O(\ell),$$

the equilibrium constant is defined as

$$K_P = \frac{1}{(P_{Na}^2 P_{O_2}^{1/2})_B}, \tag{9}$$

which can be simplified as follows:

$$1/K_P = P_t^{5/2}(Y_{Na}^2 Y_{O_2}^{1/2})_B$$

$$= P_t^{5/2}(1 - Y_{N_2} - Y_{O_2,B})^2(Y_{O_2,B})^{1/2}$$

$$= P_t^{5/2}(Y_{O_2,A} - Y_{O_2,B})^2(Y_{O_2,B})^{1/2}. \tag{10}$$

The equilibrium constant is related to the free energy change for the reaction by

$$\Delta F = -RT \ln K_P. \tag{11}$$

The above set of equations contains two unknowns: T_B and $Y_{O_2,B}$. These can be solved by means of the Newton-Raphson Method* and the CDC-3600 computer.

Typical results of the calculations are presented in Figs. IV.A.1 and IV.A.2. These figures show the effects of velocity and particle diameter, respectively, when burning temperature and burning rate are plotted as functions of oxygen concentration in the ambient atmosphere. When the oxygen concentration in the atmosphere falls below 5 m/o, the burning temperature rapidly approaches the boiling point of sodium (1177°K) and the vapor-phase combustion model is no longer valid.

In the next phase of the theoretical analysis, a quasi-steady-state approach and an averaging technique will be used in correlating the reaction rates of the individual particles with the burning rate of the spray and the pressure rise rate of the enclosed volume.

*Ralson, A., A First Course in Numerical Analysis, p. 349, McGraw-Hill Book Co., Inc., New York (1965).

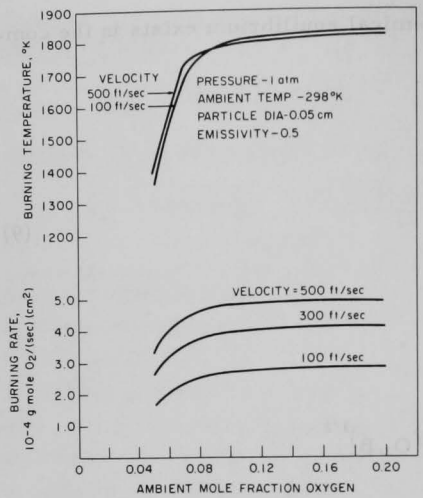

Fig. IV.A.1. Effect of Velocity on the Theoretical Burning Temperature and Burning Rate of Sodium Spheres

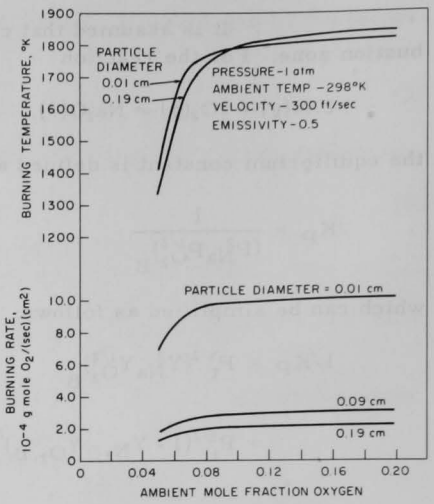

Fig. IV.A.2. Effect of Particle Diameter on the Theoretical Burning Temperature and Burning Rate of Sodium Spheres

(iii) Segregation in Ceramic Fuels (M. G. Chasanov)

Last Reported: ANL-7391, pp. 178-179 (Oct. 1967).

Migration and segregation of fissile and fertile material within a fast reactor fuel during its operational lifetime could have significant effects on the operational safety of the fuel. Investigation of the migration of plutonium and fission products in a thermal gradient is underway for mixed-oxide fuels. Extension of the program to carbide fuels is planned.

The thermal-gradient furnace used in these migration studies and several preliminary experiments with UO_2-CeO_2 pellets have been previously described (see Progress Reports for September 1966, ANL-7255, p. 87, and March 1967, ANL-7317, p. 110). Experiments are in progress with cylindrical $(U_{0.8}Pu_{0.2})O_{2.00}$ pellets, 1/2 in. high by 1/2 in. in diameter. Two experiments reported in ANL-7391 indicated no significant migration had occurred for these samples (sample top temperatures were about 2000°C).

Two 500-hr duration experiments were carried out in the thermal-gradient apparatus by heating the pellets in an atmosphere of several hundred Torr of argon. In experiment P-3 (T_{top} = 1980°C; T_{bottom} = 1250°C), the sample was heated in an inverted tungsten metal

crucible which served as a barrier to loss of material by vaporization; in experiment P-4 (T_{top} = 2040°C; T_{bottom} = 960°C), no crucible was used. The thermal gradient obtained in experiment P-3 was somewhat smaller because of conduction losses resulting from the use of the metal crucible.

An electron microprobe scan along the longitudinal axis of Sample P-3 revealed no significant migration of plutonium. This was also the case for the corresponding 100-hr experiment, P-1. For Sample P-4, the electron microprobe analysis gives an indication of some enhancement in plutonium concentration in the hotter portion of the pellet (a peak concentration of 22 w/o PuO_2 versus a nominal average composition of 20 w/o). This observation may be the result of enhanced migration due to stoichiometry changes (loss of oxygen from the hotter end). Portions of this sample are being analyzed for any changes in the ratio of oxygen to metal.

A 1000-hr experiment utilizing a tungsten-covered sample has now been completed and is currently being examined.

3. Coolant Dynamics

a. Critical Flow (H. K. Fauske)

Last Reported: ANL-7403, pp. 147-148 (Dec 1967).

(i) Sodium Tests. Preliminary shakedown tests and calibration of the sodium loop are in progress. Data on pressure drop of single-phase liquid sodium in the cylindrical-divergent nozzle test section indicate that all eight pressure taps are functioning properly. Measured friction factors are within 5% of the Moody friction-factor curve for smooth tubes. The test section is being calibrated for heat loss, and the twenty thermocouples are being checked.

(ii) Sonic Velocity. The effect of flow regime on the speed of pressure-wave propagation in two-phase flows is being investigated; air-water mixtures serve as the working fluid. Flows being tested include bubble, slug, annular, and dispersed flows. Data obtained for the bubble, the slug, and the stratified flow regimes are being compared with theoretical analysis.

b. Coolant Dynamics (R. M. Singer)

Last Reported: ANL-7403, p. 148 (Dec 1967).

(i) Superheat. The superheat tests in the polished test vessel have been completed, and data are being reduced and analyzed. Samples of the sodium will be analyzed chemically, and the test vessel wall will be

examined for metallurgical effects caused by contact with sodium for approximately 14 months. A new test section with a sandblasted surface (i.e., a rough, porous finish) is being prepared.

(ii) Expulsion. Work continues on the safety-interlock systems and on filament-alignment problems. To ensure reproducibility, we will fabricate our own filaments. During preliminary tests, heat fluxes to a solid bar up to about 500 W/cm^2 were achieved. The pulsing circuits of the heater are being tested.

Initial assembly of the sodium system will begin in one to two months.

c. Convective Instability (R. P. Heinisch)

Last Reported: ANL-7403, p. 148 (Dec 1967).

The runs with a solid test section are complete and the data have been reduced. Interestingly, if the heat flux incident upon the wall is above a certain value Q_c, then the mode of heat transfer, up to boiling of mercury, is by pure conduction. The amazing factor of importance is that the heat-flux value for Q_c is relatively small.

d. Core Component Dynamics (M. W. Wambsganss)

Last Reported: ANL-7403, pp. 148-150 (Dec 1967).

In the investigation of the plastic deformation of cylindrical shells under impulsive loads, information concerning the region of energy deposition has been obtained by studying the static yield conditions corresponding to an arbitrary load shape.

Consider a circular cylindrical shell of radius R and thickness h with the applied load distribution $P(z,t)$ symmetric about $z = 0$. Define the dimensionless axial coordinate ξ and dimensionless time τ by

$$\xi = z/\sqrt{R}h; \qquad \tau = t/T, \tag{1}$$

where T is a time interval associated with the particular problem under consideration. Let

$$\phi(\xi)\,\psi(\tau) = RP(z,t)/\sigma_0 h, \tag{2}$$

where σ_0 is the yield stress of the material of the shell, ϕ is the dimensionless load-shape function, and ψ is the dimensionless pulse shape. Because of the assumed symmetry it is necessary to consider only $\xi \geq 0$.

Given an arbitrary monotonically decreasing load-shape function ϕ, as $\psi(\tau)$ increases from zero the shell will just begin to yield at some time τ_0. Hinge circles initially form at $\xi = 0$ and $\xi = \xi_1(\tau_0)$, where the function $\xi_1(\tau)$, which gives the location of the outer hinge circle, is the solution of a nonlinear differential equation. However, $\psi(\tau_0)$ and $\xi_1(\tau_0)$ coincide with the static-yield amplitude ψ_s and the static-yield hinge-circle location ξ_s, which can be found by limit-analysis techniques. Using a limited-interaction yield condition, we can show that ψ_s and ξ_s are the simultaneous solutions of

$$\psi_s \int_0^{\xi_s} \phi(\xi)\, d\xi = \xi_s; \qquad 2\psi_s \int_0^{\xi_s} \xi\phi(\xi)\, d\xi = \xi_s^2 - 1. \tag{3}$$

To demonstrate the implications of Eqs. (3), consider a family of load-shape functions ϕ_γ such that

$$\phi_\gamma(\xi) = \begin{cases} \left(\dfrac{\gamma+1}{a\gamma}\right)\left[1 - \left(\dfrac{\xi}{a}\right)^\gamma\right]; & 0 \le \xi < a; \quad 0 < \gamma < \infty; \\ 0, & \xi \ge a; \end{cases}$$

$$\phi_0(\xi) = \lim_{\gamma \to 0} \phi_\gamma = \frac{1}{a} \log\left(\frac{a}{\xi}\right); \qquad 0 \le \xi < a;$$

$$\phi_\infty(\xi) = \lim_{\gamma \to \infty} \phi_\gamma = \frac{1}{a}; \qquad 0 \le \xi < a, \tag{4}$$

where $a\sqrt{Rh}$ is the length of the region of load application and a is dimensionless. The multiplicative factor $(\gamma+1)/a\gamma$ in the definition of ϕ_γ is such that

$$\int_0^a \phi_\gamma\, d\xi = 1, \qquad 0 \le \gamma \le \infty, \tag{5}$$

so that the total load on the shell for a given value of ψ is independent of γ and a. Graphs of ϕ_γ for various values of the load-shape parameter γ (see Fig. IV.A.3) show that a variety of plausible load shapes are included in the family.

The solution to Eqs. (3) for various load shapes ϕ_γ are given by Figs. IV.A.4 and IV.A.5. The available solutions in the literature are for a rectangular load shape ($\gamma = \infty$) and for a concentrated load ($a \to 0$).

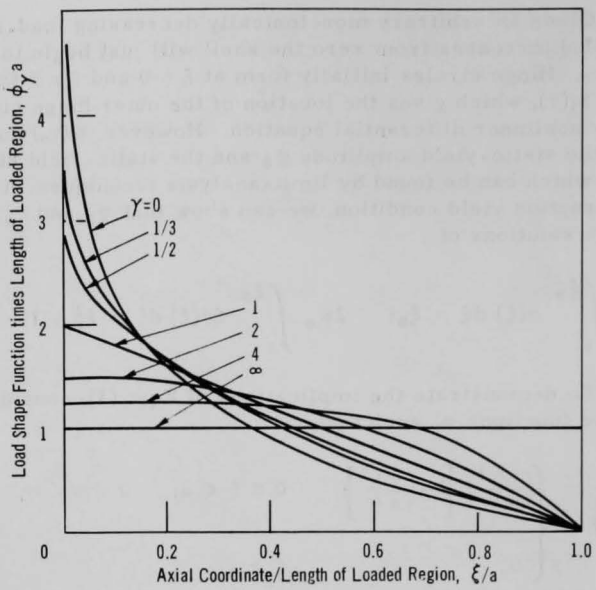

Fig. IV.A.3. Load-shape Function ϕ_γ for Various Shape Parameters γ

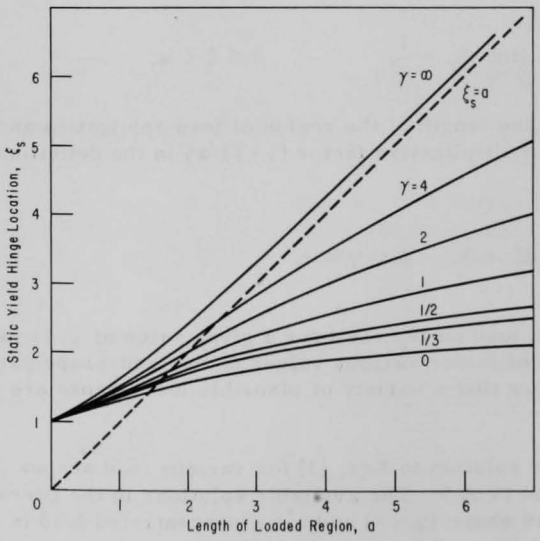

Fig. IV A.4. Location of Hinge Circle at Static Yielding ξ_s as a Function of Length of the Loaded Region a for Various Shape Parameters γ

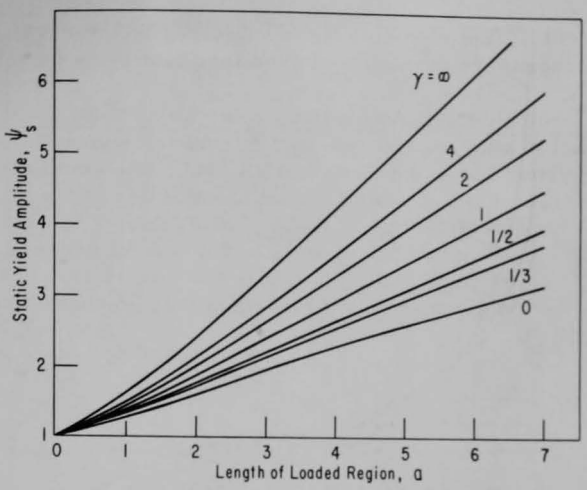

Fig. IV.A.5. Static-yield Amplitude ψ_s as a Function of Length of the Loaded Region a for Various Shape Parameters γ

In Fig. IV.A.4. we see that in both cases $\xi_s > a$, i.e., the hinge circle is outside the region of load application. This has led some investigators to conclude that the region of energy deposition is larger than the loaded region of the shell. However, as we see in Fig. IV.A.4, $\xi_s < a$ for load shapes and load-region lengths more physically realistic than those for the two idealized cases. Consequently, in practical situations the hinge circles are likely to be inside the region of load application and the region of energy deposition is smaller than the loaded region.

Figure IV.A.5 shows that the total load necessary to cause yielding increases almost linearly with the length of the loaded region for any given load shape.

B. Operations

1. TREAT Operations (J. F. Boland)

Last Reported: ANL-7403, p. 151 (Dec 1967).

a. Reactor Operations. Renovation of the control-rod drive mechanisms was completed. This work included: (a) replacement of bolts and studs, which had shown a tendency to loosen during operation, by self-locking fasteners, (b) installation of electric terminal blocks of higher quality, and (c) replacement of wiring which had deteriorated insulation.

EBR-II fuel elements were subjected to steady-state irradiation as part of a program to develop a method for identifying defective elements.

b. Development of Automatic Power Level Control System. Development of reactor kinetics and reactivity-feedback subroutines for the IBM "Continuous System Modeling Program" (CSMP) was completed, and the computer program now provides adequate simulation of transient power-versus-time characteristics of TREAT. Initial efforts to simulate reactor operation with closed-loop control were unsuccessful because of programming limitations that were not explained in the description of the CSMP. A different program arrangement which should avoid these limitations is being investigated.

PUBLICATIONS

NUCLEAR SAFETY

A Hybrid-computer Program for Transient Temperature Calculations on TREAT Fast Reactor Safety Experiments
Lawrence T. Bryant, Lawrence W. Amiot, Charles E. Dickerman, and William P. Stephany
ANL-7374 (Sept 1967)

An Electron-bombardment-heated Sodium Experiment
Robert E. Holtz
ANL-7364 (Sept 1967)

Experimental Investigation of Low-pressure Alkali-metal Thermionic Converters for DC and RF Power
Hans K. Richards
ANL-7377 (Sept 1967)

ARGONNE NATIONAL LAB WEST
3 4444 00011236 7
ARGONNE NATIONAL LAB WEST
3 4444 00011236 7
ARGONNE NATIONAL LAB WEST
3 4444 00011236 7
ARGONNE NATIONAL LAB WEST
3 4444 00011236 7
ARGONNE NATIONAL LAB WEST
3 4444 00011236 7
ARGONNE NATIONAL LAB WEST
3 4444 00011236 7
ARGONNE NATIONAL LAB WEST
3 4444 00011236 7
ARGONNE NATIONAL LAB WEST
3 4444 00011236 7
ARGONNE NATIONAL LAB WEST
3 4444 00011236 7
ARGONNE NATIONAL LAB WEST
3 4444 00011236 7